Electrochemistry of Palladium with Emphasis on Size Dependent Electrochemistry of Water Soluble Palladium Nanoparticles

by

Ashok Kumar

A Dissertation Presented in Partial Fulfillment
of the Requirements for the Degree
Doctor of Philosophy

Approved March 2016 by the
Graduate Supervisory Committee:

Daniel A. Buttry, Chair
Ian R. Gould
Giovanna Ghirlanda

ARIZONA STATE UNIVERSITY

May 2016

ABSTRACT

Palladium metal in its various forms has been heavily studied for many catalytic, hydrogen storage and sensing applications and as an electrocatalyst in fuel cells. A short review on various applications of palladium and the mechanism of Pd nanoparticles synthesis will be discussed in chapter 1. Size dependent properties of various metal nanoparticles and a thermodynamic theory proposed by Plieth to predict size dependent redox properties of metal nanoparticles will also be discussed in chapter 1.

To evaluate size dependent stability of metal nanoparticles using electrochemical techniques in aqueous media, a synthetic route was designed to produce water soluble Pd nanoparticles. Also, a purification technique was developed to obtain monodisperse metal nanoparticles to study size dependent stability using electrochemical methods. Chapter 2 will describe in detail the synthesis, characterization and size dependent anodic dissolution studies of water soluble palladium nanoparticles.

The cost associated with using expensive metal catalysts can further decreased by using the underpotential deposition (UPD) technique, in which one metal is electrodeposited in monolayer or submonolayer form on a different metal substrate. Electrochemically, this process can be detected by the presence of a deposition peak positive to the bulk deposition potential in a cyclic voltammetry (CV) experiment. The difference between the bulk deposition potential and underpotential deposition peak (i.e. the UPD shift), which is a measure of the energetics of the monolayer deposition step, depends on the work function difference between the metal pairs. Chapter 3 will explore how metal nanoparticles of different sizes will change the energetics of the UPD

phenomenon, using the UPD of Cu on palladium nanoparticles as an example. It will be shown that the UPD shift depends on the size of the nanoparticle substrate in a way that is understandable based on the Plieth model.

High electrocatalytic activity of palladium towards ethanol oxidation in an alkaline medium makes it an ideal candidate for the anode electrocatalyst in direct ethanol based fuel cells (DEFCs). Chapter 4 will explore the poisoning of the catalytic activity of palladium in the presence of halide impurities, often used in synthesis of palladium nanoparticles as precursors or shape directing agents.

Dedicated to my family and teachers……

ACKNOWLEDGMENTS

I would like to express my first and foremost gratitude to my advisor, Professor Daniel A. Buttry. I have been incredibly privileged to be his Ph.D. student; he gave me the freedom to explore on my own, and at the same time challenged me to the greatest extent possible. I am highly indebted for his excellent guidance to recovery when my steps faltered, patience and in providing me with an exceptional environment for doing research. All of these assisted me in developing my own independent and pioneering problem solving aptitudes that will greatly benefit me during my career.

I would like to extend my gratitude to Professor Ian Gould, who played a very significant role in my choice to attend Arizona State University, for his constant help and assistance through my comprehensive examination, my progression through the graduate program, technical review and dissertation defense. I would like to thank my committee member, Professor Giovanna Ghirlanda, for her time and assistance through my comprehensive examination, technical review and dissertation defense. I would like to thank my comprehensive examination chair, Prof. Thomas Moore and comprehensive examination committee member, Dr. Alexandra Ross for their time and assistance. I would also like to thank Prof. Hao Yan and Prof. Yan Liu for giving me an opportunity to work in their lab. I would like to thank Prof. Prashant Mishra, department of Biochemical Engineering and Biotechnology at IIT Delhi who introduced me to the world of nanotechnology and played a crucial role in paving the way for my graduate career.

It wouldn’t have been possible to complete this thesis without constant support, help and enthusiasm of the people around me. I am thankful to Dr. Harish Bhat for initial

training during my first semester. I would like to thank Dr. Poonam Singh, Dr. Rajeev Ranjan, Joseph Rheinhardt, Tim Lamb, Chris Starr, Jarred Olson, Megan Sparks, Kate Parent and Russel Jacobs. I would like to thank Dr. Tylan Watkins for his company and discussion on scientific and non-scientific issues and inspiring me to be a better scientist and a better human being. I would like to thank Dr. Karl Weiss, Dr. Zhenquan Liu and Dr. Toshihiro Aoki from LeRoy Eyring Center for Solid State Science, ASU and David Lowry, laboratory manager CLAS Bioimaging facility at ASU for training and assistance with Electron Microscopy.

I would like to thank my friends outside the realms of our lab. I would like to thank Rajeev, Shikha, Rumit and Dinesh for their help and care. I would like to thank all my roommates during my graduate period, Fernando, Swapnil, Wilman and Arif for their company. I would like to thank my very friendly neighbors next door, Raja Pal and Shibom Basu. I am very thankful to my friend Parvez Alam for his company, help and taking care of me during our stay at ASU. I am also thankful to Palash Kanti Dutta for his friendship.

Last but not the least; I would like to express my heartiest gratitude to my parents and my younger brother, Amrit Kumar for their unconditional love and support. I am thankful to my grandparents for their love. I am thankful to my maternal uncle Mr. Navraj Pant for inspiring me to pursue my career in science.

TABLE OF CONTENTS

Page

LIST OF TABLES…..viii

LIST OF FIGURES……ix

LIST OF SCHEMES…….....xii

LIST OF ABBREVIATIONS……..…..xiii

CHAPTER

1. INTRODUCTION……..1

1.1. Theory of Nucleation and Growth of Nanoparticles: LaMer Mechanism……..4

1.2. Size Dependent Redox Properties of Metal Nanoparticles: Theory……8

1.3. Size Dependent Electrochemical Oxidation of Metal Nanoparticles……....11

1.4. Size Dependent Catalytic Properties of Metal Nanoparticles……12

1.5. Other Size Dependent Properties of Metal Nanoparticles.....14

1.6. References…….....16

2. SYNTHESIS CHARACTERIZATION AND SIZE DEPENDENT ANODIC DISSOLUTION OF WATER SOLUBLE PALLADIUM NANOPARTICLES…….24

2.1. Abstract……..25

2.2. Introduction……26

2.3. Experimental Section……...……..29

2.3.1. Synthesis of Water Soluble Palladium Nanoparticles……..……...29

2.3.2. Size Selection of Water Soluble Palladium Nanoparticles……..30

2.3.3. Characterization……...31

2.3.4. Electrochemical Measurements……...……32

2.4. Results and Discussion……..34

2.5. Conclusions……40

CHAPTER Page

2.6. References……..51

3. SIZE DEPENDENT UNDERPOTENTIAL DEPOSITION OF COPPER ON PALLADIUM NANOPARTICLES……..55

3.1. Abstract……..56

3.2. Introduction……57

3.3. Experimental…….60

3.4. Results and Discussion……..62

3.5. Conclusions……69

3.6. References……..80

4. INFLUENCE OF HALIDE IONS ON ANODIC OXIDATION OF ETHANOL ON PALLADIUM……85

4.1. Abstract……..86

4.2. Introduction……87

4.3. Experimental…….....91

4.4. Results and Discussion……..93

4.5. Conclusions……..…98

4.6. References……..…..104

APPENDIX

A. COPYRIGHT PERMISSION……110

LIST OF TABLES

Table Page

2.1. Structural and Electrochemical Data for Pd-BCA NPs……42

3.1. Work Functions and UPD Shifts for the Pd/Cu^{2+} System……70

LIST OF FIGURES

Figure Page

1.1. Various Aromatic Carbon-Carbon Bond Coupling Reactions Catalyzed by Pd……1

1.2. Oxygen Reduction Activity of Various Metals vs. O and OH Binding Energy……3

1.3. LaMer Growth Model……...6

1.4. Derivation of Plieth's Theory Using Two Half Cells……..…..…..10

2.1. Powder X-ray Diffraction for Pd-BCA NPs Samples of Varying Size Used for Size Dependent Anodic Dissolution Studies……43

2.2. TEM Micrograph of BCA Stabilized Water Soluble Palladium Nanoparticles Synthesized Under (a) Higher (Pd:BCA:BH_4^--1:5:10) and (b) Lower (Pd:BCA:BH_4^--1:1:10) Ligand Ratio……44

2.3. Low Resolution TEM and High Resolution TEM (inset) of Water Soluble Pd-BCA NPs (Pd:BCA:BH4$^-$-1:5:10) Purified Using Centrifugation Filters (a).Supernatant of 100 KDa (b).Supernatant of 30 KDa (c).Supernatant of 3 KDa……...45

2.4. Size Dependent Anodic Dissolution of Pd-BCA NPs Deposited on Glassy Carbon Electrode in 0.1M HClO4 Containing 10 mM NaCl at 1mV/s Under Nitrogen……...46

2.5. Experimentally Observed Oxidation Potential for Pd-BCA NPs as a Function of Particle Size (in Red) and Comparison with the Theoretical Values Predicted by the Plieth's Model (in Black)……47

Figure Page

2.6. TEM of Pd-BCA NPs Synthesized Under Different Conditions…….....48

2.7. TEM Images of Pd-BCA NPs Synthesized at Different Ratio of Sodium Borohydride…….....48

2.8. LSV Showing Anodic Dissolution Process of 30 KDa Sample…….....…49

2.9. LSV Showing Anodic Dissolution Process of 100 KDa Sample Obtained Under Different Coverage Conditions in 0.1 M $HClO_4$ Containing 10 mM NaCl at 1 mV/s……...….50

3.1. UPD of Cu on Pd in 0.5 M $NaClO_4$ + 10 mM $NaClO_4$ + 1 mM $Cu(ClO_4)_2$ (Black Line) and Control Experiment in 0.5 M $NaClO_4$ + 10 mM $HClO_4$ (Red Line) at 10 mV/s……71

3.2. Underpotential Deposition of Copper on Palladium at Different Negative Potential Limit in 0.5 M $NaClO_4$ + 10 mM $HClO_4$ + 1 mM $Cu(ClO_4)_2$ at 10 mV/sec……...72

3.3. Transmission Electron Miscroscopy (TEM) of BCA Capped Pd NPs Obtained After Purification. ……..……73

3.4. Size Dependent UPD Stripping of Cu From Pd NPs……..74

3.5. Theoretical (Black) and Experimental (Red) UPD Shifts for Size Dependent Cu UPD on Pd NPs…….75

3.6. Effect of Chloride Ions on Cu UPD on 50 KDa Pd NPs……76

3.7. TEM of Pd-BCA NPs Used as a Bulk Sample for Size Dependent Study…….……77

Figure Page

3.8. UPD of Cu on Pd NPs (Average Size: 98 + 38 nm) in 0.5 M $NaClO_4$ + 10 mM $HClO_4$ + 1 mM $Cu(ClO_4)_2$. (A). Before Removal of BCA Ligands by Electrochemical Cycling in the Oxide Region (Black Line). (B). After Removal of BCA Ligands by Electrochemical Cycling in the Oxide Region Scan Rate: 10 mV/sec…….78

3.9. EDX of BCA Capped Pd NPs Supported on Glassy Carbon Electrode (A). Before Electrochemical Cycling in Oxide Region (B). After Electrochemical Cycling in the Oxide Region……....79

4.1. CV of Palladium Electrode (a). 1 M NaOH (b). 1 M NaOH + 1 M EtOH Scan Rate: 100 mV/sec…….....99

4.2. LSV Showing Influence of [Cl^-] on Ethanol Oxidation on Palladium……100

4.3. LSV Showing Influence of [Br^-] on Ethanol Oxidation on Palladium……101

4.4. LSV Showing Influence of [I^-] on Ethanol Oxidation on Palladium……....102

4.5. Plot of the Relative Decrease in Anodic Peak Current for Ethanol Oxidation vs. Log[X^-] for Each of the Halides……..…103

LIST OF SCHEMES

Scheme Page

2.1. Synthesis Scheme of BCA Capped Pd NPs……41

LIST OF ABBREVIATIONS

Pd	palladium
CO	carbon monoxide
NO	nitric oxide
N_2	nitrogen
H_2O	hydrogen
PEMFCs	proton exchange membrane fuel cells
ORR	Oxygen Reduction Reaction
PVP	Poly (N-vinyl 2-pyrrolidone)
PVA	Poly (vinyl) alcohol
S	sulfur
C_s	saturation concentration
ΔG	total free energy
γ	surface energy
ΔG_v	free energy of the bulk crystal
ΔG_s	surface free energy
T	temperature
r	radius
S	supersaturation of the solution
V_m	molar volume
k_B	Boltzmann's constant
$r_{critical}$	critical radius
$\Delta G_{critical}$	critical free energy
dN/dt	rate of nucleation

A	pre-exponential factor
LSW	Lifshitz-Slyozov-Wagner
NPs	nanoparticles
fcc	face centered cubic
TEM	transmission electron microscope
nm	nanometer
Ag	silver
O_2	oxygen
Cl^-	chloride ion
Fe^{3+}	iron (III)
M_b	bulk metal
M_d	metal in dispersed form
M^{z+}	metal ion with charge z+
e^-	electronc charge
ΔG_d	free energy change associated with the conversion of one mole of bulk metal to its dispersed form
G_d	free energy of metal in dispersed state
G_b	free energy of metal in bulk state
ΔE	potential difference
z	number of electrons
F	Faraday's constant
dG	change in free energy
dA	change in surface energy
V_m	molar volume
STM	scanning tunneling microscope

ITO	indium tin oxide
H_2SO_4	sulfuric acid
LSV	linear sweep voltammetry
V	Volt(s)
mV	milliVolt(s)
Pt	platinum metal
Pt^{2+}	platinum (II) cation
BCA	2,2’-bicinchoninic acid
$HClO_4$	perchloric acid
NaCl	sodium chloride
Au	gold
ATP	adenosine triphosphate
P-XRD	powder X-ray diffraction
GCE	glassy carbon electrode
$PdCl_2$	palladium (II) chloride
$NaBH_4$	sodium borohydride
K_2BCA	2,2’-bicinchoninic acid dipotassium salt
HCl	hydrochloric acid
H_2PdCl_4	dihydrogen tetrachloropalladate (II)
mL	millilitre
°C	degree Celsius
µM	micromolar
mM	millimolar
M	molar
AA	ascorbic acid

BH_4^-	borohydride anion
µm	micrometer
MWCO	molecular weight cut-off
KDa	kiloDalton
Å	Angstrom
Θ	theta
HRTEM	high resolution transmission electron microscopy
AgCl	silver chloride
mM	millimeter
$PdCl_4^{2-}$	tetra chloropalladate (II) anion
E_0	standard reduction potential
R	universal gas constant
m	meter
J	Joule
C	Coulomb
UPD	underpotential deposition
Cu	copper
$NaClO_4$	sodium perchlorate
$Cu(ClO_4)_2.6H_2O$	copper perchlorate hexahydrate
Cu^{2+}	copper (II) ion
E_{pzc}	potential of zero charge
Φ	work function
OH^-	hydroxide anion
EDX	energy-dispersive X-ray analysis

Br^-	bromide anion
I^-	iodide anion
DAFCs	direct alcohol fuel cells
EOR	ethanol oxidation reaction
MnO_2	manganese dioxide
^{14}C	carbon-14 radioisotope
O	oxygen atom
EtOH	ethanol
NaOH	sodium hydroxide
NaBr	sodium bromide
NaI	sodium iodide
CV	cyclic voltammetry
CH_3CO	ethoxy species

CHAPTER 1

INTRODUCTION

Palladium (Pd), named after the asteroid Pallas, is arguably the most versatile and ubiquitous metal in various applications like catalytic hydrogenation-dehydrogenation reactions, petroleum cracking, modern organic synthesis and electrocatalysis.[1–9] Palladium is a noble metal with high catalytic activity, and is used in several industrial processes. Palladium in various forms is used in aromatic carbon-carbon bond coupling reactions. These coupling reactions have been used in preparation of complex organic molecules such as pharmaceuticals.[5,10–13] Examples of common coupling reactions of this kind such as Heck, Suzuki, Sonogashira and Stille coupling are shown in figure 1.1.

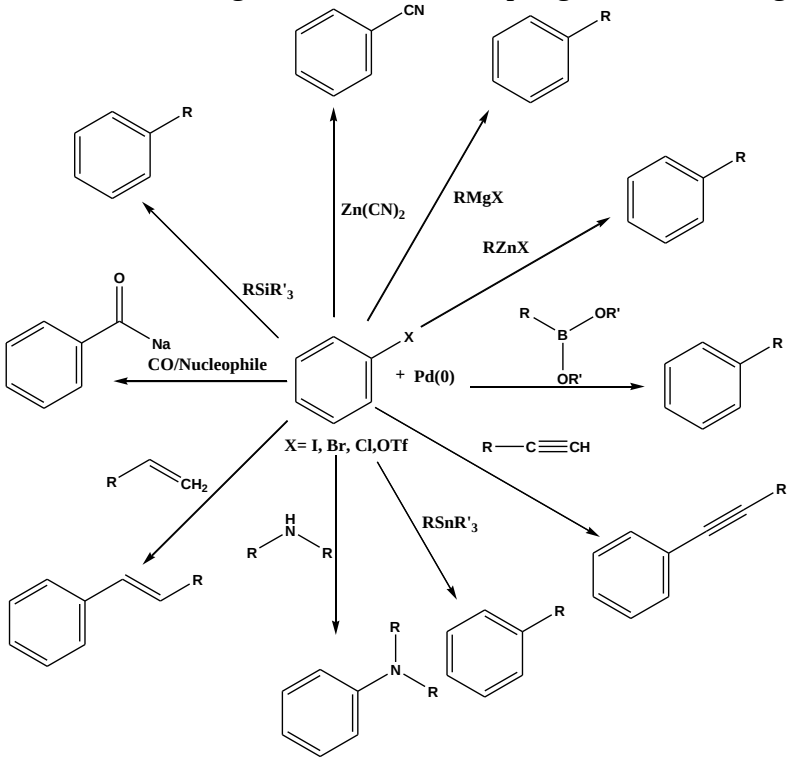

Figure 1.1. Various Carbon-Carbon Bond Coupling Reactions Catalyzed by Pd.

The ability of palladium to absorb significant amounts of hydrogen at room temperature makes it an ideal candidate for efficient and safe storage of hydrogen gas.[14,15] Palladium metal is largely used in catalytic convertors, where it converts harmful gases like hydrocarbons, CO and NO from auto exhaust into less harmful compounds like CO_2, N_2 and H_2O.[10,16]

In proton exchange membrane fuel cells (PEMFCs), platinum is the best catalyst for anode and cathode reactions. The anodic reaction involves oxidation of hydrogen, whereas at the cathode reduction of oxygen occurs. For platinum, kinetics of hydrogen oxidation are fast, and the kinetic overpotential is negligible. However, the oxygen reduction reaction occurs at larger overpotential. Because of this, the final performance of the fuel cell is controlled by the oxygen reduction reaction.[17–22] Again, cheaper alternatives are available as the catalyst for the anodic reaction.[23–27] For the cathode reaction, platinum is the best among all metals.[20] As compared to platinum, palladium is more abundant in the earth's crust and less expensive.[28] As we can see from the volcano plot in figure 1.2, palladium is the next best catalyst for the oxygen reduction reaction (ORR) in acidic media, after platinum metal.[20] However, experimental evidence confirms that the catalytic activity of palladium towards ORR is comparable to platinum, in alkaline media. Hence, palladium provides a cheaper alternative to platinum for the reactions at anode as well as cathode in alkaline fuel cells.[25,28–30]

Using metal catalysts in their bulk state is quite expensive and tends to be one of the many reasons behind failure of large scale commercialization of many technologies

like fuel cells. This issue can be resolved by using these metals in nanoparticle form, thereby requiring small amounts of precious metal to attain the desired current density.

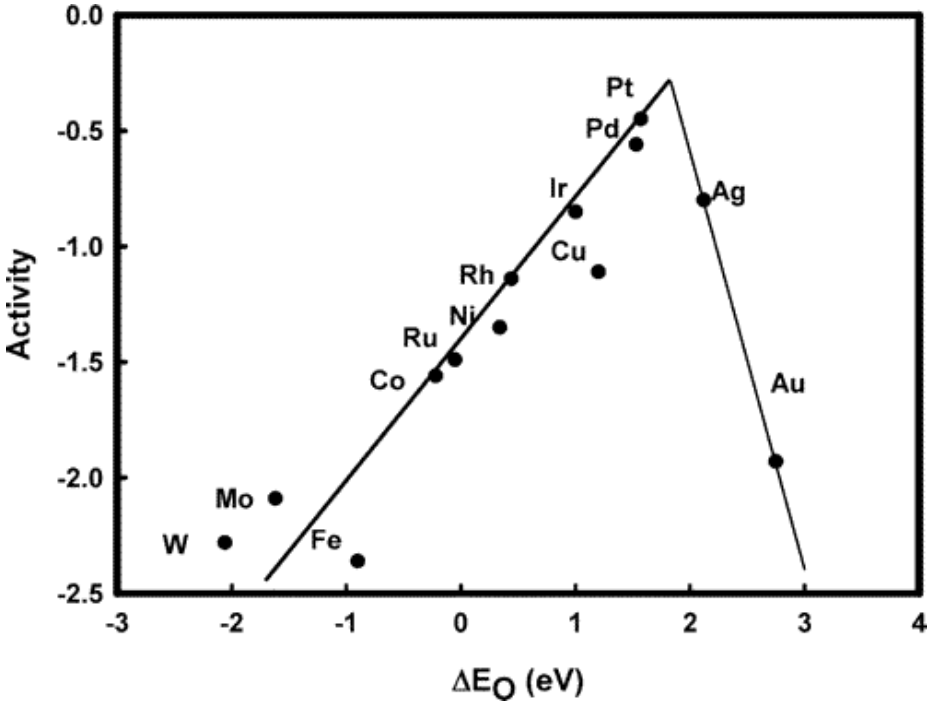

Figure 1.2. Oxygen Reduction Reaction Activity of Various Metals vs. O and OH Binding Energy. With Permission from Reference 20.

Thermodynamically, nanoparticles are unstable and tend to agglomerate to generate bulk metal. They can be obtained via chemical reduction of metal ion precursors by arresting their growth at the nanoparticle stage using capping ligands (kinetic stabilization). The stabilization provided by these capping ligands can be electrostatic or steric in nature or a combination of both. The extent of stabilization provided by these capping ligands depends on the extent of interaction between the capping ligands and the metal surface. The interaction between the ligand and the metal surface can be covalent, chemisorptive or electrostatic in nature.[31]

In the case of palladium, the capping ligand is generally an organic molecule containing a heteroatom with an available lone pair of electrons. Commonly used ligands to prepare palladium nanoparticles are based on sulphur, nitrogen and phosphorus.[18,32–36] Also, dendrimers and polymers like poly(N-vinyl 2-pyrrolidone) (PVP) and poly(vinyl alcohol) (PVA) are used to stabilize palladium nanoparticles by providing steric stabilization.[37–41] Surfactants like tetra-n-octylammonium bromide, which stabilize nanoparticles by steric as well as electrostatic means, have also been used to prepared palladium nanoparticles.[42] We will describe the use of a novel bidentate ligand for capping of water soluble Pd nanoparticles in chapter 2.

1.1. Theory of Nucleation and Growth of Nanoparticles: LaMer Mechanism

In 1950, LaMer and Dinegar proposed a theory to explain nanoparticle formation using nucleation and growth steps.[43] This theory involves conceptual separation of nucleation and growth into two steps. LaMer studied the formation of sulfur sols from the decomposition of sodium thiosulfate and proposed that the formation of sulfur sols consists of two steps: formation of free sulfur (S^0) from the thiosulfate in the first step and formation of sulfur sols in the second.

According to the model, zero-valence sulfur (S^0) should be continuously provided to maintain growth of sulfur sols. As a result, an appropriate chemical reaction is first chosen to maintain the continuous supply of S^0 in the solution. As long as more S^0 are produced, the solution is saturated with S^0 quickly. Even after attaining a saturation concentration (C_s), condensation of S^0 to solid nuclei is non-spontaneous because of the

energy consuming nature of formation of new solid phase in the homogeneous liquid environment. Hence, only after reaching a critical concentration, can the S^0 condense to form nuclei. After formation of stable nuclei, further growth takes place at lower concentration of S^0 that is slightly above C_s as this process is less energy consuming.[43,44]

Total free energy (ΔG) of a spherical nanoparticle of radius 'r' can be defined as the sum of the surface free energy and the bulk free energy:

$$\Delta G = 4\pi r^2\gamma + 4/3\pi r^3\Delta G_v$$

where, γ is surface energy, ΔG_v is the free energy of the bulk crystal and surface free energy $\Delta G_s = 4\pi r^2\gamma$. Crystal free energy ΔG_v depends on temperature T, Boltzmann's constant k_B, the supersaturation of the solution S, and its molar volume V_m.

$$\Delta G_v = -k_B T \, In(S)/V_m$$

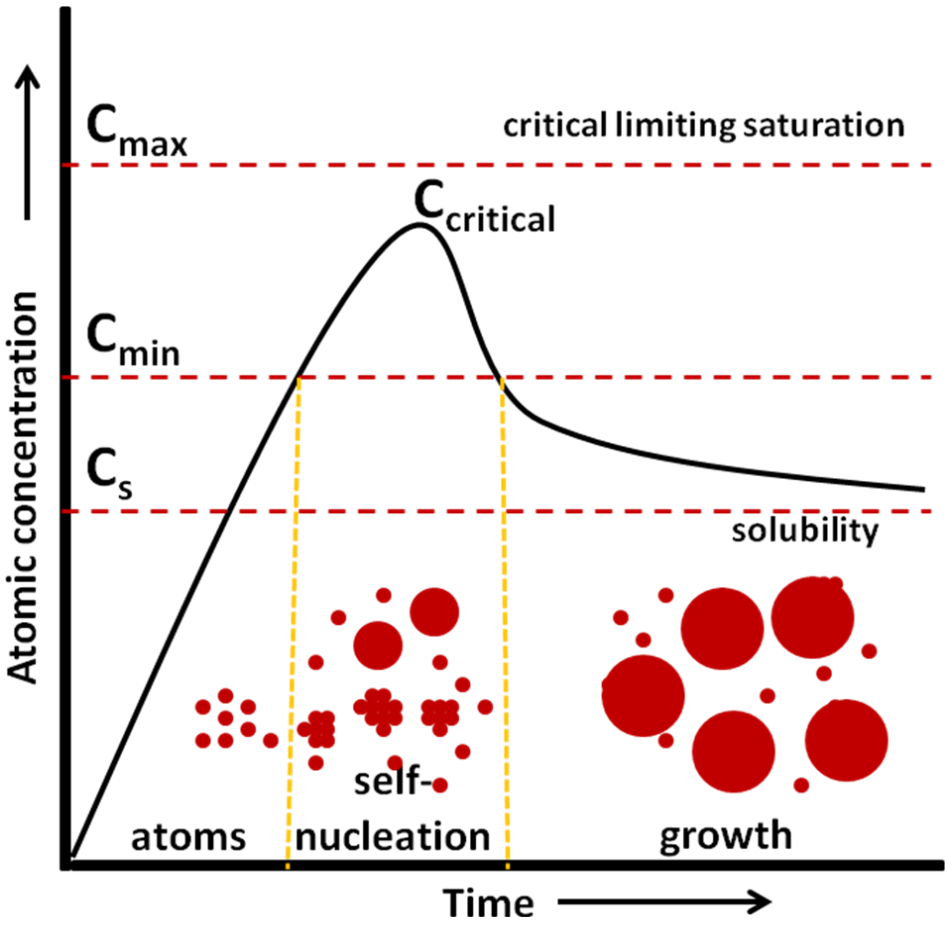

Figure 1.3. LaMer Growth Model. Adapted with permission from Reference 43.

Evolution of nuclei depends on the competition between a decrease in ΔG_v, which favors condensation of solvated atoms into nuclei and an increase in ΔG_s, destabilizing the nuclei towards solvation. When the nuclei are too small, the ΔG_s term is positive in nature dominates, leading the small nuclei to be dissolved. As nuclei grow, the total free energy reaches a maximum at a critical size with radius ($r_{critical}$) and then turns over and continuously decreases to favor the stabilization and growth of the nuclei. Since the surface free energy term is always positive and crystal free energy term ΔG_v is always

negative as solid state crystals are more stable than the solvated precursors, it is possible to find the critical radius of nanoparticles by differentiating ΔG with respect to r and setting dΔG/dr=0.

$$r_{critical} = -2\gamma/\Delta G_v = 2\gamma V_m/k_B T \ln(S)$$

The critical radius can be defined as the minimum size at which a particle can exist in solution without being re-dissolved. Also, the critical free energy ($\Delta G_{critical}$) which can be described as the minimum energy that is required to obtain stable particles can be given by:

$$\Delta G_{critical} = 4\pi\gamma r_{critical}^2$$

Rate of nucleation can be given by:

$$dN/dt = A \exp(-\Delta G_{critical}/k_B T)$$

$$dN/dt = A \exp\{16\pi\gamma^3 v^2/3k_B^3 T^3 (\text{In } S)^2\}$$

where, N is number of nuclei and A is pre-exponential factor. As evident from the equation, supersaturation, surface energy and the temperature are three experimental parameters that can be varied to control the nucleation rate.[44,45]

It is also worth mentioning that findings of recent studies using advanced in situ techniques have revealed the complex and multistep nature of the nucleation process which is not reflected in the classical nucleation theory. Models like Lifshitz-Slyozov-Wagner (LSW) and the two step Finke-Watzky mechanism have been proposed to describe the nucleation process.[45–47]

Information discussed above can be used to explain nanoparticle size control by considering the factors changed during the nanoparticle synthesis and how those factors control the nucleation and growth steps. However, to understand shape evolution of nanoparticles we need to consider the mechanism of shape evolution of nanocrystals separately.

1.2. Size Dependent Redox Properties of Metal NPs: A Thermodynamic Model

Metal nanoparticles can show properties that are entirely different from the bulk metal. In the case of gold, catalytically inactive bulk gold when used in nanoparticle form becomes catalytically active towards the oxidation of carbon monoxide.[48, 49] This early report by Haruta generated a huge amount of interest in the catalytic properties of nanoparticles. Also, many other properties of nanoparticles can be tuned by changing the size of the nanoparticle. Using metal in nanoparticle form can allow many technologies to be commercialized by substantially decreasing the cost associated with the usage of metal. At the same time it also raises a few questions. Is the activity of nanoparticles higher or lower than the bulk metal? What is the optimum size to attain the maximum performance? Experimental evidence described above suggests that nanoparticles can be better catalysts compared to bulk, as seen in the case of gold. However, in most cases the activity of metal nanoparticles is inferior to the bulk counterpart. In the case of platinum, the specific activity (i.e. catalytic activity per exposed surface atom) of bulk metal for the oxygen reduction reaction in acidic media was higher than the nanoparticles. Specific activity decreased with decreasing particle size, which was attributed to change in the distribution of surface atoms at (111) and (100) crystal faces.[50]

Two of the most important questions that need to be asked are: How the stability of metal nanoparticles compares to the bulk metal? And how does the stability of nanoparticles change with the size? Depending upon the medium, metal nanoparticles can oxidize to form metal oxide or metal ions, which can lead to loss of catalytic activity or loss of precious metal catalyst by dissolution. An estimate or understanding of their stability can be helpful for selecting the proper nanoparticle size for the application.

In 1982, Plieth proposed a thermodynamic model which suggests that the redox potential of metal nanoparticles is different from the bulk metal. The extent of deviation depends on the nanoparticle size.[51] An equation showing the relation between redox potential of metal in its nanoparticle (dispersed) form and the bulk form was derived by considering two half cells, with the first half cell containing metal in its bulk state (M_b) and the second half cell containing the metal in its dispersed form (M_d). The cell reaction can be shown as:

$$M_b \rightarrow M^{z+}_{solv.} + ze- \qquad \text{Oxidation Half} \qquad (1)$$

$$M^{z+}_{solv.} + ze- \rightarrow M_d \qquad \text{Reduction Half} \qquad (2)$$

$$M_b \rightarrow M_d \qquad \text{Overall Reaction} \qquad (3)$$

The overall reaction is the conversion of one mole of bulk metal into its dispersed form. The free energy change associated with this process can be given as:

$$\Delta G_{dispersion} = G_d - G_b \qquad (4)$$

And, the voltage of a cell compromising two half reactions can be given as:

$$\Delta E = \varepsilon_d - \varepsilon_b = -\Delta G_D/zF \quad (5)$$

where, ΔE is the difference in the equilibrium oxidation potentials between the dispersed and the bulk form of the metal.

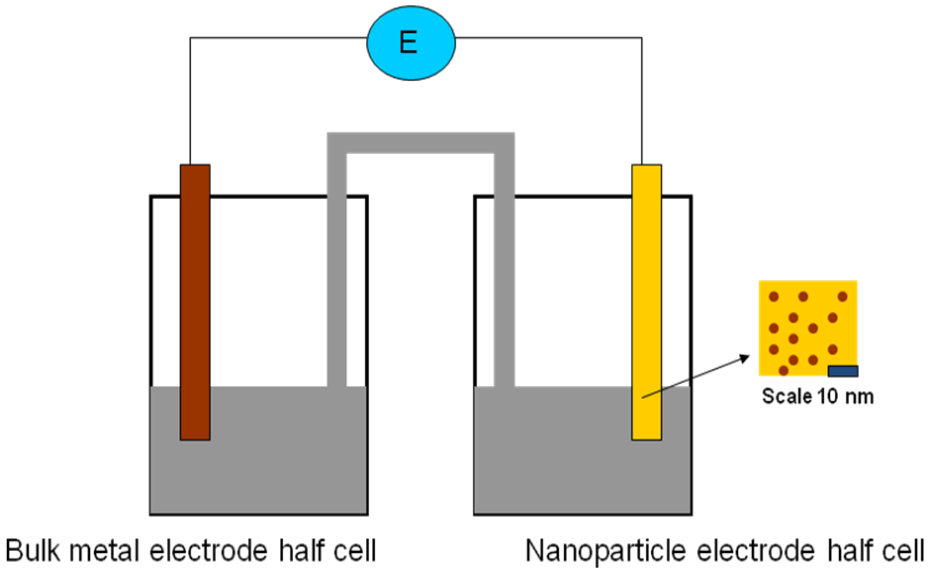

Figure 1.4. Derivation of Plieth's Theory Using Two Half Cells.

The change in free energy for the dispersion (ΔG_D) is related to the change in surface area and can be given as:

$$dG = \gamma dA \quad (6)$$

Where, γ is surface energy of the metal and dA is change in surface area.

Also,

$$dA = 8\pi r dr \quad (7)$$

$$dr = (V_m/4\pi r^2)dn \quad (8)$$

where, V_m is molar volume of the metal and *n* is the number of moles of metal converted into clusters. Integrating between *n* = 0 to *n* = 1 gives the free energy change when one mole of bulk metal is converted into its dispersed form.

$$\Delta G_D = 2\gamma V_m/r \quad (9)$$

The final equation for ΔE can be written as:

$$\Delta E = -2\gamma V_m/zFr \quad (10)$$

where, ΔE is difference in oxidation potential of dispersed metal with respect to the bulk metal, γ is the surface energy of the metal; V_m is the molar volume of the metal, z is the number of electrons, F is the Faraday's constant and r is the nanoparticle radius.

As is clear from the equation, it is expected for nanoparticles to show a negative cathodic shift in the oxidation potential as compared to the bulk metal. Also, depending upon the size of the metal nanoparticle, the extent of shift will vary. In terms of stability, nanoparticles are unstable towards oxidation as compared to their bulk counterpart, with the extent of destabilization depending on the size of the nanoparticles.

1.3. Size Dependent Electrochemical Oxidation of Metal Nanoparticles:

Electrochemical stability of metal nanoparticles has been studied by many groups. Kolb *et al.* studied electrochemical stability of nanofabricated copper clusters on a gold surface by using a tip of scanning tunneling microscope (STM). These nanofabricated copper clusters were reported to show high stability against anodic dissolution.[52] Penner *et al.* reported high stability of silver nanoclusters during anodic dissolution experiments,

which was tentatively attributed to a metal to non-metal transition and strong stabilization from an adsorbing anion layer.[53] Zamborini *et al.* reported size dependent electrochemical oxidation of citrate capped silver nanoparticles attached to an ITO electrode surface by electrostatic interaction. Electrochemical oxidation studies were done in 0.1M H_2SO_4 solution using linear sweep voltammetry (LSV) technique. A shift in oxidation potential of 275 to 385 mV was observed for silver nanoparticles (from size 8 nm to 50 nm) from bulk silver oxidation potential.[54] In another study, the same group reported size dependent oxidation of gold nanoparticles (4 nm to 250 nm on glass/indium-tin oxide electrodes) in the presence of bromide ions.[55] The experimental values of oxidation potential obtained from both these studies were in good agreement with Plieth's model.[55, 56] Recently, they also reported destabilization of gold nanoparticles by as much as 850 mV when the particles under study were less than 4 nm in size.[57] Sieradzki *et al.* studied oxidative dissolution of platinum nanoparticles in 0.1 M H_2SO_4 and were able to observe real time size dependent dissolution of platinum nanoparticles. They observed that particles less than 4 nm dissolve via a direct electrochemical dissolution pathway, $Pt \rightarrow Pt^{2+} + 2e^-$ whereas larger nanoparticles formed an oxide film before dissolution.[58, 59] Our group also reported size dependent anodic dissolution of water soluble palladium nanoparticles which will be discussed in more detail in chapter 2.

1.4. Size Dependent Catalytic Properties of Metal Nanoparticles

The driving force behind introduction of nanoparticles in catalysis was to achieve higher surface area, thus making the commercialization of technology more feasible by reducing the loading of precious metal. This was the rationale until Haruta *et al.* reported high

catalytic activity from gold nanoparticles (size less than 5 nm) towards a carbon monoxide oxidation reaction, for which bulk gold was catalytically inactive. Also, a size dependent catalytic behavior was observed for gold nanoparticle sizes below 5 nm.[49, 60] This finding acted as a catalyst for further exploration of size dependent behavior of metal nanoparticles in catalytic applications. The aim of these studies was to find a particle size that will give the highest specific or mass activity, providing information that can be used depending upon the need of the application. Kinoshita reported size dependent catalytic behavior of platinum nanoparticles for oxygen reduction reaction in acidic medium. The maximum mass activity for platinum nanoparticles was obtained at 3.5 nm, which was attributed to highest mass average distribution of catalytically active (100) and (111) crystal faces at 3.5 nm. However, the average distribution of the most catalytically active (100) crystal face for oxygen reduction reaction (ORR) decreased with the decrease in platinum particle size. Specific activity for ORR of nanoparticles was inferior as compared to the bulk platinum and showed a decrease in specific activity with decreasing particle size.[50] Size dependent electrochemical oxidation of formic acid, formaldehyde and methanol in acidic medium was studied using carbon supported platinum particles. Rate of methanol oxidation was found to be size dependent, with particles having diameter greater than 4 nm showing similar activity as compared to bulk polycrystalline platinum. For sizes less than 4 nm the rate of electrooxidation decreased with decrease in particle size. In the case of formic acid, the electrooxidation rate increased below 4 nm whereas electrooxidation of formaldehyde lacked appreciable difference.[61] El-Sayed *et al.* used PVP-capped palladium nanoparticles of sizes 3.0, 3.9,

5.2 and 6.6 nm to study size dependence of Suzuki reactions in aqueous medium. Highest catalytic activity was reported for PVP capped Pd NPs of 3.9 nm.[62] Solvent free aerobic oxidation (non electrochemical) of ethanol was studied using silica-alumina supported palladium nanoparticles with average sizes ranging from 2.2 nm to 10 nm. Particle size ranges from 3.6 nm to 4.3 nm expressed maximum catalytic activity.[63] Size dependent oxygen reduction reaction in alkaline medium was studied using carbon supported palladium catalysts prepared by high temperature reduction synthetic route using hydrazine as reducing agent. A 4 electron transfer pathway was found to be the dominant pathway and the maximum mass activity of palladium nanoparticles was observed at 5 nm.[64] There are numerous reports showing size dependent catalytic behavior of metal nanoparticles, and only few selected examples have been discussed.[65-68] In the next section we will discuss a few different examples of size dependent properties of metal nanoparticles.

1.5. Other Size Dependent Properties of Metal Nanoparticles

Apart from showing size dependent stability and catalytic properties, size dependent optical, electrochemical, physical and biological properties of metal nanoparticles have also been reported. Plasmonic properties and fluorescence of gold and silver nanoparticles, which are very important for their application in sensors, are also size dependent.[68-71] Melting points of many metal nanoparticles were also reported to show size dependent behavior.[72-80] For example, bulk gold melts around 1064°C, whereas a gold nanoparticle around 1.5 nm melts near 350°C.[75] In another study, it was found that hydriding and dehydriding kinetics of palladium nanoparticles is size dependent. This

study was performed with palladium nanoparticles in size ranges 1.8 to 5.4 nm, using gold nanoparticles as a nanoplasmonic sensor to sense hydrogen intake and desorption.[81] Metal nanoparticles have been seen as promising candidates for imaging, targeting and drug delivery inside biological systems.[82-85] Also, antimicrobial properties of metal nanoparticles show size dependent behavior with the smallest sized metal nanoparticles showing the highest antimicrobial activity as compared to the larger nanoparticles.[86-95] Recently, our group reported a size dependent study of underpotential deposition of copper on palladium nanoparticle which will be discussed in detail in chapter 3. Chapter 4 describes a follow-on study of halide adsorption at Pd electrodes that was motivated by the results of the UPD study.[96]

1.6. References:

(1) Guo, X. F.; Jang, D. Y.; Jang, H. G.; Kim, G. J. Hydrogenation and Dehydrogenation Reactions Catalyzed by CNTs Supported Palladium Catalysts. *Catal. Today* **2012**, *186*, 109–114.

(2) Xiu-Tian-Feng, E.; Zhang, Y.; Zou, J. J.; Wang, L.; Zhang, X. Oleylamine-Protected Metal (Pt, Pd) Nanoparticles for Pseudohomogeneous Catalytic Cracking of JP-10 Jet Fuel. *Ind. Eng. Chem. Res.* **2014**, *53*, 12312–12318.

(3) Wu, X. F.; Anbarasan, P.; Neumann, H.; Beller, M. From Noble Metal to Nobel Prize: Palladium-Catalyzed Coupling Reactions as Key Methods in Organic Synthesis. *Angew. Chemie - Int. Ed.* **2010**, *49*, 9047–9050.

(4) Miyaura, N.; Suzuki, A. Palladium-Catalyzed Cross-Coupling Reactions of Organoboron Compounds. *Chem. Rev.* **1995**, *95*, 2457–2483.

(5) Yin, L.; Liebscher, J. Carbon-Carbon Coupling Reactions Catalyzed by Heterogeneous Palladium Catalysts. *Chem. Rev.* **2007**, *107*, 133–173.

(6) Bianchini, C.; Shen, P. K. Palladium-Based Electrocatalysts for Alcohol Oxidation in Half Cells and in Direct Alcohol Fuel Cells. *Chem. Rev.* **2009**, *109*, 4183–4206.

(7) Therrien, J. A.; Wolf, M. O.; Patrick, B. O. Electrocatalytic Reduction of CO_2 with Palladium Bis-N-Heterocyclic Carbene Pincer Complexes. *Inorg. Chem.* **2014**, *53*, 12962–12972.

(8) Jiang, L.; Hsu, A.; Chu, D.; Chen, R. Size-Dependent Activity of Palladium Nanoparticles for Oxygen Electroreduction in Alkaline Solutions. *J. Electrochem. Soc.* **2009**, *156*, B643.

(9) Gao, D.; Zhou, H.; Wang, J.; Miao, S.; Yang, F.; Wang, G.; Wang, J.; Bao, X. Size-Dependent Electrocatalytic Reduction of CO_2 over Pd Nanoparticles. *J. Am. Chem. Soc.* **2015**, 150306114146006.

(10) Adams, K. M.; Gandhl, H. S. Palladium-Tungsten Catalysts for Automotive Exhaust Treatment. **1983**, 207–212.

(11) Gildner, P. G.; Colacot, T. J. Reactions of the 21st Century: Two Decades of Innovative Catalyst Design for Palladium-Catalyzed Cross-Couplings. *Organometallics* **2015**, *34*, 5497–5508.

(12) Gonzalo Rodríguez, J.; Lafuente, A. Effective Elimination of PCBs Catalyzed by the Palladium/hydrazine System as an Ecological Sustainable Process. *Ind. Eng. Chem. Res.* **2008**, *47*, 7993–7996.

(13) Shao, Y.; Cheng, Y.; Duan, W.; Wang, W.; Lin, Y.; Wang, Y.; Liu, J. Nanostructured Electrocatalysts for PEM Fuel Cells and Redox Flow Batteries: A Selected Review. *ACS Catal.* **2015**, *5*, 7288–7298.

(14) Yamauchi, M.; Ikeda, R.; Kitagawa, H.; Takata, M. Nanosize Effects on Hydrogen Storage in Palladium. *J. Phys. Chem. C* **2008**, *112*, 3294–3299.

(15) Wu, S.; Zhou, H.; Hao, M.; Wei, X.; Li, S.; Yu, H.; Wang, X.; Chen, Z. Fast Response Hydrogen Sensors Based on Anodic Aluminum Oxide with Pore-Widening Treatment. *Appl. Surf. Sci.* **2016**.

(16) Van Meel, K.; Smekens, A.; Behets, M.; Kazandjian, P.; Van Grieken, R. Determination of Platinum, Palladium, and Rhodium in Automotive Catalysts Using High-Energy Secondary Target X-Ray Fluorescence Spectrometry. *Anal. Chem.* **2007**, *79*, 6383–6389.

(17) Colón-Mercado, H. R.; Popov, B. N. Stability of Platinum Based Alloy Cathode Catalysts in PEM Fuel Cells. *J. Power Sources* **2006**, *155*, 253–263.

(18) Debe, M. K. Electrocatalyst Approaches and Challenges for Automotive Fuel Cells. *Nature* **2012**, *486*, 43–51.

(19) Lin, S. P.; Wang, K. W.; Liu, C. W.; Chen, H. S.; Wang, J. H. Trends of Oxygen Reduction Reaction on Platinum Alloys: A Computational and Experimental Study. *J. Phys. Chem. C* **2015**, *119*, 15224–15231.

(20) Nørskov, J. K.; Rossmeisl, J.; Logadottir, A.; Lindqvist, L.; Kitchin, J. R.; Bligaard, T.; Jónsson, H. Origin of the Overpotential for Oxygen Reduction at a Fuel-Cell Cathode. *J. Phys. Chem. B* **2004**, *108*, 17886–17892.

(21) Stephens, I. E. L.; Bondarenko, A. S.; Grønbjerg, U.; Rossmeisl, J.; Chorkendorff, I. Understanding the Electrocatalysis of Oxygen Reduction on Platinum and Its Alloys. *Energy Environ. Sci.* **2012**, *5*, 6744.

(22) Wu, J.; Yang, H. Platinum-Based Oxygen Reduction Electrocatalysts. *Acc. Chem. Res.* **2013**, *46*, 1848–1857.

(23) Jervis, R.; Mansor, N.; Gibbs, C.; Murray, C. a.; Tang, C. C.; Shearing, P. R.; Brett, D. J. L. Hydrogen Oxidation on PdIr/C Catalysts in Alkaline Media. *J. Electrochem. Soc.* **2014**, *161*, F458–F463.

(24) Schwartz, S. 00/02619 Long-Term Hydrogen Oxidation Catalysts in Alkaline Fuel Cells. *Fuel Energy Abstr.* **2000**, *41*, 292.

(25) Shao, M. Palladium-Based Electrocatalysts for Hydrogen Oxidation and Oxygen Reduction Reactions. *J. Power Sources* **2011**, *196*, 2433–2444.

(26) Sheng, W.; Bivens, A. P.; Myint, M.; Zhuang, Z.; Forest, R. V.; Fang, Q.; Chen, J. G.; Yan, Y. Non-Precious Metal Electrocatalysts with High Activity for Hydrogen Oxidation Reaction in Alkaline Electrolytes. *Energy Environ. Sci.* **2014**, *7*, 1719.

(27) St. John, S.; Atkinson, R. W.; Unocic, R. R.; Zawodzinski, T. A.; Papandrew, A. B. Ruthenium-Alloy Electrocatalysts with Tunable Hydrogen Oxidation Kinetics in Alkaline Electrolyte. *J. Phys. Chem. C* **2015**, *119*, 13481–13487.

(28) Antolini, E. Palladium in Fuel Cell Catalysis. *Energy Environ. Sci.* **2009**, *2*, 915.

(29) Koenigsmann, C.; Sutter, E.; Chiesa, T. A.; Adzic, R. R.; Wong, S. S. Highly Enhanced Electrocatalytic Oxygen Reduction Performance Observed in Bimetallic Palladium-Based Nanowires Prepared under Ambient, Surfactantless Conditions. *Nano Lett.* **2012**, *12*, 2013–2020.

(30) Antolini, E.; Zignani, S. C.; Santos, S. F.; Gonzalez, E. R. Palladium-Based Electrodes: A Way to Reduce Platinum Content in Polymer Electrolyte Membrane Fuel Cells. *Electrochim. Acta* **2011**, *56*, 2299–2305.

(31) Cookson, J. The Preparation of Palladium Nanoparticles. *Platin. Met. Rev.* **2012**, *56*, 83–98.

(32) Kim, S. W.; Park, J.; Jang, Y.; Chung, Y.; Hwang, S.; Hyeon, T.; Kim, Y. W. Synthesis of Monodisperse Palladium Nanoparticles. *Nano Lett.* **2003**, *3*, 1289–1291.

(33) Chen, S.; Huang, K.; Stearns, J. A. Alkanethiolate-Protected Palladium Nanoparticles. *Chem. Mater.* **2000**, *12*, 540–547.

(34) Son, S. U.; Jang, Y.; Yoon, K. Y.; Kang, E.; Hyeon, T. Facile Synthesis of Various Palladium Nanoparticles through the Understanding of Coordination Chemistry of the Nanoparticles. *Nano Lett.* **2004**, *4*, 1147–1151.

(35) Li, Z.; Gao, J.; Xing, X.; Wu, S.; Shuang, S.; Dong, C.; Paau, M. C.; Choi, M. M. F. Synthesis and Characterization of N -Alkylamine-Stabilized Palladium Nanoparticles for Electrochemical Oxidation of Methane. *J. Phys. Chem. C* **2010**, *114*, 723–733.

(36) Tamura, M.; Fujihara, H. Chiral Bisphosphine BINAP-Stabilized Gold and Palladium Nanoparticles with Small Size and Their Palladium Nanoparticle-Catalyzed Asymmetric Reaction. *J. Am. Chem. Soc.* **2003**, *125*, 15742–15743.

(37) Calo, V.; Nacci, A.; Monopoli, A.; Montingelli, F.; Suzuki, P. Pd Nanoparticles as Efficient Catalysts for Suzuki and Stille Coupling Reactions of Aryl Halides in Ionic Liquids Vincenzo Calo. **2005**, 6040–6044.

(38) Stevens, P. D.; Li, G.; Fan, J.; Yen, M.; Gao, Y. Recycling of Homogeneous Pd Catalysts Using Superparamagnetic Nanoparticles as Novel Soluble Supports for Suzuki, Heck, and Sonogashira Cross-Coupling Reactions. *Chem. Commun. (Camb).* **2005**, 4435–4437.

(39) Andrés, R.; de Jesús, E.; Flores, J. C. Catalysts Based on Palladium Dendrimers. *New J. Chem.* **2007**, *31*, 1161.

(40) Yeung, L. K.; Crooks, R. M. Heck Heterocoupling within a Dendritic Nanoreactor. *Nano Lett.* **2001**, *1*, 14–17.

(41) Toshima, N.; Yonezawa, T. Bimetallic Nanoparticles—novel Materials for Chemical and Physical Applications. *New J. Chem.* **1998**, *22*, 1179–1201.

(42) Bönnemann, H.; Brinkmann, R.; Köppler, R.; Neiteler, P.; Richter, J. A General Approach to NR4⊖-Stabilized Metal Colloids in Organic Phases. *Adv. Mater.* **1992**, *4*, 804–806.

(43) LaMer, V. K.; Dinegar, R. H. Theory, Production and Mechanism of Formation of Monodispersed Hydrosols. *J. Am. Chem. Soc.* **1950**, *72*, 4847–4854.

(44) Thanh, N. T. K.; Maclean, N.; Mahiddine, S. Mechanisms of Nucleation and Growth of Nanoparticles in Solution. *Chem. Rev.* **2014**, *114*, 7610–7630.

(45) Kwon, S. G.; Hyeon, T. Formation Mechanisms of Uniform Nanocrystals via Hot-Injection and Heat-up Methods. *Small* **2011**, *7*, 2685–2702.

(46) Watzky, M. A.; Finke, R. G. Nanocluster Size-Control and "Magic Number" Investigations. Experimental Tests of the "Living-Metal Polymer" Concept and of Mechanism-Based Size-Control Predictions Leading to the Syntheses of Iridium(0) Nanoclusters Centering about Four Sequential Magic . *Chem. Mater.* **1997**, *9*, 3083–3095.

(47) Sugimoto, T. General Kinetics of Ostwald Ripening of Precipitates. *J. Colloid Interface Sci.* **1978**, *63*, 16–26.

(48) Haruta, M.; Kageyama, H.; Kamijo, N.; Kobayashi, T.; Delannay, F. *Successful Design of Catalysts Future Requirements and Development, Proceedings Ofthe Worldwide Catalysis Seminars, July, 1988, on the Occasion of the 30th Anniversary of the Catalysis Society of Japan*; Studies in Surface Science and Catalysis; Elsevier, 1989; Vol. 44.

(49) Choudhary, T. V.; Goodman, D. W. Oxidation Catalysis by Supported Gold Nano-Clusters. *Top. Catal.* **2002**, *21*, 25–34.

(50) Kinoshita, K. Particle Size Effects for Oxygen Reduction on Highly Dispersed Platinum in Acid Electrolytes. *J. Electrochem. Soc.* **1990**, *137*, 845.

(51) Plieth, W. J. Electrochemical Properties of Small Clusters of Metal Atoms and Their Role in the Surface Enhanced Raman Scattering. *J. Phys. Chem.* **1982**, *86*, 3166–3170.

(52) Kolb, D.; Engelmann, G.; Ziegler, J. On the Unusual Electrochemical Stability of Nanofabricated Copper Clusters This Work Was Supported by the Deutsche Forschungsgemeinschaft through Grant No. Ko 576/10-2. One of Us (G.E.E.) Gratefully Acknowledges Receipt of a Stipend from the Fonds Der Che. *Angew. Chem. Int. Ed. Engl.* **2000**, *39*, 1123–1125.

(53) Ng, K. H.; Liu, H.; Penner, R. M. Subnanometer Silver Clusters Exhibiting Unexpected Electrochemical Metastability on Graphite. *Langmuir* **2000**, *16*, 4016–4023.

(54) Ivanova, O. S.; Zamborini, F. P. Size-Dependent Electrochemical Oxidation of Silver Nanoparticles. *J. Am. Chem. Soc.* **2010**, *132*, 70–72.

(55) Ivanova, O. S.; Zamborini, F. P. Electrochemical Size Discrimination of Gold Nanoparticles Attached to Glass/indium-Tin-Oxide Electrodes by Oxidation in Bromide-Containing Electrolyte. *Anal. Chem.* **2010**, *82*, 5844–5850.

(56) Ivanova, O. S.; Zamborini, F. P. Electrochemical Size Discrimination of Gold Nanoparticles Attached to Glass/indium-Tin-Oxide Electrodes by Oxidation in Bromide-Containing Electrolyte. *Anal. Chem.* **2010**, *82*, 5844–5850.

(57) Masitas, R. A.; Zamborini, F. P. Oxidation of Highly Unstable <4 Nm Diameter Gold Nanoparticles 850 mV Negative of the Bulk Oxidation Potential. *J. Am. Chem. Soc.* **2012**, *134*, 5014–5017.

(58) Tang, L.; Li, X.; Cammarata, R. C.; Friesen, C.; Sieradzki, K. Electrochemical Stability of Elemental Metal Nanoparticles. *J. Am. Chem. Soc.* **2010**, *132*, 11722–11726.

(59) Tang, L.; Han, B.; Persson, K.; Friesen, C.; He, T.; Sieradzki, K.; Ceder, G. Electrochemical Stability of Nanometer-Scale Pt Particles in Acidic Environments. *J. Am. Chem. Soc.* **2010**, *132*, 596–600.

(60) Haruta, M.; Kobayashi, T.; Sano, H.; Yamada, N. Novel Gold Catalysts for the Oxidation of Carbon Monoxide at a Temperature Far below 0.DEG.C. *Chem. Lett.* **1987**, 405–408.

(61) Park, S.; Xie, Y.; Weaver, M. J. Electrocatalytic Pathways on Carbon-Supported Platinum Nanoparticles: Comparison of Particle-Size-Dependent Rates of Methanol, Formic Acid, and Formaldehyde Electrooxidation. *Langmuir* **2002**, *18*, 5792–5798.

(62) Li, Y.; Boone, E.; El-Sayed, M. A. Size Effects of PVP−Pd Nanoparticles on the Catalytic Suzuki Reactions in Aqueous Solution. *Langmuir* **2002**, *18*, 4921–4925.

(63) Chen, J.; Zhang, Q.; Wang, Y.; Wan, H. Size-Dependent Catalytic Activity of Supported Palladium Nanoparticles for Aerobic Oxidation of Alcohols. *Adv. Synth. Catal.* **2008**, *350*, 453–464.

(64) Jiang, L.; Hsu, A.; Chu, D.; Chen, R. Size-Dependent Activity of Palladium Nanoparticles for Oxygen Electroreduction in Alkaline Solutions. *J. Electrochem. Soc.* **2009**, *156*, B643.

(65) Fenger, R.; Fertitta, E.; Kirmse, H.; Thünemann, A. F.; Rademann, K. Size Dependent Catalysis with CTAB-Stabilized Gold Nanoparticles. *Phys. Chem. Chem. Phys.* **2012**, *14*, 9343–9349.

(66) Gao, D.; Zhou, H.; Wang, J.; Miao, S.; Yang, F.; Wang, G.; Wang, J.; Bao, X. Size-Dependent Electrocatalytic Reduction of CO_2 over Pd Nanoparticles. *J. Am. Chem. Soc.* **2015**, *137*, 4288–4291.

(67) Wang, H.; Wang, Y.; Zhu, Z.; Sapi, A.; An, K.; Kennedy, G.; Michalak, W. D.; Somorjai, G. A. Influence of Size-Induced Oxidation State of Platinum Nanoparticles on Selectivity and Activity in Catalytic Methanol Oxidation in the Gas Phase. *Nano Lett.* **2013**, *13*, 2976–2979.

(68) Yahia-Ammar, A.; Sierra, D.; Mérola, F.; Hildebrandt, N.; Le Guével, X. Self-Assembled Gold Nanoclusters for Bright Fluorescence Imaging and Enhanced Drug Delivery. *ACS Nano* **2016**, *10*, 2591–2599.

(69) Li, Z.-Y.; Wu, Y.-T.; Tseng, W.-L. UV-Light-Induced Improvement of Fluorescence Quantum Yield of DNA-Templated Gold Nanoclusters: Application to Ratiometric Fluorescent Sensing of Nucleic Acids. *ACS Appl. Mater. Interfaces* **2015**, *7*, 23708–23716.

(70) Yuan, X.; Luo, Z.; Zhang, Q.; Zhang, X.; Zheng, Y.; Lee, J. Y.; Xie, J. Synthesis of Highly Fluorescent Metal (Ag, Au, Pt, and Cu) Nanoclusters by Electrostatically Induced Reversible Phase Transfer. *ACS Nano* **2011**, *5*, 8800–8808.

(71) Le Guével, X.; Hötzer, B.; Jung, G.; Hollemeyer, K.; Trouillet, V.; Schneider, M. Formation of Fluorescent Metal (Au, Ag) Nanoclusters Capped in Bovine Serum Albumin Followed by Fluorescence and Spectroscopy. *J. Phys. Chem. C* **2011**, *115*, 10955–10963.

(72) Castro, T.; Reifenberger, R.; Choi, E.; Andres, R. P. Size-Dependent Melting Temperature of Individual Nanometer-Sized Metallic Clusters. *Phys. Rev. B* **1990**, *42*, 8548–8556.

(73) Allen, G. L.; Bayles, R. A.; Gile, W. W.; Jesser, W. A. Small Particle Melting of Pure Metals. *Thin Solid Films* **1986**, *144*, 297–308.

(74) Jiang, Q.; Zhang, S.; Zhao, M. Size-Dependent Melting Point of Noble Metals. *Mater. Chem. Phys.* **2003**, *82*, 225–227.

(75) Dick, K.; Dhanasekaran, T.; Zhang, Z.; Meisel, D. Size-Dependent Melting of Silica-Encapsulated Gold Nanoparticles. *J. Am. Chem. Soc.* **2002**, *124*, 2312–2317.

(76) Lai, S.; Guo, J.; Petrova, V.; Ramanath, G.; Allen, L. Size-Dependent Melting Properties of Small Tin Particles: Nanocalorimetric Measurements. *Phys. Rev. Lett.* **1996**, *77*, 99–102.

(77) Liu, M.; Wang, R. Y. Size-Dependent Melting Behavior of Colloidal In, Sn, and Bi Nanocrystals. *Sci. Rep.* **2015**, *5*, 16353.

(78) Qi, W. H.; Wang, M. P. Size and Shape Dependent Melting Temperature of Metallic Nanoparticles. *Mater. Chem. Phys.* **2004**, *88*, 280–284.

(79) Wronski, C. R. M. The Size Dependence of the Melting Point of Small Particles of Tin. *Br. J. Appl. Phys.* **1967**, *18*, 1731–1737.

(80) Guisbiers, G.; Abudukelimu, G.; Hourlier, D. Size-Dependent Catalytic and Melting Properties of Platinum-Palladium Nanoparticles. *Nanoscale Res. Lett.* **2011**, *6*, 396.

(81) Langhammer, C.; Zhdanov, V. P.; Zorić, I.; Kasemo, B. Size-Dependent Kinetics of Hydriding and Dehydriding of Pd Nanoparticles. *Phys. Rev. Lett.* **2010**, *104*, 135502.

(82) Liong, M.; Lu, J.; Kovochich, M.; Xia, T.; Ruehm, S. G.; Nel, A. E.; Tamanoi, F.; Zink, J. I. Multifunctional Inorganic Nanoparticles for Imaging, Targeting, and Drug Delivery. *ACS Nano* **2008**, *2*, 889–896.

(83) Pelgrift, R. Y.; Friedman, A. J. Nanotechnology as a Therapeutic Tool to Combat Microbial Resistance. *Adv. Drug Deliv. Rev.* **2013**, *65*, 1803–1815.

(84) Kim, J. S.; Kuk, E.; Yu, K. N.; Kim, J.-H.; Park, S. J.; Lee, H. J.; Kim, S. H.; Park, Y. K.; Park, Y. H.; Hwang, C.-Y.; *et al*. Antimicrobial Effects of Silver Nanoparticles. *Nanomedicine* **2007**, *3*, 95–101.

(85) Adeyemi, O. S.; Sulaiman, F. A. Evaluation of Metal Nanoparticles for Drug Delivery Systems. *J. Biomed. Res.* **2015**, *29*, 145–149.

(86) Dizaj, S. M.; Lotfipour, F.; Barzegar-Jalali, M.; Zarrintan, M. H.; Adibkia, K. Antimicrobial Activity of the Metals and Metal Oxide Nanoparticles. *Mater. Sci. Eng. C. Mater. Biol. Appl.* **2014**, *44*, 278–284.

(87) Badwaik, V. D.; Vangala, L. M.; Pender, D. S.; Willis, C. B.; Aguilar, Z. P.; Gonzalez, M. S.; Paripelly, R.; Dakshinamurthy, R. Size-Dependent Antimicrobial Properties of Sugar-Encapsulated Gold Nanoparticles Synthesized by a Green Method. *Nanoscale Res. Lett.* **2012**, *7*, 623.

(88) Adams, C. P.; Walker, K. A.; Obare, S. O.; Docherty, K. M. Size-Dependent Antimicrobial Effects of Novel Palladium Nanoparticles. *PLoS One* **2014**, *9*, e85981.

(89) Lu, Z.; Rong, K.; Li, J.; Yang, H.; Chen, R. Size-Dependent Antibacterial Activities of Silver Nanoparticles against Oral Anaerobic Pathogenic Bacteria. *J. Mater. Sci. Mater. Med.* **2013**, *24*, 1465–1471.

(90) Konopsky, V. N.; Basmanov, D. V.; Alieva, E. V.; Sekatskii, S. K.; Dietler, G. Size-Dependent Hydrogen Uptake Behavior of Pd Nanoparticles Revealed by Photonic Crystal Surface Waves. *Appl. Phys. Lett.* **2012**, *100*, 083108.

(91) Wang, S.-H.; Lee, C.-W.; Chiou, A.; Wei, P.-K. Size-Dependent Endocytosis of Gold Nanoparticles Studied by Three-Dimensional Mapping of Plasmonic Scattering Images. *J. Nanobiotechnology* **2010**, *8*, 33.

(92) Jiang, W.; Kim, B. Y. S.; Rutka, J. T.; Chan, W. C. W. Nanoparticle-Mediated Cellular Response Is Size-Dependent. *Nat. Nanotechnol.* **2008**, *3*, 145–150.

(93) Pan, Y.; Neuss, S.; Leifert, A.; Fischler, M.; Wen, F.; Simon, U.; Schmid, G.; Brandau, W.; Jahnen-Dechent, W. Size-Dependent Cytotoxicity of Gold Nanoparticles. *Small* **2007**, *3*, 1941–1949.

(94) Zhang, S.; Li, J.; Lykotrafitis, G.; Bao, G.; Suresh, S. Size-Dependent Endocytosis of Nanoparticles. *Adv. Mater.* **2009**, *21*, 419–424.

(95) Ivask, A.; Kurvet, I.; Kasemets, K.; Blinova, I.; Aruoja, V.; Suppi, S.; Vija, H.; Käkinen, A.; Titma, T.; Heinlaan, M.; *et al*. Size-Dependent Toxicity of Silver Nanoparticles to Bacteria, Yeast, Algae, Crustaceans and Mammalian Cells in Vitro. *PLoS One* **2014**, *9*, e102108.

(96) Kumar, A.; Buttry, D. A. Influence of Halide Ions on Anodic Oxidation of Ethanol on Palladium. *Electrocatalysis*, **2016**, 1-6.

CHAPTER 2

Synthesis, Characterization and Size-Dependent Anodic Dissolution of Water Soluble Palladium Nanoparticles

Ashok Kumar and Daniel A. Buttry*

Department of Chemistry and Biochemistry, Arizona State University, Tempe, AZ, 85287-1604, USA

Reproduced by permission of American Chemical Society

Journal of Physical Chemistry, 2013, 117, 23334-23347

2.1. Abstract: 2,2'-bicinchoninic acid capped palladium nanoparticles (Pd-BCA NPs) were synthesized using a one pot chemical reduction route. Monodisperse Pd-BCA NPs of different size ranges were obtained using a purification technique employing low molecular weight cutoff centrifuge filters. Size dependent anodic dissolution of Pd-BCA NPs was studied in 0.1 M $HClO_4$ containing 10 mM NaCl. Experimental data were shown to be in excellent agreement with theoretical values calculated using the Plieth model. For Pd NPs with 1.0 nm diameter, the oxidation was shifted to less positive potentials by over a third of a volt, representing substantial destabilization of the NP due to its small size.

2.2. Introduction:

Metal NPs have been studied extensively because of their interesting optical, electronic, catalytic and magnetic properties as compared to bulk materials, making them an ideal candidate for a variety of applications.[1-6] A variety of studies have addressed the stability of NPs against aggregation, structural transformations, oxidation and dissolution.[7-11] An especially important issue is the stability of metal NPs toward anodic dissolution, given the broad range of electrocatalytic applications that have been investigated for metal NPs. Plieth used thermodynamics to theoretically predict the size dependence of the dissolution potential of metal NPs. According to that model, NP stability toward oxidation should decrease as NP size decreases, producing a negative shift in dissolution potential with decrease in size.[12] This results from the increasing contribution of surface energy to the overall NP stability as size decreases. Data consistent with Plieth's theory were demonstrated by Zamborini *et al.* with silver and gold nanoparticles.[13-15] Also, Tang *et al.* studied the dissolution of Pt NPs using scanning tunneling microscopy and showed smaller particles ($d < 4$ nm) dissolve at lower potential compared to the bulk metal redox potential.[16, 17] They used a more correct model involving the surface stress of both the metal and metal oxide interfaces for the Pt case. As expected, size dependent shifts in dissolution potential were not observed when Compton and coworkers studied much larger Ag NPs in the 25-100 nm diameter range.[18] These NPs behave as bulk metal, and would not be expected to show a size dependent oxidation potential influenced by surface stress. Two other groups have reported higher dissolution potential for metal nanoparticles as compared to the bulk metal; these results remain unexplained.[19, 20]

The Compton and Zamborini studies also confirmed theoretical work by Brainina *et al.* who studied the effect of surface coverage on the oxidation potential of nanoparticles.[21] They showed that at low scan rates and with relatively fast electron transfer kinetics, the peak potentials reflect true thermodynamic oxidation potentials. These conditions remove the influence of overlapping diffusion profiles for the dissolved metal ions produced from the dissolution process, and constitute the approach used here.

Increasing interest in Pd and its alloys for electrocatalytic and other applications has motivated us to develop a new synthetic approach for producing Pd NPs. The synthetic method is modeled after previously published methods for Au and Ag NPs capped with the nucleoside adenosine triphosphate.[22, 23] This method produces water soluble metal NPs that are isolable as solids, allowing storage and redissolution. The ATP capping ligand binds at the metal NP surface via its nitrogen functional groups. Reasoning by analogy to older work by Schmid and coworkers on production of Pd NPs (so-called "giant clusters") with phenanthroline capping ligands, a new synthesis of water soluble Pd NPs is reported here that uses bicinchoninic acid (BCA) as the capping ligand (Scheme 1).[24] These BCA-capped palladium nanoparticles (Pd-BCA NPs) are easily synthesized, storable as solids, water soluble, and provide an attractive platform for electrochemical and other investigations. We report here the synthesis, characterization and size dependent anodic dissolution behavior of these NPs. The general approach for the study involved synthesis followed by size fractionation using centrifuge filters typically employed for size-based protein purification. The different size fractions of Pd-BCA NPs were characterized using powder X-ray diffraction (P-XRD) and transmission

electron microscopy (TEM). Size dependent dissolution studies were performed with drop-cast Pd-BCA NPs trapped by Nafion on a glassy carbon electrode (GCE). The anodic dissolution results are seen to be in excellent agreement with predictions by the Plieth model.

2.3. Experimental Section:

Palladium (II) chloride ($PdCl_2$, 99%) and sodium borohydride ($NaBH_4$, 99.9%) were purchased from Sigma-Aldrich, and 2,2'-bicinchoninic acid dipotassium salt hydrate (K_2BCA, >98%) was purchased from TCI America. All reagents were used as obtained. Water of resistivity 18.3 MΩ (Millipore MQ Reference) was used to prepare all the solutions.

2.3.1. Synthesis of Water Soluble Palladium Nanoparticles: In the synthesis of water-soluble BCA-Pd NPs, the molar ratio Pd:BCA:BH_4^- has a strong influence on the size and stability of the NPs. For the present study, the Pd:BCA:BH_4^- molar ratio was mostly held constant at 1:5:10, though a few other sets of ratios were examined. In a typical 1:5:10 synthesis, 6.0 mL of 10 mM H_2PdCl_4 (produced by dissolution of $PdCl_2$ in dilute HCl) was stirred with 6.0 mL of 50 mM K_2BCA and 222.0 mL of water under nitrogen for 30 minutes. To this solution (pH ~8), 6.0 mL of freshly prepared 100 mM $NaBH_4$ (in nitrogen saturated water) was rapidly added while stirring. The solution with final Pd concentration of 250 μM, turned dark purple and then finally brown in color after the addition of $NaBH_4$ indicating the reduction of H_2PdCl_4 to Pd NPs capped by BCA. The solution was further stirred for 4 hours under nitrogen for complete growth of the nanoparticles. To obtain solid Pd-BCA NPs, the solution was reduced in volume to ~3 mL using a rotary evaporator at 37° C, and then the NPs were precipitated with ~ 1 mL of isopropanol. Solid nanoparticles were isolated by centrifugation for 15 minutes at 5000 rpm. The isolated nanoparticles were dried under nitrogen and re-dispersed in ~ 2 mL water after which they were re-precipitated using isopropanol. The process of

precipitation, centrifugation and drying under nitrogen was repeated three times to obtain pure BCA-Pd NPs free of excess BCA, which were then dried and stored.

A sample containing much larger Pd NPs, with mean diameter in the range 50 – 100 nm, was also prepared. This "bulk" sample was used to obtain the oxidation potential for a bulk Pd sample free of size effects, since there should be no influence of size in this range of diameters. These NPs were prepared by using a weak reducing agent (Ascorbic acid) instead of sodium borohydride.

2.3.3. Size Selection of Water Soluble Palladium Nanoparticles: Synthesis of Pd NPs with different sizes can be achieved by controlling either nucleation or growth of the nanoparticles through control of the BCA to Pd ratio (to control growth) and $NaBH_4$ to Pd ratio (to control nucleation). However, strict control of size is difficult, especially with regard to the population of outliers (small numbers of NPs well outside of the main population distribution). This is an important point, since even a small number of NPs significantly larger than the main population can substantially skew the electrochemical results because of their potentially much larger electrochemical charge for anodic dissolution. Thus, in the present case, rather than attempting to achieve monodispersity in the size of the NPs through control of the synthetic conditions, we chose to use a size-base separation approach employing centrifuge filters typically used for size-based protein purification (Amicon® Ultra-4 Centrifugal Filter Units-Millipore). Thus, for size selection the initially synthesized Pd-BCA NP solution (1Pd:5BCA:10BH_4^-) was concentrated to ~10 mL using rotatory evaporator. This solution was passed through a 0.1 µm syringe filter to remove any aggregated particles. The obtained solution was then

passed through a series of centrifuge filters of different MWCO (molecular weight cut-off) values, with intermediate separation of the filtrate (containing smaller NPs) from the supernatant (containing larger NPs). This allowed size-based separation of the NPs within certain range limits defined by the characteristics of the filters. For example, a typical separation started with centrifugation through a 100 KDa filter at 10,000 rpm for 5 minutes. The supernatant was collected and labeled as 100 KDa sample. The filtrate obtained was then passed through 30 KDa filter, and the supernatant was laballed as 30 KDa sample. Finally, the filtrate of the second centrifugation step was passed through a 3 KDa filter at 12,000 rpm for 15 minutes to obtain a 3 KDa sample. All filtered samples were further diluted using MQ water and stored at 4° C to avoid any agglomeration. The sizes and histograms of the BCA-Pd NPs obtained from this separation method were determined using TEM and will be shown below.

2.3.4. Characterization: X-ray diffraction of the solid BCA-Pd NPs was carried out on a Siemens D 5000 X-ray diffractometer using the Cu-K_α radiation of 1.541 Å wavelength for 2θ values ranging between 10° and 90° and a scan rate of 2.5° per minute. To prepare sample for powder X-ray diffraction, Pd-BCA NPs solutions of different sizes were dried on sample holders under nitrogen. Transmission electron microscopy measurements were carried out using a Phillips CM12 microscope and HRTEM measurements were done using a JEOL 2010F operated at 80 kV. TEM samples were prepared by drop coating 5.0 μL of a dilute sonicated solution of the BCA-Pd NPs onto a formvar coated 400 mesh copper grid (Ted Pella Inc.), which was then allowed to dry for 4 hours. Histograms were obtained by selecting an area and counting 100 particles from that area.

2.3.5. Electrochemical Measurements: All electrochemical measurements were carried out on a CHI760c potentiostat. Ag/AgCl saturated with 1 M NaCl was used as the reference electrode, while a spiral Pt wire was used as a counter electrode. Glassy carbon electrode (GCE), 3mm in diameter, was used as a working electrode after polishing consecutively on 1 μm, 0.3 μm and 0.05 μm Alumina powder for 5 minutes each and then sonicated for 10 minutes in MQ water (Millipore) followed by drying under nitrogen flow. Nitrogen was purged through all solutions before electrochemical measurements. For size dependent electrochemical studies a drop of a solution containing Pd-BCA NPs evaporated on a clean GCE and dried very slowly under nitrogen using an inverted beaker to attain uniform coverage. The NPs were the entrapped at the surface by casting a film of Nafion from a 1.0% solution. The Nafion solution was allowed to dry slowly. This method gave surface coverages that were reproducible to roughly 10-20%. Electrochemical dissolution studies were performed using linear sweep voltammetry in 0.1 M $HClO_4$ containing 0.01 M NaCl. Control experiments were done using a glassy carbon electrode coated with Nafion. No redox peaks were observed when Nafion coated glassy carbon electrodes without Pd-BCA NPs were used. The 50 nm diameter "bulk" Pd NP samples were used to calibrate the oxidation potential for bulk Pd under the specific conditions of the experiment (i.e. to account for reference electrode offsets, junction potentials, any influence from capping ligands, Nafion entrapment, etc.). See Figure S1 in supporting information for TEM images of this sample. Larger Pd particles were used in preference to a pure Pd electrode so that well-defined LSV peaks could be obtained for direct comparison to the LSV data for the BCA-Pd NPs. The dissolution experiments

were reproduced three times for the smallest NP sample with average size 1.0 ± 0.3 nm, whereas for other samples it was reproduced seven times to give adequate statistics.

2.4. Results and Discussion:

P-XRD scans of various Pd-BCA NPs are shown in Figure 2.1. The P-XRD of the "bulk" control sample shows peaks near 40°, 46°, 68°, 82° and 86° corresponding to the (111), (200), (220), (311) and (222) planes of the face-centered cubic (fcc) crystal structure of palladium.[25] As compared to this sample, the Pd-BCA NPs samples showed a broadening of peaks with decreasing size and a reduction in intensity of the higher 2Θ angles, as reported in the literature for other Pd NPs.[26] Prior to any size fractionation the Pd-BCA NPs showed peaks at 39.5°, 67.4° and 81.2° corresponding to the (111), (220) and (311) planes. The large fraction of small sized nanoparticles in this "as-synthesized" sample caused the peak at 39.5° to broaden and obscure the peak at 46° corresponding to the (200) plane. This peak reappeared in the diffraction scan of the 100 KDa sample which was obtained after separating smaller sized nanoparticles from synthesized Pd-BCA NPs using centrifuge filters. The peak broadening becomes more severe for the 30 KDa sample and the 3 KDa sample shows only a hint of a peak near 40^{o}. These results are consistent with a very significant reduction in the NP size as lower MWCO filters are used for size fractionation. Debye-Scherrer analysis also was used for size estimation from peak broadening; the estimated diameters are given in Table 2.1.

In addition to peak broadening, decreasing NP size also led to a shift in the peak position to smaller angle showing an increase in lattice parameter. The value for the d-spacing obtained from the (111) peak is 2.25 Å for the "bulk" sample and the 100 KDa sample and then appears to increase to 2.36 Å for the 30 KDa NPs (shown in Table 2.1

for all Pd-BCA NPs). A reliable d-value could not be obtained for the 3 KDa sample because of the breadth of the peak.

Previous reports have discussed changes in the lattice parameter with size for Pd NPs.[27-29] Theoretically, nanoparticles are expected to show lattice contraction with a decrease in size because of an increase in surface stress. This has been observed for a variety of different metal NPs, except palladium which sometimes shows lattice expansion for smaller NPs.[30-33] For the case of Pd, dilation of the lattice with decrease in size has been explained by structural changes induced by surface oxidation or incorporation of hydrogen, carbon or oxygen into the lattice.[34-36] In the present case, these effects should not influence the experimental determination of the oxidation potential since the NPs are held at negative potentials prior to the anodic scans used in the determination (see below), maintaining the Pd NPs in their metallic state.

TEM images of BCA-Pd NPs produced using a few different Pd:BCA:BH_4^- molar ratios are shown in Figure 2.2. At a lower BCA ratio (Pd:BCA:BH_4^- of 1:1:10) NPs of average diameter 2.1 ± 0.8 nm were obtained. There is also some evidence for aggregation for these NPs in the EM images, consistent with less efficient capping at the lower BCA ratio. In contrast, a higher BCA ratio (Pd:BCA:BH_4^- of 1:5:10) produced smaller particles of average diameter 1.4 ± 0.8 nm as expected. (See Figure 2.6 for TEM images showing larger views of the samples) At higher ratios of BH_4^-, smaller particles along with several aggregated particles were obtained (See Figure 2.7 for TEM). Thus, the trends in size and aggregation behavior follow the expected behavior for a nucleation and growth mechanism.[37]

For all of the sizes described, the accompanying size histograms show that the samples are fairly polydisperse. These experiments suggested that it would be challenging to obtain sufficiently monodisperse Pd-BCA NPs for size-dependent studies by varying synthetic conditions alone. Thus, size fractionation using a select range of MWCO centrifuge filters was used. Based on its smaller mean diameter and sample stability, a sample produced using the 1:5:10 molar ratio was used for the size fractionation process. As described in the experimental section, these NPs were separated into different size ranges by successively centrifuging through centrifuge filters of MWCO of 100 KDa, 30 KDa and 3 KDa. TEM images of Pd-BCA NPs obtained after size fractionation are shown in Figure 2.3. The 100 KDa, 30 KDa and 3 KDa Pd-BCA NPs had an average diameters of 3.2 ± 0.9 nm, 1.5 ± 0.3 nm and 1.0 ± 0.3 nm, respectively. The obtained fractions were reasonably monodisperse, as shown in the histograms. These samples were then used in anodic dissolution experiments to explore the size dependence of oxidation.

Linear sweep voltammograms (LSVs) of anodic dissolution of Pd-BCA NPs of different sizes entrapped on a glassy carbon surface are shown in Figure 2.4. Voltammetric scans were done from -0.2 V to 1.0 V in 0.1 M $HClO_4$ containing 10 mM NaCl at 1 mV/s. The low scan rate ensured the experimental conditions would provide thermodynamic oxidation potentials from the LSV peak potentials, as predicted by Brainina and validated in experiments by Compton and coworkers and Zamborini and coworkers.[13, 14, 15, 18, 21] To ensure the dissolution process was complete another LSV was recorded after the first dissolution scan using the same electrode in fresh electrolyte; no

peaks were observed during the second scan which confirms that all NPs dissolved completely during the first scan. (See Figure 2.8 for LSVs). Control experiments were also done at a variety of surface coverage values to verify that the oxidation potential obtained from the LSV peak potentials was invariant with coverage, a requirement of the conditions delineated by Brainina.[20] Figure 2.9 shows results of selected experiments. These results show a lack of coverage dependence in the low coverage range, with some evidence of coverage dependence at the highest coverages examined. Thus, only low coverage data were used in the samples statistically analyzed to obtain oxidation potentials as a function of size. The strong dependence on chloride concentration necessitated care in preparation of solutions with precisely reproduced [Cl^-]. Multiple scans were done on each sample to obtain statistically relevant values (Shown in Table 2.1).

The data in Figure 4 clearly show dissolution peaks for Pd oxidation to $PdCl_4^{2-}$ that are strongly size dependent. These are similar to the data previously reported for Ag and Au NPs.[13, 14, 15] For the "bulk" sample, the oxidation peak appears at +0.70 V (black curve), consistent with expectations for bulk-like behavior. This value was used in calculations of the effect of size on the potential shift away from the bulk value (see below). The lowest oxidation potential is observed at +0.34 V for the 1.0 ± 0.3 nm diameter NPs. This demonstrates a destabilization of these types of Pd NPs by over a third of a volt due to the small size of the 3 KDa sample. The scan for the 3 KDa sample (diameter 1.0 ± 0.3 nm) seems to show a smaller peak near the value expected for bulk

Pd. This suggests that this sample may have contained a small fraction of much larger particles, perhaps due to aggregation at some point during sample processing.

The dissolution process is interpreted based on the predicted behavior for Pd dissolution to $PdCl_4^{2-}$. The more rigorous analysis described by Tang and coworkers was not needed in the present case because the mechanism did not involve generation of a palladium oxide as part of the oxidation process.[16, 17] Dissolution of palladium is a two electron process in the presence of chloride ions to form $PdCl_4^{2-}$, as shown in Equation 1. The redox potential (E_0) for this process is highly dependent on chloride ion concentration, as shown in Equation 2.

$$PdCl_4^{2-} + 2e^- \rightarrow Pd^0 + 4Cl^- \quad ; E_0 = 0.391 \text{ V vs Ag/AgCl} \qquad (1)$$

$$E = E_0 - 2.303RT/nF \log[Cl^-]^4 \qquad (2)$$

The oxidation potentials for the anodic dissolution process corresponding to Pd-BCA NPs of average size 3.2 ± 0.9 nm, 1.5 ± 0.3 nm and 1.0 ± 0.3 nm were found to be 570 ± 12 mV, 467 ± 10 mV and 343 ± 15 mV, respectively. As qualitatively predicted by the Plieth model and experimentally observed by Zamborini and coworkers for silver and gold nanoparticles, the present results show a size dependent shift in oxidation potential for Pd NPs over the size range investigated.[12-15]

Figure 5 shows a plot of the experimental oxidation potentials for BCA-Pd NPs as a function of NP radius, based on the model proposed by Plieth (equation 3):

$$\Delta E = E_{0,\text{ Pd NP}} - E_{0,\text{ bulk Pd}} = -(2\gamma V_m/zFr) \qquad (3)$$

where $E_{0,\ Pd\ NP}$ is the oxidation potential of the variously sized BCA-Pd NPs, $E_{0,\ bulk\ Pd}$ is the oxidation potential of bulk Pd (i.e. the 0.70 V oxidation potential for the "bulk" >50 nm diameter Pd NP samples), γ is the surface energy of Pd (J m^{-2}), V_m is the molar volume of palladium (m^3 mol^{-1}), z is the number of electrons, F is Faraday's constant (96485.34 C × mol^{-1}), and r is the nanoparticle radius (m). The calculations used a surface energy value of bulk palladium of 2.0 J m^{-2}, as reported in the literature.[38-40]

The plot shows an excellent fit of the data to the Plieth model using a value of the surface energy of 2.0 J m^{-2}. As for previous work on Pt, Au and Ag, these anodic dissolution experiments reveal the intrinsic instability of very small metal NPs toward oxidation and dissolution. This will have substantial impact on any applications that require exposure of metal NPs to oxidizing potentials or oxidizing chemical conditions.

2.5. Conclusions:

This study reports the synthesis of a new class of water soluble Pd NPs. Capping with BCA endows the NPs with water solubility, an attractive feature. A simple purification procedure using centrifuge filters was developed to provide NPs with well-defined and narrow size distributions. Using these samples, a size dependent shift in oxidation potential for anodic dissolution of Pd NPs was observed. The data are in excellent agreement with a model proposed by Plieth. The purification strategy employed here can be used to obtain monodisperse nanoparticles of different sizes that can be used to examine the size dependence of catalytic activity, studies that are now underway.

SCHEME

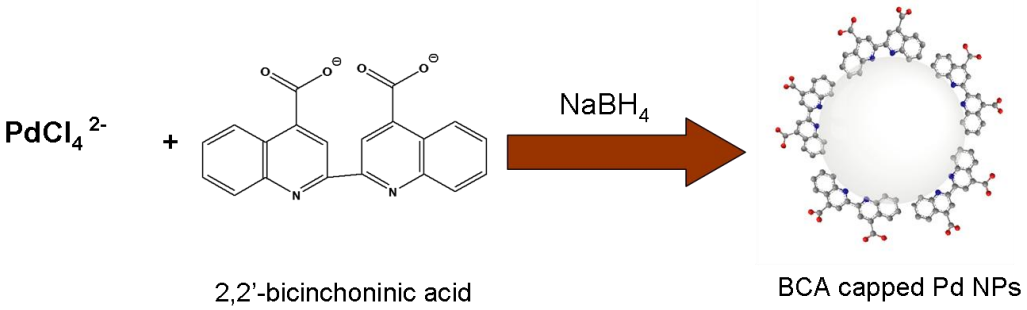

Scheme 2.1. Synthesis Scheme of BCA Capped Pd NPs.

TABLES

Sample	Mean Diameter (in nm) TEM	Mean Diameter (in nm) TEM	Interplanar spacing (d) (in Å)	Theo. E_0 (in mV)	Exp. E_0 (in mV)
Bulk	>50	20	2.25		700 ± 14
100 KDa sup.	3.2 ± 0.9	3.0	2.27	586	570 ± 10
Pd-BCA NPs	1.4 ± 0.8	1.4	2.29	NA	NA
30 KDa sup.	1.5 ± 0.3	1.0	2.33	456	467 ± 12
3 KDa sup.	1.0 ± 0.3	NA	> 2.33	334	343 ± 15

Table 2.1. Structural and Electrochemical Data for Pd-BCA NPs.

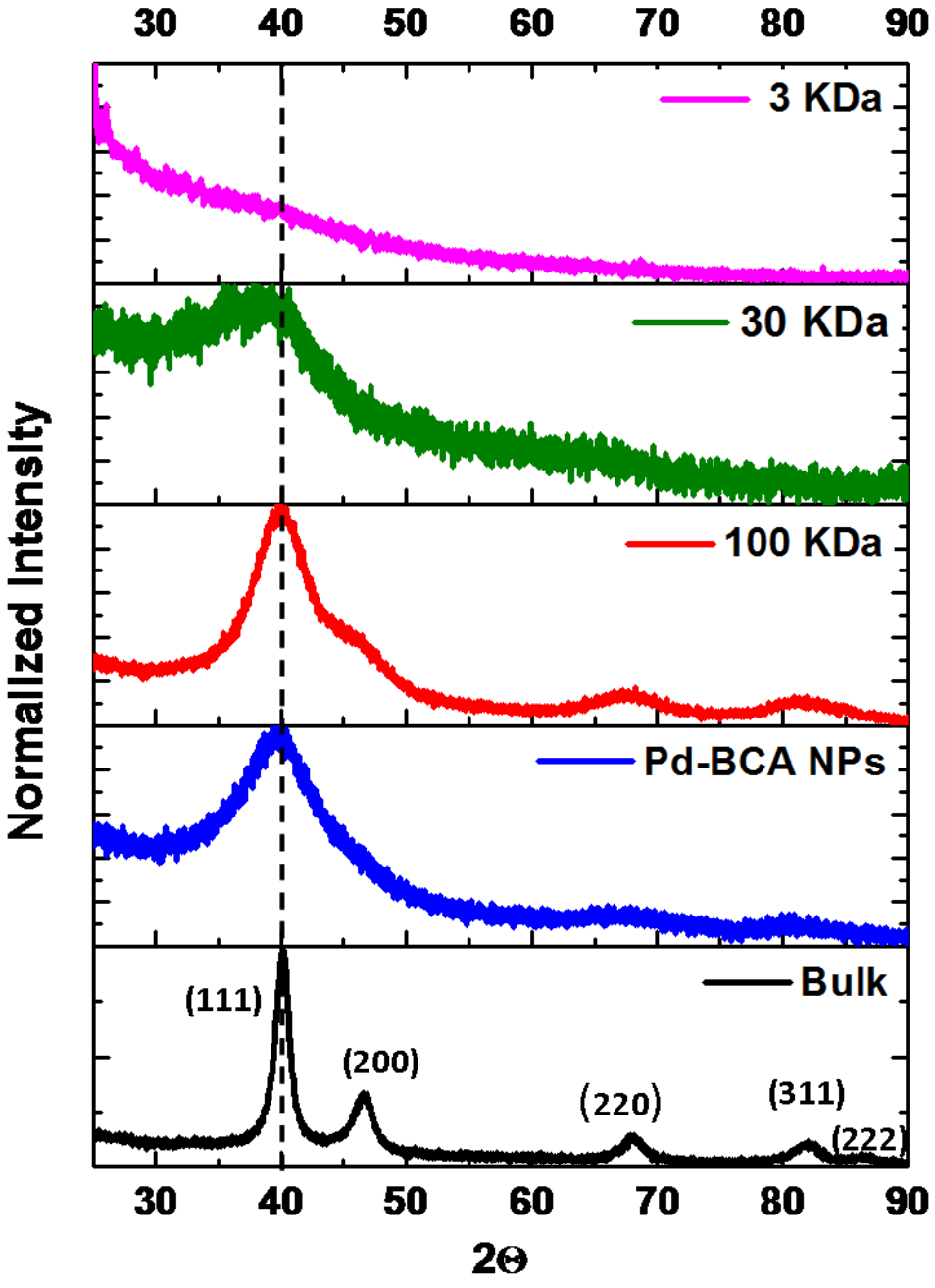

Figure 2.1. Powder X-ray Diffraction for Pd-BCA NPs Samples of Varying Size Used for Size Dependent Anodic Dissolution Studies.

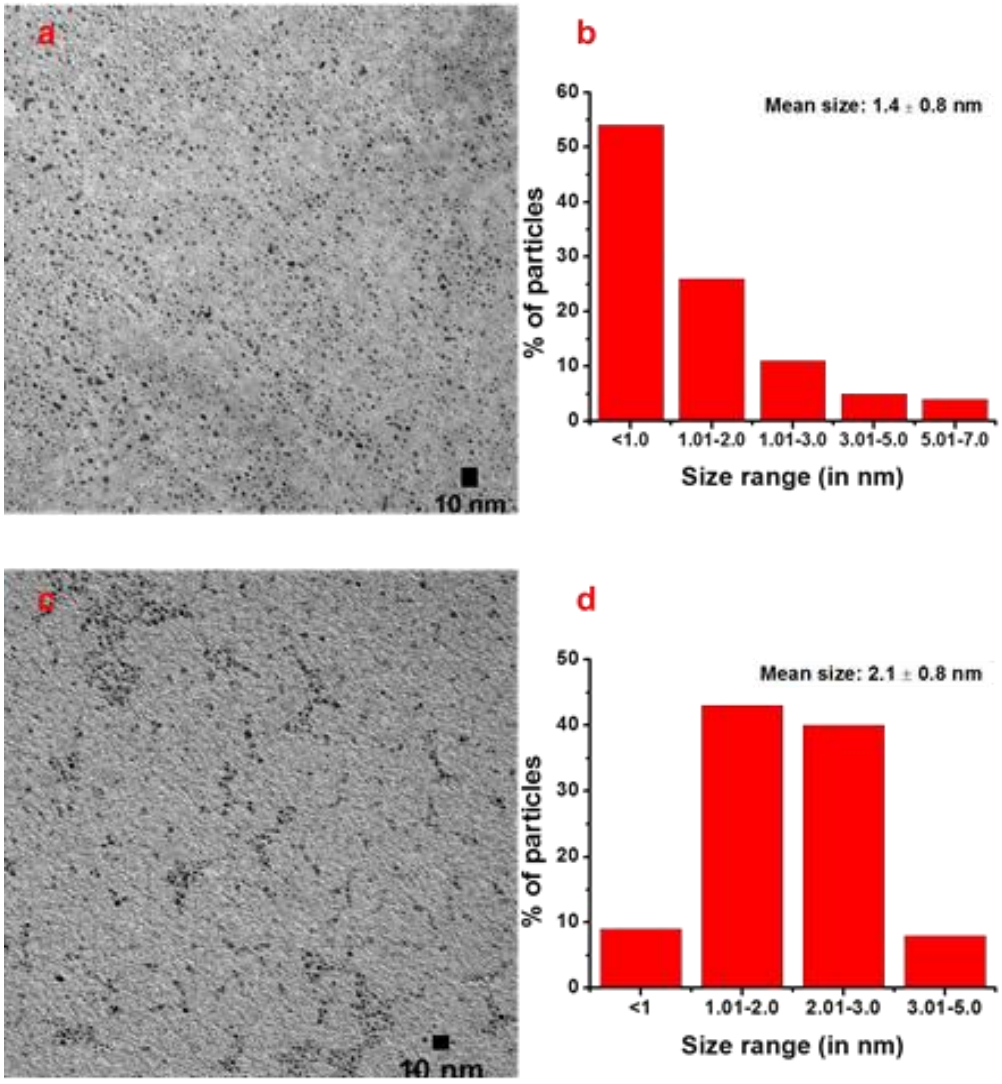

Figure 2.2. TEM Micrograph of BCA Stabilized Water Soluble Palladium Nanoparticles Synthesized Under (a) Higher (Pd:BCA:$BH4^-$-1:5:10) and (c) Lower (Pd:BCA:BH_4^--1:1:10) Ligand Ratio.Nanoparticles are Observed as Black Circles Scattered Across the Mesh Grid.

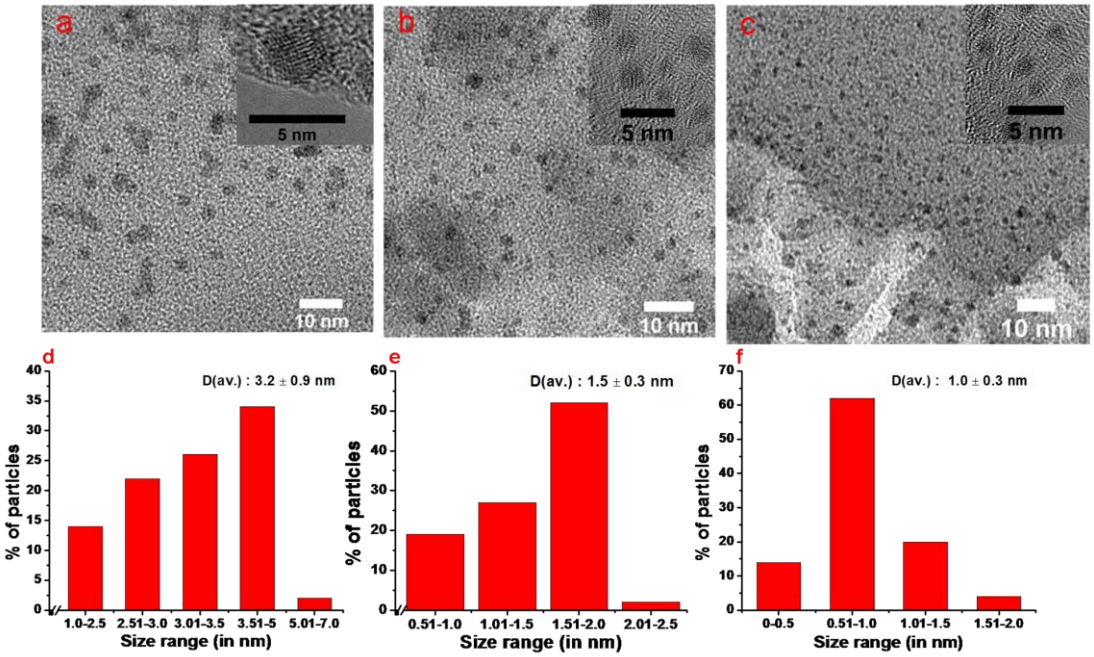

Figure 2.3. Low Resolution TEM and High Resolution TEM (inset) of Water Soluble Pd-BCA NPs (Pd:BCA:BH_4^--1:5:10) Purified Using Centrifugation Filters.(a).Supernatant of 100 KDa (b).Supernatant of 30 KDa (c).Supernatant of 3 KDa.

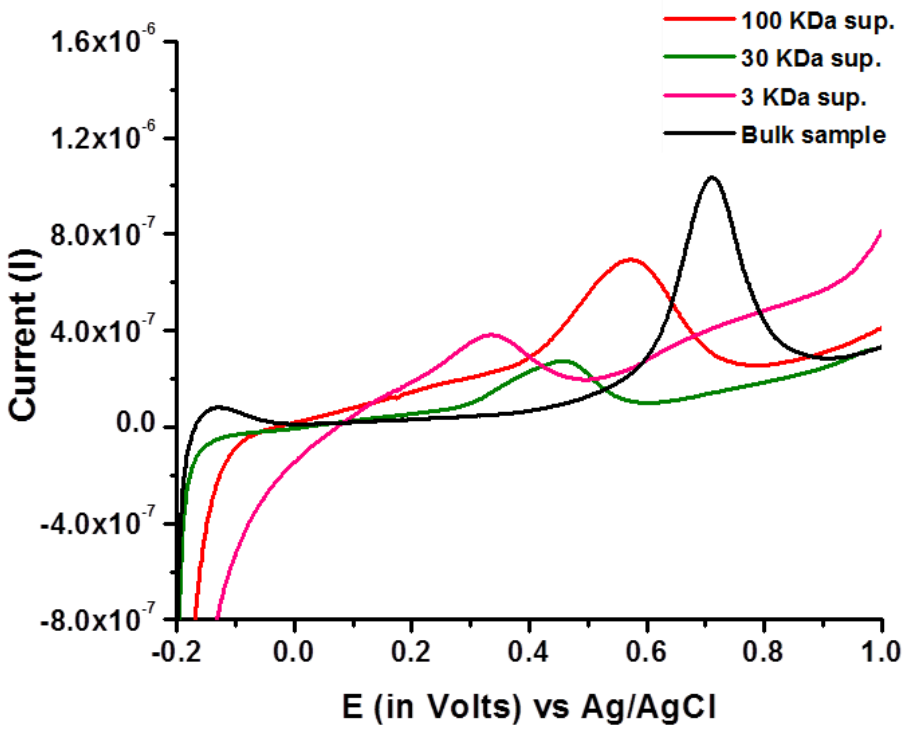

Figure 2.4. Size Dependent Anodic Dissolution of Pd-BCA NPs Deposited on Glassy Carbon Electrode in 0.1 M $HClO_4$ Conatining 10 mM NaCl at 1 mV/s Under Nitrogen. Bulk Sample (in Black), 100 KDa Sample (in Red), 30 KDa Sample (in Green) and 3 KDa Sample (in Magenta). Average Particle Size was 3.2 ± 0.9 nm, 1.5 ± 0.3 nm and 1.0 ± 0.3 nm for 100 KDa, 30 KDa and 3 KDa Sample Respectively. Average Particle Size of Bulk Sample was > 50 nm.

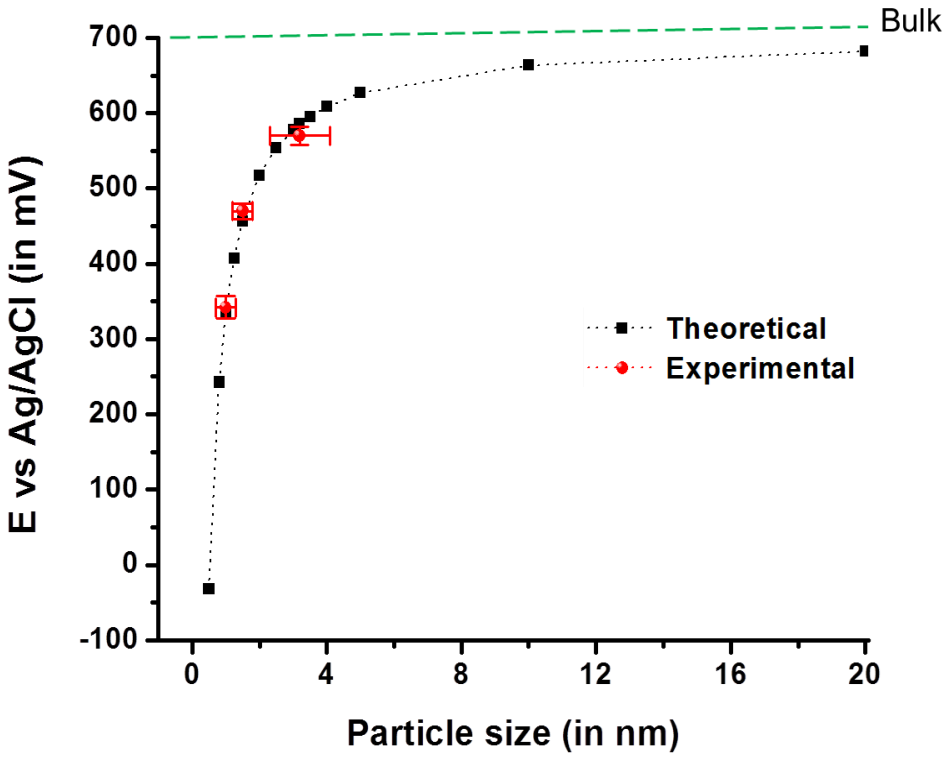

Figure 2.5. Experimentally Observed Oxidation Potential for Pd-BCA NPs as a Function of Particle Size (in **Red**) and Comparison with the Theoretical Values Predicted by the Plieth Model (in **Black**).

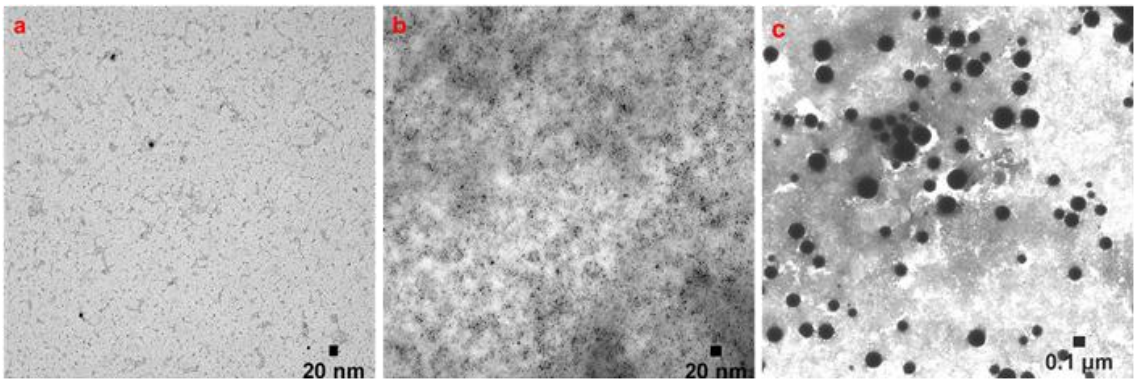

Figure 2.6. TEM of Pd-BCA NPs Synthesized Under Different Conditions. (a). Pd:BCA:BH_4^--1:1:10 (b). Pd:BCA:BH_4^--1:5:10 (c). Pd:BCA:Ascorbic acid-1:1:10. Sample c as Used as Bulk Sample in Anodic Dissolution Studies.

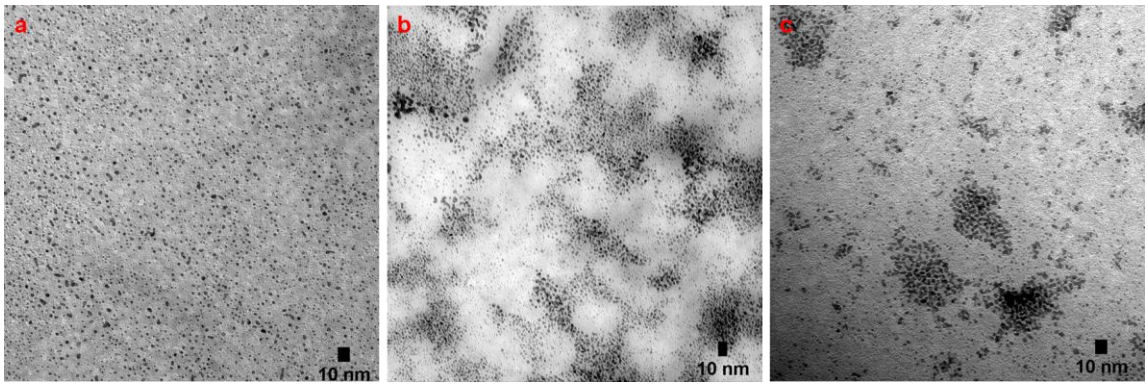

Figure 2.7. TEM Images of Pd-BCA NPs Synthesized at Different Ratio of Sodium Borohydride.(a). Pd:BCA:BH_4^--1:5:10 (b). Pd:BCA:BH_4^--1:5:20 (c). Pd:BCA:BH_4^--1:5:30.

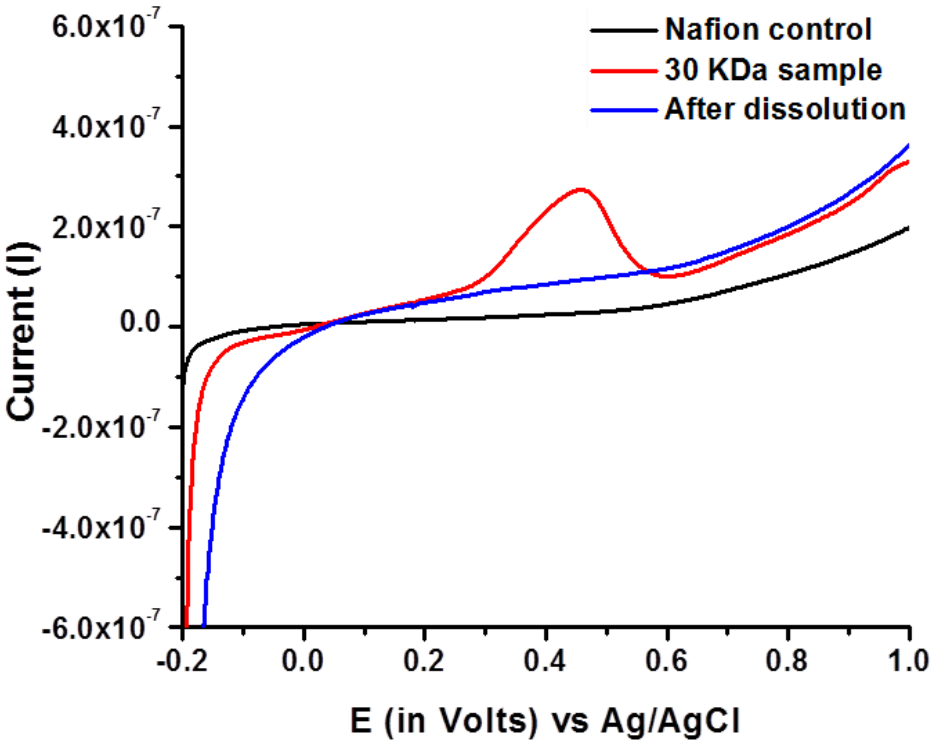

Figure 2.8. LSV Showing Anodic Dissolution Process of 30 KDa Sample (Shown in **Red**), Just After Dissolution Using Same Electrode and Fresh Electrolyte to Show the Dissolution Process is Complete (Shown in **Blue**) and Nafion Control (Without Any Pd-BCA NPs) to Show Nafion Doesn't Show Any Redox Activity During the Process (Shown in **Black**). All LSV were Recorded in 0.1 M $HClO_4$ Containing 10 mM NaCl at 1 mV/s.

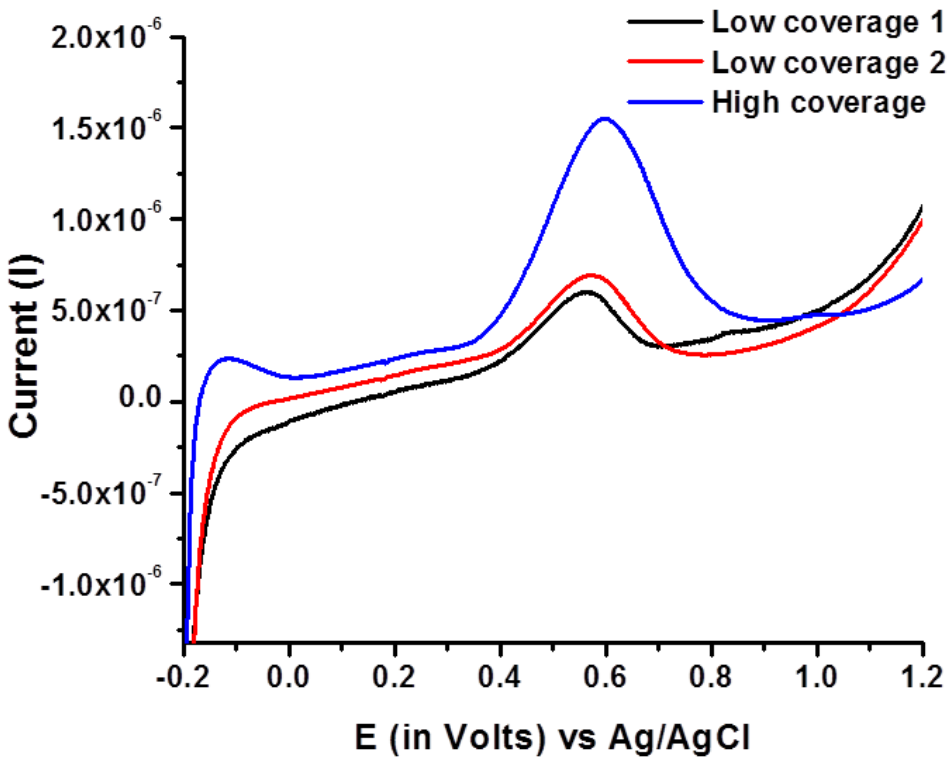

Figure 2.9. LSV Showing Anodic Dissolution Process of 100 KDa Sample (Average Diameter ~3.2 ± 0.9 nm) Obtained Under Different Coverage Conditions in 0.1 M $HClO_4$ Containing 10 mM NaCl at 1 mV/s.

2.6. References:

1. Emory, S. R.; Haskins, W. E.; Nie, S. Direct Observation of Size-Dependent Optical Enhancement in Single Metal Nanoparticles. *JACS* **1998**, *120*, 8009-8010.

2. Jain, P. K., Huang, X.; El-Sayed, I. H.; El-Sayed, M. A. Noble Metals on the Nanoscale: Optical and Photothermal Properties and Some Applications in Imaging, Sensing, Biology, and Medicine. *Acc. Chem. Res.* **2008**, *41*, 1578-1586.

3. Mulvaney, P. Surface Plasmon Spectroscopy of Nanosized Metal Particles. *Langmuir* **1996**, *12*, 788-800.

4. Corma, A.; Garcia, H. Supported Gold Nanoparticles as Catalysts for Organic Reactions. *Chem. Soc. Rev.* **2008**, *37*, 2096-2126.

5. McFarland, A. D.; Van Duyne, R. P. Single Silver Nanoparticles as Real-Time Optical Sensors with Zeptomole Sensitivity. *Nano lett.* **2003**, *3*, 1057-1062.

6. Nam, J. M.; Park, S. J.; Mirkin, C. A. Bio-Barcodes Based on Oligonucleotide-Modified Nanoparticles. *JACS* **2002**, *124*, 3820-3821.

7. Keller, A. A.; Wang, H.; Zhou, D.; Lenihan, H. S.; Cherr, G.; Cardinale, B. J.; Miller, R.; Ji, Z. Stability and Aggregation of Metal Oxide Nanoparticles in Natural Aqueous Matrices. *Environ. Sci. Technol.* **2010**, *44*, 1962-1967.

8. Zhang, H.; Gilbert, B.; Haung, F., Banfield, J. F. Water Driven Structure Transformation in Nanoparticles at Room Temperature. *Nature* **2003**, *424*, 1025-1029.

9. Chernavskii, P. A.; Peskov, N. V.; Mugtasimov, A. V.; Lunin, V. V. Oxidation of Metal Nanoparticles: Experiment and Model. *Russian Journal of Physical Chemistry B* **2007**, *4*, 394-411.

10. Sutter, E.; Sutter, P. Size-Dependent Room Temperature Oxidation of In Nanoparticles. *J. Phys. Chem. C* **2012**, *116*, 20574-20578.

11. Li, X.; Lenhart, J. J. Aggregation and Dissolution of Silver Nanoparticles in Natural Surface Water. *Environ. Sci. Technol*. **2012**, *46*, 5378-5386.

12. Plieth, W. J. On The Electrochemical Properties of Small Clusters of Metal Atoms and Their Role in the Surface Enhanced Raman Scattering. *J. Phys. Chem.* **1982**, *86*, 3166-3170.

13. Zamborini, F. P.; Ivanova, O. S. Size-Dependent Electrochemical Oxidation of Silver Nanoparticles. *JACS* **2010**, *132*, 70-72.

14. Zamborini, F. P.; Ivanova, O. S. Electrochemical Size Discrimination of Gold Nanoparticles Attached to Glass/Indium-Tin-Oxide Electrodes by Oxidation in Bromide-Containing Electrolyte. *Anal. Chem.* **2010**, *82*, 5844-5850.

15. Masitas, R. A.; Zamborini, F. P. Oxidation of Highly Unstable < 4 nm Diameter Gold Nanoparticles 850 mV Negative of the Bulk Oxidation Potential. *JACS* **2012**, *134*, 5014-5017.

16. Tang, L.; Han, B.; Persson, K.; Friesen, C.; He, T.; Sieradzki, K.; Ceder, G. Electrochemical Stability of Nanometer-Scale Pt Particles in Acidic Environments. *JACS* **2010**, *132*, 596-600.

17. Tang, L.; Li, X.; Cammarata, R. C.; Friesen, C.; Sieradzki, K. Electrochemical Stability of Elemental Metal Nanoparticles. *JACS* **2010**, *132*, 11722-11726.

18. Ward Jones, S. E.; Campbell, F. W.; Baron, R.; Xiao, L.; Compton, R. G. Particle Size and Surface Coverage Effects in the Stripping Voltammetry of Silver Nanoparticles: Theory and Experiment. *J. Phys. Chem. C* **2008**, *112*, 17820-17827.

19. Kolb, D. M.; Englemann, G. E.; Ziegler, J. C. On the Unusual Electrochemical Stability of Nanofabricated Copper Clusters. *Angew. Chem., Int. Ed*. **2000**, *39*, 1123-1125.

20. Ng, K. H.; Liu, H.; Penner, R. M. Subnanometer Silver Clusters Exhibited Unexpected Electrochemical Metastability on Graphite. *Langmuir* **2000**, *16*, 4016-4023.

21. Brainina, K.Z.; Galperin, L.G.; Vikulova, E.V. Electrochemistry of Metal Nanoparticles: The Effect of Substrate. *Journal of Solid State Electrochemistry* **2012**, *16*, 2357-2363.

22. Zhao, W.; Gonzaga, F.; Li, Y.; Brook, M. A. Highly Stabilized Nucleotide-Capped Small Gold Nanoparticles with Tunable Size. *Advanced Materials* **2007**, *13*, 1776-1771.

23. Singh, P.; Buttry, D. A. Comparison of Oxygen Reduction Reaction at Silver Nanoparticles and Polycrystalline Silver Electrodes in Alkaline Solution. *J. Phys. Chem. C.* **2012**, *116*, 1056-10663.

24. Schmid, G.; Harms, M.; Malm, J. O.; Bovin, J. O.; Ruitenbeck, J. V.; Zandbergen, H. W.; Fu, W.T. Ligand-Stabilized Giant Palladium Clusters: Promising Candidates in Heterogeneous Catalysis. *JACS* **1993**, *115*, 2046-2048.

25. Teranishi, T.; Miyake, M. Size Control of Palladium Nanoparticles and Their Crystal Structures. *Chem. Mater.* **1998**, *10*, 594-600.

26. Lin, C. M.; Hung, T. L.; Huang, Y. H.; Wu, K. T.; Tang, M. T.; Lee, C. H.; Chen, C. T.; Chen, Y. Y. Size-Dependent Lattice Structure of Palladium Studied by X-Ray Absorption Spectroscopy. *Phys. Rev. B* **2007**, *75*, 125426-6.

27. Heinemann, K.; Poppa, H. In-Situ TEM Evidence of Lattice Expansion of Very Small Supported Palladium Particles. *Surf. Sci.* **1985**, *156*, 265-274.

28. Giorgio, S.; Henry, C. R.; Chapon, C.; Penisson, J. M. Structure and Morphology of Small Palladium Particles (2-6 nm) Supported on MgO Micro-Cubes. *J. Cryst. Growth* **1990**, *100*, 254-260.

29. Goyhenex, C.; Henry, C. R.; Urban, J. Measurements of the Lattice Parameter of Supported Palladium Clusters. *J. Philos. Mag. A* **1994**, *69*, 1073-1084.

30. Vermaak, J.S.; Mays, C. W.; Kuhlmann-Wilsdorf, D. On Surface Stress and Surface Tension: I. Theoritical Considerations. *Surf. Sci.* **1968**, *12*, 128-133.

31. Mays, C. W.; Vermaak, J. S.; Kuhlmann-Wilsdorf, D. On Surface Stress and Surface Tension: II. Determination of the Surface Stress of Gold. *Surf. Sci.* **1968**, *12*, 134-140.

32. Wassermann, H. J.; Vermaak, J. S. On the Determination of the Surface Stress of Copper and Platinum. *Surf. Sci.* **1972**, *32*, 168-174.

33. Montano, P. A.; Zhao, J.; Ramanathan, M.; Shenoy, G. K.; Schulze, W.; Urban, J. Structure of Silver Microclusters. *Chem. Phys. Lett.* **1989**, *164*, 126-130.

34. Jacobs, J. W.; Schryvers, D. S. A High-Resolution Electron Microscopy Study of Photodeposited Pd Particles on TiO_2 and Their Oxidation in Air. *J. Catal.* **1987**, *103*, 436-449.

35. Lamber, R.; Jaeger, N.; Schulz-Ekloff, G. Electron Microscopy Study of the Interaction of Ni, Pd and Pt with Carbon: II. Interaction of Palldium with Amorphous Carbon. *Surf. Sci.* **1990**, *227*, 15-23.

36. Kuhrt, C.; Anton, R. On the Origin of a Lattice Expansion in Palladium and Pd-Au Vapor Deposits on Various Substrates. *Thin Solid Films* **1991**, *198*, 301-315.

37. Xia, Y.; Xiong, Y.; Lim, B.; Skrabalak, S. E. Shape-Controlled Synthesis of Metal Nanocrystals: Simple Chemistry Meets Complex Physics? *Angew. Chem. Int. Ed.* **2008,** *48*, 60-103.

38. Qi, W. H.; Wang, M. P. Size and Shape Dependent Lattice Parameters of Metallic Nanoparticles. *J. Nanopart. Res.* **2005**, *7*, 51-57.

39. Redjala, T.; Remita, H.; Apostolescu, G.; Mostafavi, M.; Thomazeau, C.; Uzio, D. Bimetallic Au-Pd and Ag-Pd Clusters Synthesized by γ or Electron Beam Radiolysis and Study of the Reactivity/Structure Relationships in the Selective Hydrogenation of Buta-1,3-Diene. *Oil & Gas Science and Technology – Rev. IFP*. **2006**, *61*, 789-797.

40. Tyson, W. R.; Miller, W. A. Surface Free Energies of Solid Metals: Estimation from Liquid Surface Tension Measurements. *Surf. Sci.* **1972**, *62*, 267-276.

CHAPTER 3

Size-Dependent Underpotential Deposition of Copper on Palladium Nanoparticles

Ashok Kumar and Daniel A. Buttry*

Department of Chemistry and Biochemistry, Arizona State University, Tempe, AZ, 85287-1604, USA

Reproduced by permission of American Chemical Society

Journal of Physical Chemistry, 2015, 117, 23334-23347

3.1. Abstract: The underpotential deposition (UPD) of copper on palladium nanoparticles (NPs) with sizes in the range 1.6 – 98 nm is described. A dependence of the UPD shift on size of the nanoparticle is observed, with the UPD shift decreasing as the particle size decreases. This size dependence is consistent with the known dependence of UPD shift on work function difference between the substrate metal (Pd) and the depositing metal (Cu). The shift suggests the work function of the NPs decreases with decreasing size as expected (i.e. the smaller nanoparticles are more easily oxidized and therefore have lower work functions than larger NPs). For the smallest nanoparticles, the UPD shift does not follow the expected trend based solely on predictions of work function changes with size. Based on preliminary competitive anion adsorption experiments, it is speculated that strong chloride absorption on the smallest nanoparticles may be responsible for this deviation.

3.2. Introduction:

Underpotential deposition (UPD) is the deposition of a monolayer or a submonolayer amount of a metal on a foreign metal substrate at potentials positive of the bulk deposition. The difference between the potential at which UPD occurs and the potential for bulk deposition is referred as the UPD shift.[1] The UPD shift is known to depend on the difference in work function between the substrate metal and the depositing metal.[2] Given that the work function for very small (<3 nm diameter) NPs is size dependent, one might expect that UPD would depend on NP size in this same size range.[3–5] We demonstrate this effect for the first time using Cu UPD on Pd NPs with diameters ranging from 1.6 nm to 98 nm.

UPD has been used to deposit a wide variety of metals onto different metal substrates, allowing studies to elucidate catalytic mechanisms as well as to prepare new catalytic materials. It has been widely used to prepare inexpensive catalysts by depositing monolayer amounts of noble metals on less expensive substrates.[6–12] Given that many electrocatalytic materials are used in nanoparticle form, understanding UPD at metal NPs is an important issue.

UPD has been studied for both polycrystalline and single crystal metals showing differences in UPD voltammetric features between the two. UPD peaks on single crystals with a high degree of order and large domain sizes tend to be sharp while UPD features on polycrystalline metals are broad.[13–20] Previous reports of UPD on NPs reveal broad features that are similar to responses on polycrystalline substrates.[18,21] The magnitude of

UPD responses also depends on the available surface area of the substrate. Thus, UPD has been routinely used as a method of choice to determine electroactive surface area of electrodes and catalysts.[7,18–22]

UPD of Cu on polycrystalline and single crystal Pd substrates has been examined by several groups. On a Pd(111) surface, a single sharp UPD peak is preceded by a small shoulder, while on a Pd(100) surface the Cu UPD gives two sharp peaks with a small preceding peak. Polycrystalline samples show what appears to be a mixture of these two responses, with generally broader features.[13] These same workers compared experimental UPD shifts with work function differences between Cu and Pd and found reasonable agreement, especially when using work function values for the specific single crystal faces being used. Cu UPD on Pd was found to occur without alloying.[13] However, there are a few studies suggesting Cu-Pd alloying during the UPD process in the Cu/Pd system.[23–25]

Underpotential deposition can be very effective in preparing core-shell NPs. The sequential reduction method using chemical reductants not only leads to polydispersity but also lacks control over the number of monolayers of metal atoms deposited as shells. UPD on the other hand allows strict control over the shell structure as well as selective deposition on a particular crystallographic plane of the core.[26–28] However, a more noble metal shell cannot be deposited by UPD. This can be solved by using a galvanic replacement technique. Palladium nanoparticles are excellent electrocatalysts for alcohol and formic acid oxidation but their electrocatalytic activity for oxygen reduction reaction is significantly lower than more expensive Pt NPs.[29–31] Adzic *et al.* were able to prepare

Pd-Pt core-shell NPs by depositing Cu onto Pd NPs by UPD followed by galvanic exchange of Cu for Pt.[12] Interestingly, it has proven possible to distinguish the UPD of metals onto different crystal facets of metallic nanoparticles. In one striking example, theory and experiment were used together to rationalize not only the difference in deposition potential at different crystal faces, but also the influence of absorbed anions from the supporting electrolyte on the energetics of the process.[32] Below we also describe the possible influence of anion adsorption on Cu UPD on Pd NPs.

In this paper, we demonstrate the dependence of Cu UPD on the size of Pd NPs with diameters of a few nanometers. Water soluble Pd NPs were obtained using BCA (2,2'-bicinchoninic acid dipotassium salt hydrate) as a capping ligand. Using the water soluble BCA ligand allows us to use aqueous processing methods to obtain Pd NPs of different size ranges by using the centrifuge filter technique, making size dependent electrochemical studies possible. These same NPs were used in a previous study exploring the size dependence of the anodic dissolution of very small metal NPs.[33] That study showed that the oxidation potential of Pd NPs decreases as the NPs are made smaller. This is consistent with a number of other studies on Pt, Au and Ag NPs.[34–37] Given the expected connection between NP oxidation potential and NP work function, [3,4,38] we explore here how UPD depends on the size of Pd NPs which serve as the UPD substrate. For a range of NP sizes, we show that the UPD shift depends in the expected way on the size of the metal NPs. Deviation from the expected trend for the smallest NPs is speculatively ascribed to especially strong competitive adsorption of Cl^- which is thought to influence the UPD process.

3.3. Experimental:

Palladium (II) chloride ($PdCl_2$, 99%) and sodium borohydride ($NaBH_4$, 99.9%) were purchased from Sigma-Aldrich, and 2,2'-bicinchoninic acid dipotassium salt hydrate (K_2BCA, >98%) was purchased from TCI America. These and all other reagents were reagent grade or better and were used as obtained. For UPD experiments, sodium perchlorate ($NaClO_4$, ≥98%) and perchloric acid ($HClO_4$, 70%, 99.999% trace metal basis) were purchased from Sigma-Aldrich, and copper perchlorate hexahydrate ($Cu(ClO_4)_2.6H_2O$, 99.999% metal basis) was purchased from Alfa-Aesar. Water of resistivity 18.3 MΩ (Millipore MQ Reference) was used to prepare all solutions. The synthesis of BCA-capped Pd NPs and their size fractionation using various sizes of molecular weight cut-off centrifuge filters was previously described.[33] Large, roughly spherical Pd NPs (average diameter ~ 98±38 nm) were synthesized using a previously reported synthesis in which $PdCl_4^{2-}$ is reduced and weakly capped using ascorbic acid. (See Supporting Information S1 for TEM).[33] These were used to represent the behavior of a "bulk" Pd sample, i.e. a nanoparticle sample for which the size was sufficiently large that nanoscale effects are not expected to be observed.

All Pd nanoparticle samples were characterized by transmission electron microscopy and X-ray diffraction as previously described. HRTEM measurements were done using an ARM200F (JOEL) operated at 200 KV. Histograms were obtained by selecting an area and counting 50 particles from that area. As seen from HRTEM images the Pd NPs obtained are mostly polycrystalline in nature. Samples and protocols for electrochemical experiments were also described previously.[33] Briefly, very dilute NP

solutions were evaporated on a glassy carbon electrode, followed by entrapment with an overlaying film of Nafion^{TM}. Prior to UPD studies, "bare" Pd NPs were prepared by electrochemically removing the BCA capping ligands by repetitive oxide growth and stripping cycles in deoxygenated 0.5 M $NaClO_4$ + 10 mM $HClO_4$ solution. It was found that the presence of BCA on Pd NPs surface inhibits copper UPD and that UPD peaks appeared only after removing BCA ligands from the Pd NP surface by electrochemically cycling in the oxide region (See Supporting Information Figures S2 and S3). These samples were then used to examine Cu UPD in slightly acidic solutions containing Cu(II). An Ag/AgCl reference electrode was used, against which all potentials are referred.

3.4. Results and Discussion:

A cyclic voltammogram showing copper underpotential deposition on 98 nm diameter palladium NPs is shown in Figure 3.1. This sample was used to simulate the behavior of bulk Pd using the same experimental sampling format as for the smaller NPs. In the control experiment without Cu(II) (red curve), only features corresponding to palladium oxide growth and palladium oxide stripping are observed. In the control solution, during the positive scan oxide growth starts at +0.5 V. Stripping of the oxide appears on the reverse scan as a well-formed peak at +0.42 V. No other features are observed down to 0 V. In the presence of Cu^{2+}, several additional features are observed as a result of copper deposition and stripping processes. During the negative scan, the Cu UPD process occurs simultaneously with the Pd oxide stripping process. Thus, Cu UPD appears as a single broad shoulder on the negative side of the stripping peak. Continuing in the negative direction, cathodic current increases below 0.1 V, suggesting further deposition. The current rises strongly below +0.0 V due to bulk Cu deposition. Two distinct peaks are observed on the subsequent positive scan, the first at +0.05 V and the second at +0.36 V. These are attributed to anodic dissolution of bulk Cu and stripping of UPD copper, respectively. Based on previous studies of Cu UPD on polycrystalline Pd, it is possible that the cathodic deposition process below +0.1 V and the anodic peak at +0.05 V also contain contributions from UPD.[13] However, due to the closeness of the bulk process, this was not investigated further. Instead, to study size-dependent UPD phenomena we focused on the well-formed anodic peak at +0.36 V, which corresponds to dissolution of

underpotentially deposited Cu. Both the Pd(111) and Pd(100) surfaces as well as polycrystalline Pd exhibit peaks near this potential.[13]

Figure 3.2 shows an experiment in which the negative potential limit was varied during scans through the UPD region. The data show that during the negative scan, excursions into the shoulder (UPD) region of the cathodic peak centered at 0.4 V produce the anodic peak at +0.36 V attributed to stripping of a Cu UPD deposit. The second anodic peak at +0.05 V is only observed if the negative limit exceeds 0.0 V as seen in the black curve. Scan limits more negative than -0.06 V produce very large cathodic Cu deposition currents and large anodic peaks around +0.05 V attributed to dissolution of bulk Cu (not shown), confirming this peak as having contributions from bulk dissolution. These data again show that the anodic Cu UPD stripping peak at +0.36 V is well-formed and suggest it can be used to accurately measure the dependence of UPD stripping on NP size.

Figure 3.3 shows TEM images of BCA-capped Pd NPs that were size fractionated using different kDa MW cutoff centrifuge filters. Sizes were obtained from the images as previously reported using manual analysis of a large number of NPs.[33] The sizes shown in the images correspond to a 100 kDa sample (average diameter: 3.1 ± 0.7 nm), a 50 kDa sample (average diameter: 2.4 ± 0.5 nm) and a 30 kDa sample (average diameter: 1.6 ± 0.4 nm).[33] As can be seen, not all of the particles are spherical, with some having an oblong or irregular shape. This dispersity is captured in the reported range for the diameters of each of the NP samples.

The samples from Figure 3.3 were used in separate UPD experiments along with the 98 nm diameter NP sample to serve as a bulk Pd control. These results are shown in Figure 3.4. The Cu stripping peak for the bulk sample was observed at +0.08 V. Cu UPD anodic stripping peaks were observed at +371 ± 6 mV, +320 ± 12 mV, +281 ± 10 mV and +143 ± 14 mV for the bulk Pd sample, 100 kDa sample, 50 kDa sample and 30 kDa sample, respectively. The data show a dramatic negative shift of the anodic Cu UPD stripping peak as the NP size decreases, as well as substantial broadening of the UPD stripping peak. We turn now to analysis of the shift.

Table 3.1 shows work functions for bulk Cu, bulk Pd and Pd NP substrates, and theoretical and experimental Cu UPD shifts for bulk Pd and Pd NP substrates. The bulk work function values are from the literature.[39] The NP work function values are calculated using an approach based on earlier treatments of NP thermodynamics by Plieth.[3,4,38] He proposed a relationship between the oxidation potential of metal NPs and their size that derived from the influence of surface energy on NP stability for very small NPs.[38] This is given in equation 1:

$$\Delta E_d = E_{d,NP} - E_{d,Bulk} = -(2\gamma V_m/zFr) \qquad (1)$$

where γ is surface energy of the NP material, V_m is its molar volume, z is the number of electrons involved in its oxidative dissolution, F is Faraday's constant, r is nanoparticle radius and E_d is the oxidation (dissolution) potential of the NP or bulk material. We previously showed that this equation correctly predicts the negative shift of oxidation potential with decreasing size for Pd NPs.[33] Here this relation is used to connect UPD

shifts with NP size. Trassati showed that the potential of zero charge (pzc) and work function are directly related. This implies that the pzc's for NPs ($E_{pzc,NP}$) and NP work functions (Φ_{NP}) differ from the bulk values as shown in equation 2.[39]

$$E_{pzc,NP} - E_{pzc,Bulk} = \Phi_{NP} - \Phi_{Bulk} \quad (2)$$

Plieth also showed that the changes in surface energy of NPs shift the entire electrochemical scale for the NP.[3,4] In other words, the oxidation (dissolution) potential and the potential of zero charge shift by the same amount with size, as shown in equation 3.

$$E_{pzc,NP} - E_{pzc,Bulk} = \Delta E_d \quad (3)$$

This allows one to use equation 1 to calculate shifts in work function with size as shown in equation 4. We note that this treatment neglects the size dependent image charge effect on work function that can be calculated by classical means,[40] since Plieth pointed out that the image charge effects cannot be measured in electrochemical UPD experiments.[4]

$$\Phi_{NP} - \Phi_{Bulk} = - (2\gamma V_m/zFr) \quad (4)$$

With eqn. 4 in hand, one can use the Kolb-Gerischer relation between UPD shift and work function difference between the metals to predict the shift in UPD expected as NP size decreases.[1] Equation 5 shows this prediction for the specific case of Cu UPD on Pd. In this equation the work function term for Pd is considered to be the work function relevant for whatever is the UPD substrate, whether bulk Pd or Pd NPs.

$$\Delta UPD = 0.5\ (\Phi_{Pd} - \Phi_{Cu}) \qquad (5)$$

Thus, in Table 3.1, equation 4 is used to calculate the work functions for the various Pd NP substrates and equation 5 is used to calculate the theoretical UPD shifts for those cases. A surface energy for Pd of 2 J m^{-2} was used.[41] These calculated NP UPD shifts can be compared to the experimental shifts which are given in the last column of the table. Results for a previous experimental study of Cu UPD on bulk Pd are also shown.[13]

The theoretical and experimental UPD shifts are plotted versus reciprocal diameter for all samples in Figure 3.5. This plot is in the functional form predicted by the Plieth model. The black line shows the theoretical predictions and the red points show the experimental values. The red line was drawn so it passed through the experimental value for Cu UPD on the 98 nm bulk Pd sample and had the same slope predicted by the theoretical treatment. The vertical offset between the experimental and theoretical lines of approximately 75 mV may be due to small errors in either the work functions for the two metals or the surface energy value used to predict the size dependence of the work function for the Pd NPs. Nevertheless, the experimental data show a strong dependence of the Cu UPD shift with Pd NP size, with a trend that seems to be in reasonable agreement with the Plieth model. The data show that the Cu UPD process shifts strongly in the negative direction as NP size decreases, consistent with expectations for the UPD process to track oxidation potential and work function shifts in the Pd NPs with size. These data represent the first experimental validation of this prediction, as embodied in equations 4 and 5.

The data in Fig. 3.5 deviate significantly from the theoretical predictions for the smaller NP samples, with the deviation increasing as size decreases. It seems clear from the plot that the Plieth model captures some of the processes leading to UPD shifts, but not all. In considering possible explanations of this, we focused on the effects of competitive specific adsorption. There were two reasons for this. First, it is well known that ClO_4^- solutions can contain substantial concentrations of Cl^-.[42] In our experiments we believe the concentration of chloride ion in the UPD electrolyte solution was approximately 50 μM. Further, Cl^- adsorption is known to substantially influence Cu UPD on both Pt and Pd.[43–45] Finally, Ross and coworkers have previously shown that anion adsorption is substantially enhanced with decreasing size for Pt NPs.[46–48] This effect occurs both for Cl^- and OH^- and is responsible for large reductions in catalytic activity per unit area for electrochemical reactions catalyzed at noble metal NPs, such as methanol oxidation and oxygen reduction.[42,49] A possible explanation for their observations is the increasing number of step and kink sites per unit area as NP size decreases, assuming that anion adsorption is enhanced at such sites. In contrast, for UPD the decrease in size leads to a reduction in work function for the Pd NP substrates, resulting in inhibition of the UPD process (i.e. more negative potentials are required to drive UPD as size decreases). Taken together, these ideas suggest that decreasing size should suppress UPD while enhancing the competitive adsorption of Cl^-, a combination of effects that might lead to the deviations shown in Fig. 3.5. To test this, we examined the influence of increasing Cl^- concentration on the UPD shift for the smallest NP sample.

Figure 3.6 shows the result of increasing [Cl^-] on the Cu UPD stripping process for a 1.6 nm diameter Pd NP sample. Plate B shows clearly that increasing the concentration of Cl^- from 50 to 750 µM results in a negative shift in the UPD stripping peak of approximately 100 mV. These results could be interpreted to imply that Cl^- inhibits Cu UPD, and are consistent with the speculative arguments presented above. However, these preliminary results certainly do not prove that Cl^- adsorption is responsible for the deviation observed in Fig. 3.5. More work would be needed to establish any such relationship.

3.5. Conclusions:

The results presented above comprise the first systematic demonstration of size dependent UPD on metal NP substrates. They show that UPD shifts at metal NP substrates appear to follow a size-dependent trend based on a simple work function model proposed by Plieth that derives from the influence of surface energy on NP thermodynamic stability and how this changes with NP size. Deviations from the predicted behavior were observed, with the largest deviations occurring for the smallest NPs. These were speculatively attributed to Cl^- adsorption interfering with the UPD process, with the interference becoming stronger as NP size decreased. The results provide guidance to efforts that employ UPD to prepare metal NP electrocatalysts and other nanoscale materials based on such methods.

TABLES

Substrate	Average diameter (nm)	Work function of substrate (eV)	Work function of Cu (eV)	UPD shift (Theoretical) (mV)	UPD Shift (Experimental) (mV)
Bulk[12]	NA	5.0	4.55	225	275 by Meyer
"Bulk" Pd NPs	98 ± 38	4.996	4.55	223	291
100kDa	3.1 ± 0.7	4.882	4.55	166	240
50kDa	2.4 ± 0.5	4.848	4.55	149	201
30kDa	1.6 ± 0.4	4.771	4.55	111	63

Table 3.1. Work Functions and UPD Shifts for the Pd/Cu^{2+} System.

FIGURES

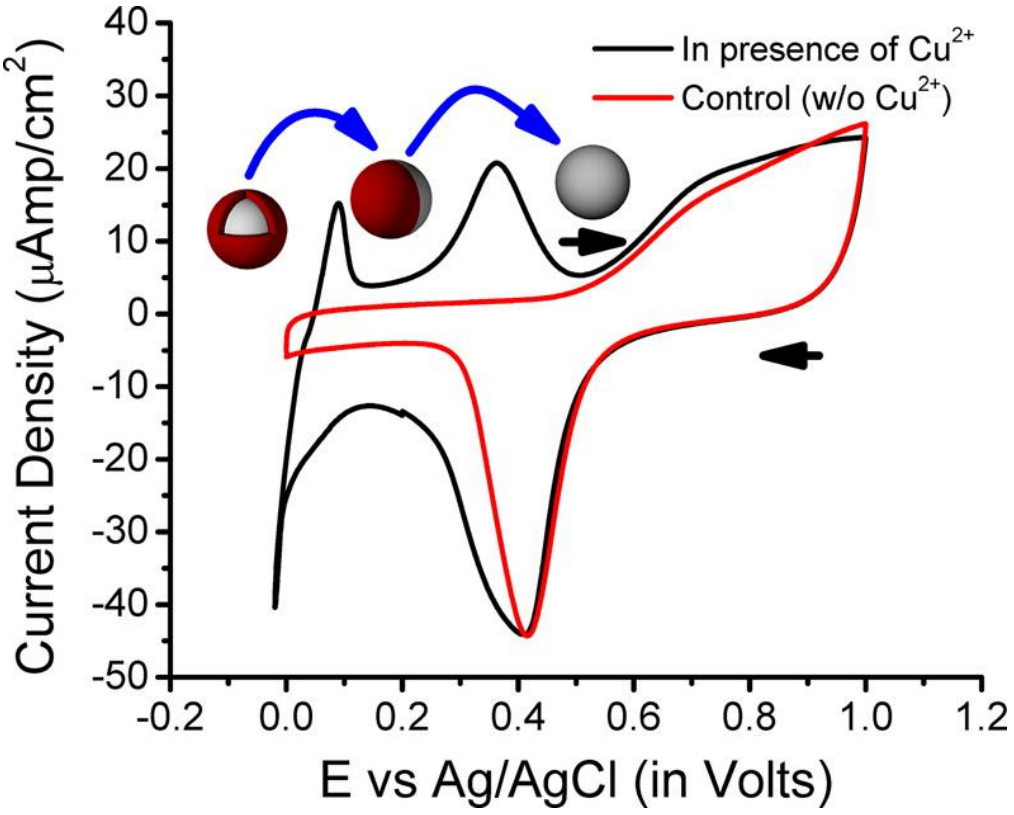

Figure 3.1. UPD of Cu on Pd in 0.5 M $NaClO_4$ + 10 mM $HClO_4$ + 1 mM $Cu(ClO_4)_2$ (Black Line) and Control Experiment in 0.5 M $NaClO_4$ + 10 mM $HClO_4$ (Red Line) at 10 mV/sec.

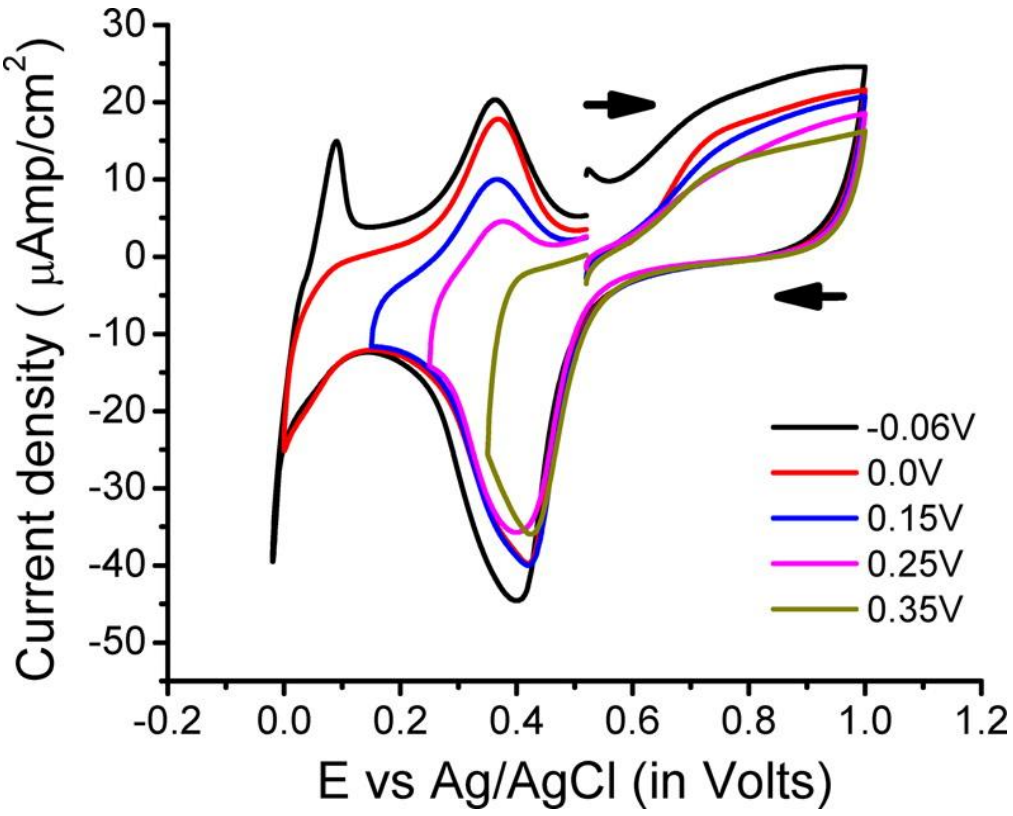

Figure 3.2. Underpotential Deposition of Copper on Palladium at Different Negative Potential Limit in 0.5 M $NaClO_4$ + 10 mM $HClO_4$ + 1 mM $Cu(ClO_4)_2$ at 10 mV/sec.

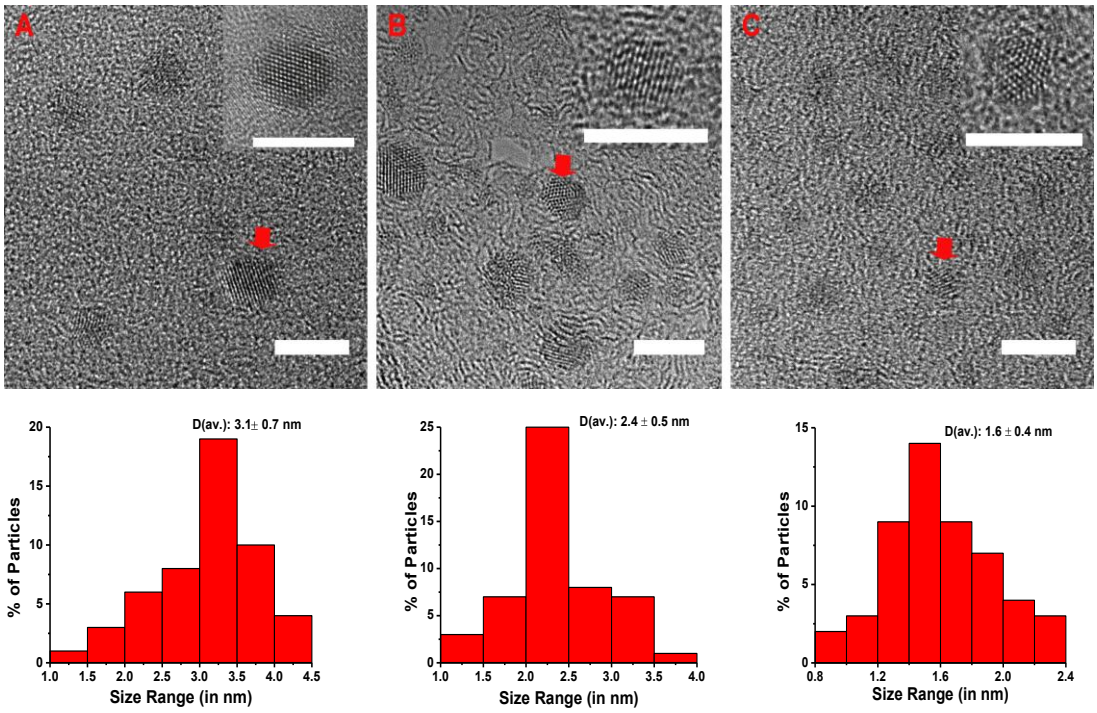

Figure 3.3. Transmission Electron Microscopy (TEM) of BCA Capped Pd NPs Obtained After Purification. Average Diameter of 100 kDa, 50 kDa and 30 kDa Sample was 3.1 ± 0.7 nm, 2.4 ± 0.5 nm and 1.6 ± 0.4 nm Respectively (Scale Bar: 5 nm).

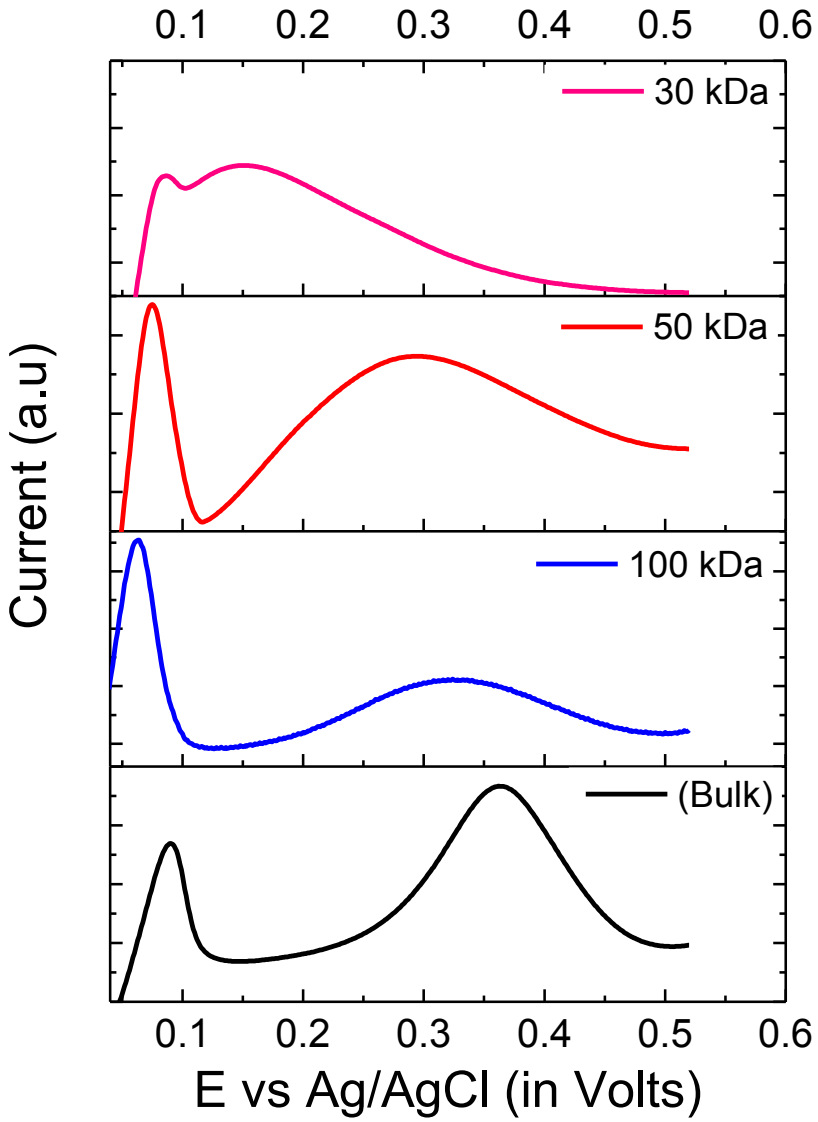

Figure 3.4. Size Dependent UPD Stripping of Cu From Pd NPs. Electrolyte: 0.5 M $NaClO_4$ + 10 mM $HClO_4$ and 1 mM $Cu(ClO_4)_2$ Solution Under N_2 Atmosphere, Scan Rate: 10 mV/s. All UPD Experiments were Performed as in Figure 1. For Simplicity, only Cu Stripping Region is Used for Comparison.

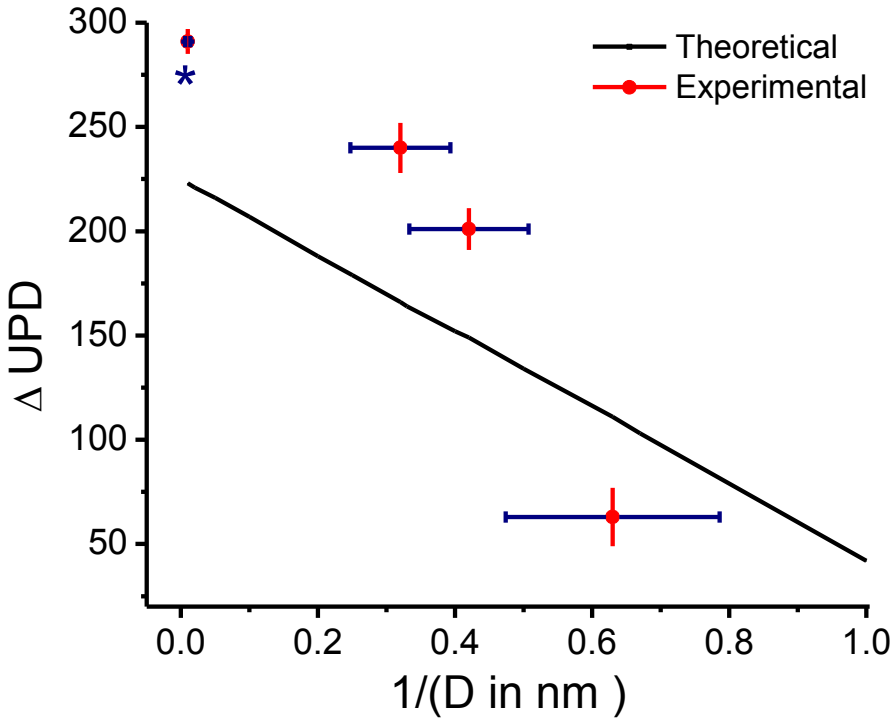

Figure 3.5. Theoretical (Black) and Experimental (Red) UPD Shifts for Size Dependent Cu UPD on Pd NPs. Vertical Error Bars are Standard Deviation from Average UPD Peak Value for Three Measurements. Horizontal Error Bars are Standard Deviation for Nanoparticle Size. Asterisk Symbol Represent UPD Shift Value for Cu on Bulk Pd Electrode Reported by Meyer *et al.* in the Reference 12.

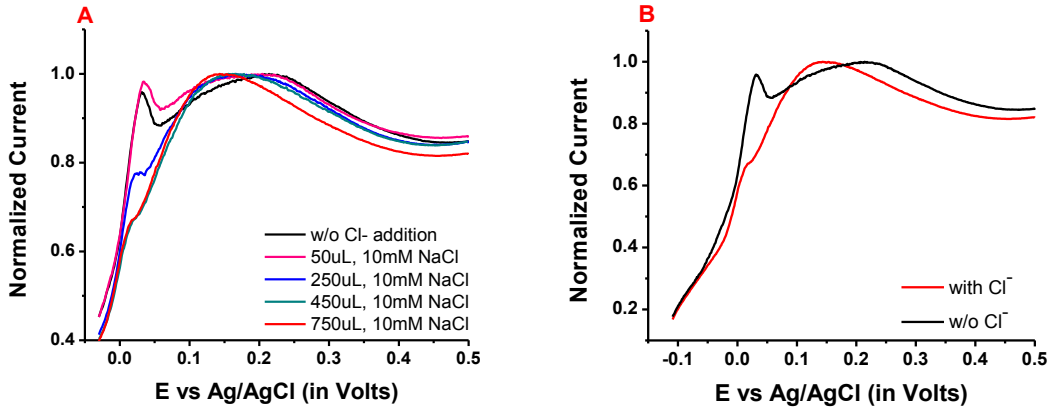

Figure 3.6. Effect of Cl^- Ions on Cu UPD on 50 kDa Pd NPs (Average Diameter 2.4 ± 0.5 nm) **A.** Result of Stepwise Chloride Addition, **B.** Cu UPD with and without Chloride Addition (Black and Red curves from **A**.) Other Conditions as in Fig. 4.

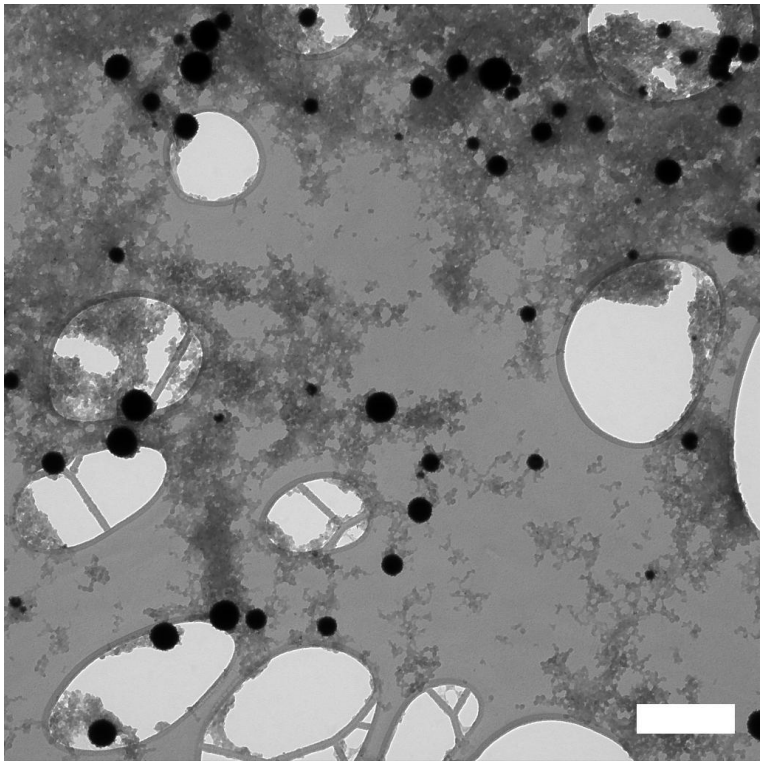

Figure 3.7. TEM of Pd-BCA NPs (Average diameter: 100 ± 38 nm) Used as a Bulk Sample for Size Dependent Study. (Scale Bar: 500 nm)

To understand the influence of BCA ligands on copper UPD at Pd NPs, Cu UPD was performed before and after removing BCA from Pd NPs by electrochemically cycling in the oxide region. As seen in Figure S2, copper deposition was completely blocked in the presence of BCA ligands on the Pd NP surface (black curve). Bulk copper deposition and the Cu UPD peak were observed only after electrochemical removal of BCA ligands from Pd NPs surface (red curve).

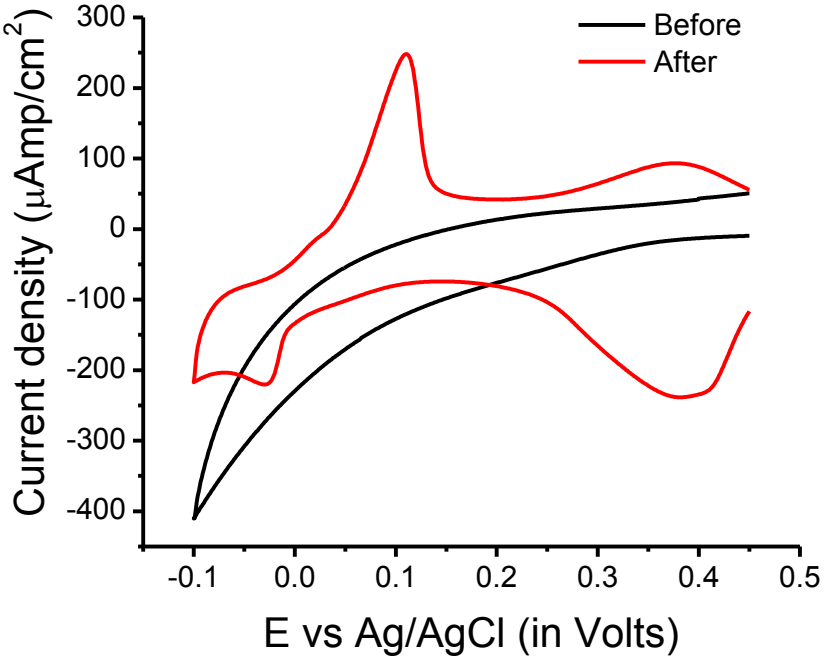

Figure 3.8. UPD of Cu on Pd NPs (Average Size: 98 ± 38 nm) in 0.5 M $NaClO_4$ + 10 mM $HClO_4$ + 1 mM $Cu(ClO_4)_2$. (A). Before Removal of BCA Ligands by Electrochemical Cycling in the Oxide Region (Black Line). (B). After Removal of BCA Ligands by Electrochemical Cycling in the Oxide Region. Scan Rate: 10 mV/sec.

To demonstrate removal of BCA ligands after cycling in the oxide region, SEM-EDS was performed before and after electrochemical cycling in the oxide region. The N/Pd (nitrogen/palladium) ratios before and after electrochemical cycling in oxide region were compared. The observed decrease in N/Pd ratio after electrochemical recycling in 0.5 M $NaClO_4$ + 10 mM $HClO_4$ at 10 mV/sec shows removal of BCA ligands from Pd NPs surface.

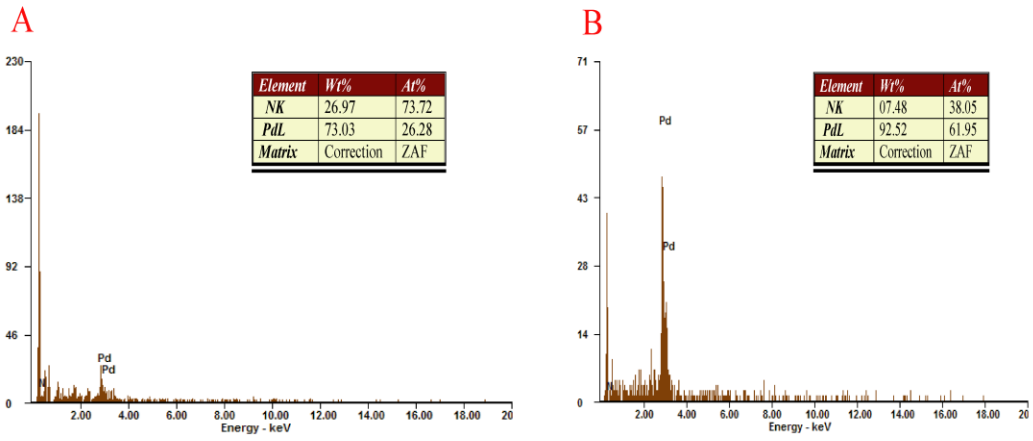

Figure 3.9. EDX of BCA Capped Pd NPs Supported on Glassy Carbon Electrode A) Before Electrochemical Cycling in Oxide Region B) After Electrochemical Cycling in Oxide Region.

3.6. References:

(1) Kolb, D. M.; Przasnyski, M.; Gerischer, H. Underpotential Deposition of Metals and Work Function Differences. *J. Electroanal. Chem. Interfacial Electrochem.* **1974**, *54*, 25–38.

(2) Gerischer, H.; Kolb, D. M.; Przasnyski, M. Chemisorption of Metal Atoms on Metal Surfaces in Correlation to Work Function Differences. *Surf. Sci.* **1974**, *43*, 662–666.

(3) Plieth, W. J. Correlations between the Equilibrium Potential and the Potential of Zero Charge of Metals in Different Modifications. *J. Electroanal. Chem. Interfacial Electrochem.* **1986**, *204*, 343–349.

(4) Plieth, W. J. The Work Function of Small Metal Particles and Its Relation to Electrochemical Properties. *Surf. Sci.* **1985**, *156*, 530–535.

(5) Khoa, N. T.; Kim, S. W.; Yoo, D.-H.; Kim, E. J.; Hahn, S. H. Size-Dependent Work Function and Catalytic Performance of Gold Nanoparticles Decorated Graphene Oxide Sheets. *Appl. Catal. A Gen.* **2014**, *469*, 159–164.

(6) Zhang, Y.; Pluchery, O.; Caillard, L.; Lamic-humblot, A.; Casale, S.; Chabal, Y. J.; Salmeron, M. Sensing the Charge State of Single Gold Nanoparticles via Work Function Measurements. **2015**, *15*, 51-55.

(7) Yancey, D. F.; Carino, E. V; Crooks, R. M. Electrochemical Synthesis and Electrocatalytic Properties of Au@ Pt Dendrimer-Encapsulated Nanoparticles. *J. Am. Chem. Soc.* **2010**, *132*, 10988–10989.

(8) Yu, Y.; Hu, Y.; Liu, X.; Deng, W.; Wang, X. The Study of Pt@Au Electrocatalyst Based on Cu Underpotential Deposition and Pt Redox Replacement. *Electrochim. Acta* **2009**, *54*, 3092–3097.

(9) Jin, Y.; Shen, Y.; Dong, S. Electrochemical Design of Ultrathin Platinum-Coated Gold Nanoparticle Monolayer Films as a Novel Nanostructured Electrocatalyst for Oxygen Reduction. *J. Phys. Chem. B* **2004**, *108*, 8142–8147.

(10) Shao, M. H.; Huang, T.; Liu, P.; Zhang, J.; Sasaki, K.; Vukmirovic, M. B.; Adzic, R. R. Palladium Monolayer and Palladium Alloy Electrocatalysts for Oxygen Reduction Palladium Monolayer and Palladium Alloy Electrocatalysts for Oxygen Reduction. **2006**, *22*, 10409–10415.

(11) Liu, P.; Ge, X.; Wang, R.; Ma, H.; Ding, Y. Facile Fabrication of Ultrathin Pt Overlayers onto Nanoporous Metal Membranes via Repeated Cu UPD and in Situ Redox Replacement Reaction. *Langmuir* **2009**, *25*, 561–567.

(12) Sasaki, K.; Wang, J. X.; Naohara, H.; Marinkovic, N.; More, K.; Inada, H.; Adzic, R. R. Recent Advances in Platinum Monolayer Electrocatalysts for Oxygen Reduction Reaction: Scale-up Synthesis, Structure and Activity of Pt Shells on Pd Cores. *Electrochim. Acta* **2010**, *55*, 2645–2652.

(13) Chierchie, T.; Mayer, C. Voltammetric Study of the Underpotential Deposition of Copper on Polycrystalline and Single Crystal Palladium Surfaces. *Electrochim. Acta* **1988**, *33*, 341–345.

(14) Hölzle, M. H.; Zwing, V.; Kolb, D. M. The Influence of Steps on the Deposition of Cu onto Au(111). *Electrochim. Acta* **1995**, *40*, 1237–1247.

(15) Hachiya, T.; Honbo, H.; Itaya, K. Detailed Underpotential Deposition of Copper on gold(III) in Aqueous Solutions. *J. Electroanal. Chem. Interfacial Electrochem.* **1991**, *315*, 275–291.

(16) Wünsche, M.; Meyer, H.; Schumacher, R. Formation and Properties of UPD Copper Deposits on Polycrystalline Platinum Electrodes. *Electrochim. Acta* **1995**, *40*, 629–635.

(17) Kirowa-Eisner, E.; Bonfil, Y.; Tzur, D.; Gileadi, E. Thermodynamics and Kinetics of Upd of Lead on Polycrystalline Silver and Gold. *J. Electroanal. Chem.* **2003**, *552*, 171–183.

(18) Singh, P.; Buttry, D. a. Comparison of Oxygen Reduction Reaction at Silver Nanoparticles and Polycrystalline Silver Electrodes in Alkaline Solution. *J. Phys. Chem. C* **2012**, *116*, 10656–10663.

(19) Chen, D.;Tao, Q.; Liao, L.W.; Liu, S. X.; Chen, Y. X.; Ye, S. Determining the Active Surface Area for Various Platinum Electrodes. *Electrocatalysis* **2011**, *2*, 207–219.

(20) Carino, E. V; Crooks, R. M. Characterization of Pt @ Cu Core @ Shell Dendrimer-Encapsulated Nanoparticles Synthesized by Cu Underpotential Deposition. *Langmuir* **2011**, *27*, 4227–4235.

(21) Herrero, E.; Buller, L. J.; Abruna, H. D. ChemInform Abstract: Underpotential Deposition at Single Crystal Surfaces of Au, Pt, Ag and Other Materials. *Chem. Rev.* **2001**, *101*, *1897-1930.*, .

(22) Sheng, W.; Chen, S.; Vescovo, E.; Shao-Horn, Y. Size Influence on the Oxygen Reduction Reaction Activity and Instability of Supported Pt Nanoparticles. *J. Electrochem. Soc.* **2012**, *159*, B96-B103..

(23) Lenz, P.; Solomun, T. Underpotential Deposition of Copper on Pd(100): An Electron Spectroscopy Study. *J. Electroanal. Chem.* **1993**, *353*, 131–145.

(24) Solomun, T. Core-Level Analyses of the Copper c(2 × 2) Lattice Formed at Underpotentials on the Pd (100) Surface. *J. Electroanal. Chem. Interfacial Electrochem.* **1989**, *261*, 229–235.

(25) Lu, D.-L.; Ichihara, M.; Tanaka, K.-I. Pt+Cu and Pd+Cu Alloy Particles Formed in the Underpotential Deposition Region of Cu2+ in Perchloric Acid Solution. *Electrochim. Acta* **1998**, *43*, 2325–2330.

(26) Rodríguez-López, M.; Solla-Gullón, J.; Herrero, E.; Tuñón, P.; Feliu, J. M.; Aldaz, A.; Carrasquillo, A. Electrochemical Reactivity of Aromatic Molecules at Nanometer-Sized Surface Domains: From Pt(hkl) Single Crystal Electrodes to Preferentially Oriented Platinum Nanoparticles. *J. Am. Chem. Soc.* **2010**, *132*, 2233–2242.

(27) Sasaki, K.; Mo, Y.; Wang, J. X.; Balasubramanian, M.; Uribe, F.; McBreen, J.; Adzic, R. R. Pt Submonolayers on Metal Nanoparticles—novel Electrocatalysts for H_2 Oxidation and O_2 Reduction. *Electrochim. Acta* **2003**, *48*, 3841–3849.

(28) Gomez, R.; Feliu, J. M.; Abruna, H. D. The Underpotential Deposition of Copper on Pt(311): Site Selective Deposition and Anion Effects. *Langmuir* **1994**, *10*, 4315–4323.

(29) Huang, J.; Zhou, Z.; Song, Y.; Kang, X.; Ke, L.; Chen, S. Electrocatalytic Activity of Palladium Nanocatalysts Supported on Carbon Nanoparticles in Formic Acid Oxidation. *J. Electrochem.* **2012**, *18*, 508-514..

(30) Zhou, Z.; Kang, X.; Song, Y.; Chen, S. Ligand-Mediated Electrocatalytic Activity of Pt Nanoparticles for Oxygen Reduction Reactions. *J. Phys. Chem. C***2012**, 116, 10592-10598.

(31) He, G.; Song, Y.; Kang, X.; Chen, S. Alkyne-Functionalized Palladium Nanoparticles: Synthesis, Characterization, and Electrocatalytic Activity in Ethylene Glycol Oxidation. *Electrochim. Acta* **2013**, *94*, 98–103.

(32) Carino, E. V.; Kim, H. Y.; Henkelman, G.; Crooks, R. M. Site-Selective Cu Deposition on Pt Dendrimer-Encapsulated Nanoparticles: Correlation of Theory and Experiment. *J. Am. Chem. Soc.* **2012**, *134*, 4153–4162.

(33) Kumar, A.; Buttry, D. a. Size-Dependent Anodic Dissolution of Water-Soluble Palladium Nanoparticles. *J. Phys. Chem. C* **2013**, *117*, 26783–26789.

(34) Ivanova, O. S.; Zamborini, F. P. Electrochemical Size Discrimination of Gold Nanoparticles Attached to Glass/indium-Tin-Oxide Electrodes by Oxidation in Bromide-Containing Electrolyte. *Anal. Chem.* **2010**, *82*, 5844–5850.

(35) Olga S. Ivanova; Francis P. Zamborini. Size – Dependent Electrochemical Oxidation of Silver Nanoparticles. *J. Am. Chem. Soc.* **2010**, *132*, 70–72.

(36) Masitas, R. a.; Zamborini, F. P. Oxidation of Highly Unstable <4 Nm Diameter Gold Nanoparticles 850 mV Negative of the Bulk Oxidation Potential. *J. Am. Chem. Soc.* **2012**, *134*, 5014–5017.

(37) Tang, L.; Li, X.; Cammarata, R. C.; Friesen, C.; Sieradzki, K. Electrochemical Stability of Elemental Metal Nanoparticles. *J. Am. Chem. Soc.* **2010**, *132*, 11722–11726.

(38) Plieth, W. J. Electrochemical Properties of Small Clusters of Metal Atoms and Their Role in Surface Enhanced Raman Scattering. *J. Phys. Chem. C* **1982**, *460*, 3166–3170.

(39) Trasatti, S. *Advances in Electrochemistry and Electrochemical Engineering*; Gerischer, H.; Tobias, C. W., Ed.; Wiley-Interscience: New York, 1977.

(40) Woord, D. M. Classical Size Dependent of the Work Function of Small Metallic Spheres. *Phys. Rev. Lett.* **1981**, *46*, 749.

(41) Tyson, W. R.; Miller, W. A. Surface Free Energies of Solid Metals: Estimation from Liquid Surface Tension Measurements. *Surf. Sci.* **1977**, *62*, 267–276.

(42) Markovic, N.; Ross, P. N. The Effect of Specific Adsorption of Ions and Underpotential Deposition of Copper on the Electro-Oxidation of Methanol on Platinum Single-Crystal Surfaces. *J. Electroanal. Chem.* **1992**, *330*, 499–520.

(43) Markovic, N.; Ross, P. N. Effect of Anions on the Underpotential Deposition of Copper on platinum(111) and platinum(100) Surfaces. *Langmuir* **1993**, *9*, 580–590.

(44) Arenz, M.; Stamenkovic, V.; Schmidt, T. J.; Wandelt, K.; Ross, P. .; Markovic, N. M . The Effect of Specific Chloride Adsorption on the Electrochemical Behavior of Ultrathin Pd Films Deposited on Pt(111) in Acid Solution. *Surf. Sci.* **2003**, *523*, 199–209.

(45) Al-Akl, A.; Attard, G. A. Anion Effects in the UPD of Copper on Pd/Pt(111) Bimetallic Electrodes. *J. Phys. Chem. B* **1997**, *101*, 4597–4606.

(46) Mayrhofer, K. J. J.; Blizanac, B. B.; Arenz, M.; Stamenkovic, V. R.; Ross, P. N.; Markovic, N. M. The Impact of Geometric and Surface Electronic Properties of Pt-Catalysts on the Particle Size Effect in Electocatalysis. *J. Phys. Chem. B* **2005**, *109*, 14433–14440.

(47) Arruda, T. M.; Shyam, B.; Ziegelbauer, J. M.; Mukerjee, S.; Ramaker, D. E. Investigation into the Competitive and Site-Specific Nature of Anion Adsorption on Pt Using in Situ X-Ray Absorption Spectroscopy. *J. Phys. Chem. C* **2008**, *112*, 18087–18097.

(48) Nesselberger, M.; Ashton, S.; Meier, J. C.; Katsounaros, I.; Mayrhofer, K. J. J.; Arenz, M. The Particle Size Effect on the Oxygen Reduction Reaction Activity of Pt Catalysts: Influence of Electrolyte and Relation to Single Crystal Models. *J. Am. Chem. Soc.* **2011**, *133*, 17428–17433.

(49) Sattler, M. L.; Ross, P. N. The Surface Structure of Pt Crystallites Supported on Carbon Black. *Ultramicroscopy* **1986**, *20*, 21–28.

CHAPTER 4

Influence of Halide Ions on Anodic Oxidation of Ethanol on Palladium

Ashok Kumar and Daniel A. Buttry*

Department of Chemistry and Biochemistry, Arizona State University

Tempe, Arizona, 85287-1604, United States

Reproduced by permission of Springer Link

Electrocatalysis, 2016, pp 1-6

4.1. Abstract:

Ethanol oxidation on polycrystalline palladium electrodes in alkaline media was studied in the presence of halide ions. Addition of halide ions decreased the ethanol oxidation peak current monotonically as a function of increasing halide concentration. The extent of poisoning was found to be in the order $I^- > Br^- > Cl^-$. Thus, Cl^- ions show appreciable inhibition of ethanol oxidation peak current at $[Cl^-] \sim 10^{-3}$ M whereas Br- and I- inhibit ethanol oxidation even at $[Br^-]$ or $[I^-] \sim 10^{-6}$ M. The potential of the ethanol oxidation peak shifted positive with increasing halide ion concentration. The extent of the shift was found to be in the order $I^- > Br^- > Cl^-$. This study is relevant due to the widespread use of palladium halide complexes in production of Pd electrocatalysts for ethanol oxidation and other electrocatalytic reactions.

4.2. Introduction:

Direct alcohol fuel cells (DAFCs) are electrochemical devices that directly convert chemical energy stored in alcohols into electricity.[1–4] Use of a liquid fuel enables them to be used as small and lightweight power sources,[5–7] without the balance of plant requirements for management of gaseous fuels, such as in hydrogen-based fuel cells. Based on the fuel type DAFCs can be further classified into various types, out of which Direct Ethanol Fuel Cells and Direct Methanol Fuel Cells are quite common and have been extensively studied.[8–11] As compared to the methanol, ethanol as a fuel has negligible toxicity, a lower crossover rate and can be easily produced in large quantity by fermentation of biomass. This helps provide sustainable pathway to commercialization of DEFCs.[12,13]

Based on the electrolyte medium, DEFCs can be further divided into two types: acid-type DEFCs and alkaline-type DEFCs. For acid-type DEFCs, platinum-based electrocatalysts have been studied extensively owing to platinum's high activity in the ethanol oxidation reaction (EOR) in acidic media.[14–17] Common drawbacks associated with Pt-based catalysts are high price, low abundance of Pt and poisoning of the catalyst surface by CO species produced as an intermediate during the EOR in acidic media.[18–21] Among Pt-free electrocatalysts for ethanol oxidation, Pd is not only tolerant against CO poisoning but also shows comparable activity to Pt for ethanol oxidation in alkaline medium despite having poor activity in acidic media. In addition, the cathodic reaction in DEFCs (oxygen reduction) can be catalyzed using non-noble-metal catalysts, such as MnO_2, providing additional cost savings.[22–25] Alkaline conditions provide an

additional advantage over acidic media because of loss of catalyst material via anodic dissolution in acidic media. This can be avoided by using alkaline conditions and electrocatalysts appropriate for such conditions.[26–31]

It is widely appreciated that halides adsorb at Pt and Pd surfaces, and can influence electrocatalytic reactions on these metals. These effects have been well studied for Pt. For example, an early study showed inhibition of ethanol oxidation on Pt by chloride. [32] The extent of inhibition was found to be dependent on the concentration of the chloride ions. In another study, methanol oxidation on Pt electrode in the presence of various anions was studied by voltammetric and radiometric methods.[33] The surface concentrations of adsorbed species on a Pt surface at +0.5 V in presence of different halides were studied using ^{14}C labelled methanol. Competitive adsorption of halide ions decreased the amount of adsorbed species relevant to the methanol oxidation mechanism. In the case of Cl^- ions, surface poisoning was achieved by complete removal of previously adsorbed methanol species by Cl^- ions from the Pt surface. This was different from the cases for Br^- and I^-, where surface poisoning was due to the formation of strongly binding products formed as a result of reaction between adsorbed methanol species and I^- or Br^-. Conway *et al.* studied competitive adsorption between halide ions and OH and O species in the Pt oxide surface film.[34] Further investigation of competitive adsorption isotherms confirmed differences in electrosorption valency (i.e. the degree of charge transfer of the ion to the surface on adsorption) of adsorbed Cl^- compared to Br^- and I^-. Br^- and I^- adsorption isotherms were Langmuirian, whereas Cl^- showed linear logarithmic behavior indicating strong lateral interactions between

adsorbed Cl^-. Breiter and coworkers studied halide adsorption on Pt surfaces in perchloric acid.[35] Cyclic voltammetric studies in 1 M $HClO_4$ solution showed a dependence of double layer capacitance on halide ion concentration in the electrolyte. Impedance studies also were done in 1 M $HClO_4$ medium. They suggested a near monolayer surface coverages of adsorbed halide ions was present at $[Cl^-] \sim 10^{-2}$ M, $[Br^-] \sim 10^{-4}$ M and $[I^-] \sim 10^{-5}$ M.

These past studies and many others reveal a considerable understanding of how halide adsorption can influence interfacial processes at Pt electrode surfaces. In contrast, surprisingly little has been published on halide adsorption at Pd electrodes, especially in the context of the influence of halides on electrocatalytic reactions at Pd. In fact, we are aware of no systematic surveys of this influence. Only a limited number of studies address halide adsorption on Pd. [36–40] Our interest in halide adsorption at Pd also derives from our recent study of the underpotential deposition (UPD) of Cu on Pd nanoparticles.[41] One result of that work was a suggestion that adsorbed Cl^- might have influenced the Cu UPD process, presumably due to adsorption of halide and consequent blocking of UPD sites. Thus, we describe here a survey of the influence of halide adsorption on ethanol oxidation on Pd in an alkaline medium, a model electrocatalytic reaction of considerable recent interest. These results are especially relevant due to the widespread use of halide complexes of Pt and Pd in the synthesis of precious metal catalysts either as a precursor salt of the metal, as a capping ligand or as an etchant to facilitate shape controlled synthesis of metal nanoparticles.[42–46] Understanding the

potentially strong adsorption of halides at Pt and Pd surfaces is key to controlling processes like catalysis and underpotential deposition.[47–49]

4.3. Experimental:

Ethanol (200 proof, ACS reagent, ≥ 99.5%), sodium hydroxide (ACS reagent, ≥ 97.0%), sodium chloride (ACS reagent, ≥ 99%), sodium bromide (BioX, ≥ 99.0%) and sodium iodide (ACS reagent, ≥ 99.5%) were purchased from Sigma-Aldrich and used as received.

All electrochemical measurements were carried out on a CHI 680 potentiostat. Ag/AgCl saturated with 1 M NaCl was used as the reference electrode, while a spiral Pt wire was used as a counter electrode. The reference electrode was isolated from the working electrode compartment. A polycrystalline palladium electrode (3.0 mm diameter) purchased from Bioanalytical Systems, Inc. was used as a working electrode. Preparation included polishing consecutively with 1 μm, 0.3 μm and 0.05 μm alumina powder for 5 minutes each, followed between polishing steps by sonication for 10 minutes in MQ water (Millipore), and ultimately by drying under a nitrogen flow. Nitrogen was purged through all electrolyte solutions before electrochemical measurements, and a nitrogen blanket was maintained over the electrolyte during experiments.

Ethanol oxidation on palladium electrodes was studied in 1 M EtOH + 1 M NaOH electrolyte medium. CV scan were performed for 20 cycles till a constant current density was obtained. Influence of halide ions on ethanol oxidation was studied by adding aliquots of stock halide solutions to the electrolyte solution after attaining constant peak

current in 1 M EtOH and 1 M NaOH. For halide effect studies, 1 M NaCl, 10 mM NaBr and 10 mM NaI were used as stock solutions.

After the addition of halide ions electrolyte was purged with N_2 and stirred for 5 minutes. CV scans were performed under N_2 atmosphere without any stirring.

4.4. Results and Discussion:

To provide a basis for interpretation of the results, we first show the electrochemistry of Pd in 1M NaOH as well as 1M NaOH + 1M EtOH medium. Fig. 4.1A shows the cyclic voltammogram (CV) for a Pd electrode in 1 M NaOH over the range -0.75 V to +0.2 V. During the positive scan, oxidation of the Pd surface starts near -300 mV leading to the formation of surface oxide, PdO, giving rise to feature A1 in the CV. Oxide growth continues up to the positive limit of the scan. During the return scan, the oxide formed during the positive scan is reduced to generate a bare Pd surface, giving rise to the symmetric oxide stripping peak C1 at -300 mV. The features labeled C2 and A2 correspond to hydrogen adsorption/absorption (C2) and desorption (A2).[50] These features are not relevant to the current study and will not be discussed further. In 1 M NaOH containing 1 M EtOH, the initial positive scan produces a large anodic peak, A1, which corresponds to ethanol oxidation.[51,52] The decrease in anodic current positive of this peak is due to oxide growth, which blocks the catalytic surface, making it unavailable for ethanol oxidation.[53,54] During the first return scan, one observes a large anodic peak, C1, which corresponds to further ethanol oxidation that becomes possible as oxide stripping produces a clean, catalytically active Pd surface poised at a potential sufficiently positive to oxidize ethanol.[53,54] A second positive scan produces an anodic peak (A2) significantly larger than the first anodic peak (A1). This is likely due to some cleaning of the Pd surface due to oxide growth and stripping, and has been observed in previous studies .[55] Following the initial scan, the anodic peaks during subsequent positive- and negative-going scans remain constant, indicating a stable, catalytically

active surface. These features are widely observed for alcohol oxidation on metals such as Pd and Pt, and are consistent with many previous studies.

Ethanol oxidation on palladium in alkaline media has been postulated to involve the following steps:[52]

$$CH_3CH_2OH + 3OH^- \leftrightarrow CH_3CO_{ads} + 3H_2O + 3e^- \quad \text{(i)}$$

$$OH^- \leftrightarrow OH_{ads} + e^- \quad \text{(ii)}$$

$$CH_3CO_{ads} + OH_{ads} \rightarrow CH_3COOH \quad \text{(iii)}$$

$$CH_3COOH + OH^- \rightarrow CH_3COO^- + H_2O \quad \text{(iv)}$$

The first step of the EOR corresponds to a dissociative oxidative adsorption of ethanol in the low-potential region leading to a strongly adsorbed ethoxy (CH_3CO) intermediate on the Pd surface sites. This intermediate is thought to suppress the hydrogen adsorption/adsorption peaks.[51] It has also been shown that optimum activity for EOR is function of the relative coverages of CH_3CO_{ads} and OH_{ads}. Thus, when the coverage of OH_{ads} is too high, it blocks the catalytic sites necessary for adsorption to produce CH_3CO_{ads} via reaction (i). When the coverage of OH_{ads} is too low, it is not sufficiently populous to drive reaction (iii).[56] This explanation for the dependence of ethanol oxidation at Pd on [OH^-] suggests that species that can compete for surface adsorption sites might interfere with the catalytic reaction sequence (i) – (iii). Thus, we turn now to an examination of how halides can suppress ethanol oxidation, presumably through adsorption that blocks the catalytically active sites.

To test the dependence of the ethanol oxidation on halide adsorption, we monitored the magnitude of the ethanol oxidation peak, A1, as halide was sequentially added to the solution. Figure 4.2 shows the linear scan voltammograms (LSVs) for the ethanol oxidation peak (A1) at increasing chloride concentrations. The effect of chloride addition is to suppress the ethanol oxidation peak, as well as to shift it in the positive direction. Over the range of concentrations studied (0-110 mM) the anodic peak current decreases by over a factor of five. This indicates substantial suppression of the ethanol oxidation reaction, most likely through adsorption of Cl^- leading to blocking of the catalytically active sites. As shown in a previous study, strong adsorption of Cl^- at Pd surfaces controls hydrogen adsorption (H_{ads}) and hydroxyl adsorption (OH_{ads}) as well as kinetics of CO oxidation.[57] It has also been shown for the case of Pt that specific adsorption of Cl^- ions and the resulting competition between Cl^- and OH^- for Pt surface sites causes the onset for Pt surface oxidation to shift toward more positive potentials.[34] These are both consistent with the present observations for the influence of Cl^- on ethanol oxidation, namely a suppression of the ethanol oxidation current and a positive shift in the feature as [Cl^-] is increased.

Figure 4.3 shows a similar experiment with Br^-, rather than Cl^-, added sequentially to the solution. As can be seen, bromide shows a qualitatively similar behavior. However, suppression of the ethanol oxidation occurs over a much lower concentration range. For example, the concentration of Cl^- necessary for a 50% reduction in the anodic peak current is ca. 25 mM, while for Br^- it is only ca. 50 µM. Thus, Br^- is more than two orders of magnitude more effective as a poison for the ethanol oxidation

reaction compared to Cl^-. Bromide also results in a substantially larger positive shift in the anodic peak. Both effects are consistent with the expected stronger adsorption of Br^- on Pd compared to Cl^-.[34,38]

Figure 4.4 shows the results for the case of I^- addition to the solution. The data show that I^- has the strongest effect of the halides, producing the strongest suppression of the anodic peak and the largest positive potential shifts for the anodic peak with $[I^-]$. For this case, only a 10 μM concentration of I^- is needed to reduce the anodic peak current by 50%, making I^- roughly five times more effective as a poison than Br^- and 2,500x more effective than Cl^-.

Figure 4.5 summarizes the results presented above. It shows a plot of the relative decrease in anodic peak current density as a function of the logarithm of the halide concentration for each of the halides studied. These data are consistent with the expectation that the adsorption strength for these halides should follow the trend $I^- > Br^- > Cl^-$, as has been observed for halide adsorption on Au(111).[34,38] Interestingly, for both Cl^- and Br^-, the suppression of ethanol oxidation saturates at higher concentrations. In other words, above a certain concentration, further addition of Cl^- or Br^- does not cause additional decreases in the anodic peak current. This manifests as a roll-off, or saturation, of the curves for these two species in Figure 4.5. This may be due to the achievement of saturation surface coverages for these species at a coverage below the closest-packed condition. This might leave a subset of surface sites available for ethanol oxidation, even at very high concentrations. Such an explanation would be consistent with electrosorption valency arguments, since the electrosorption valencies follow the trend $I^- > Br^- > Cl^-$,

meaning that iodide is the most fully discharged in its adsorbed state (i.e. has the lowest negative charge). [34,38]

4.5. Conclusions:

We have shown that halides are effective poisons for the ethanol oxidation reaction at Pd electrodes under alkaline conditions. The trends observed are consistent with expectations for the strength of adsorption and electrosorption valencies on Pd expected for the three halides studied: $I^- > Br^- > Cl^-$. Significant inhibition of the EOR can occur with iodide concentrations at low as a few tens of micromolar. The results are relevant to the use of Pd in DEFCs, especially when halide precursors are used for catalyst preparation.

FIGURES

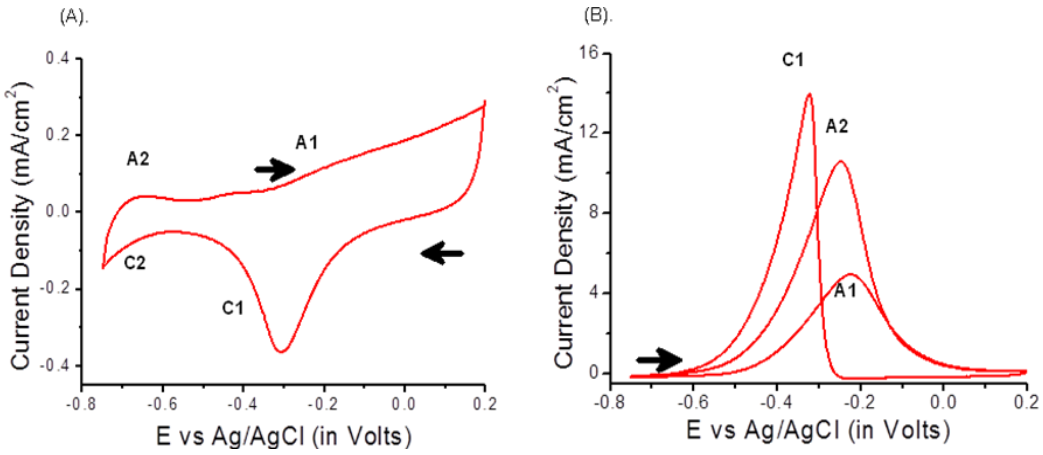

Figure 4.1. CV of Palladium Electrode a). 1 M NaOH b). 1 M NaOH + 1 M EtOH. Scan Rate = 100 mV/s.

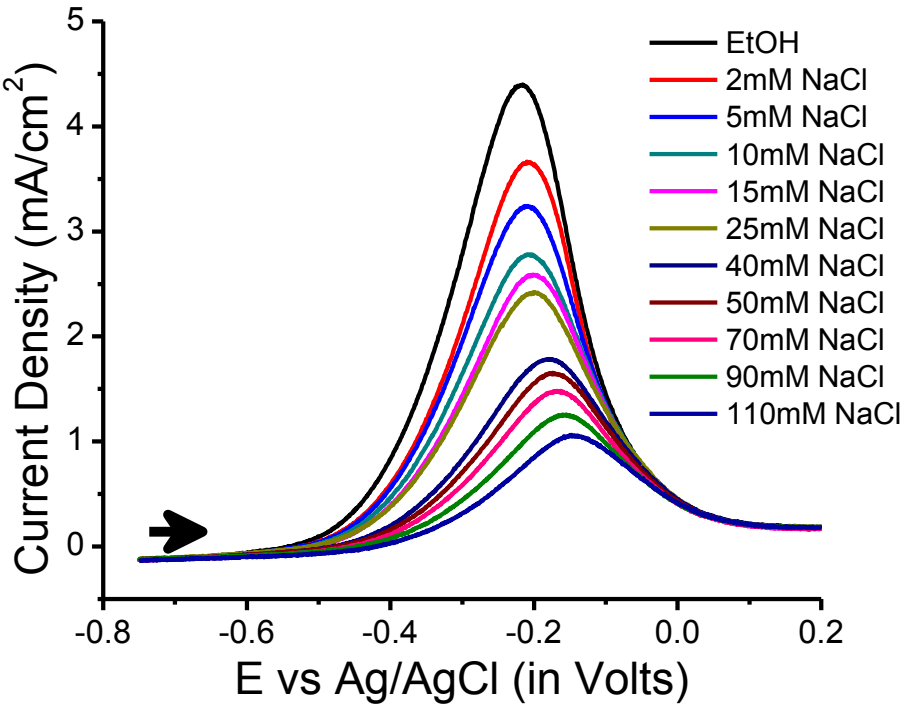

Figure 4.2. LSV Showing Influence of [Cl^-] on Ethanol Oxidation on Palladium. Electrolyte: 1 M NaOH + 1 M EtOH Solution. Scan Rate = 100 mV/s. Influence of [Cl^-] was Studied by Stepwise Addition of Different Aliquots of 1 M NaCl Stock Solution to the Electrolyte Solution to Produce the Final Concentrations Shown.

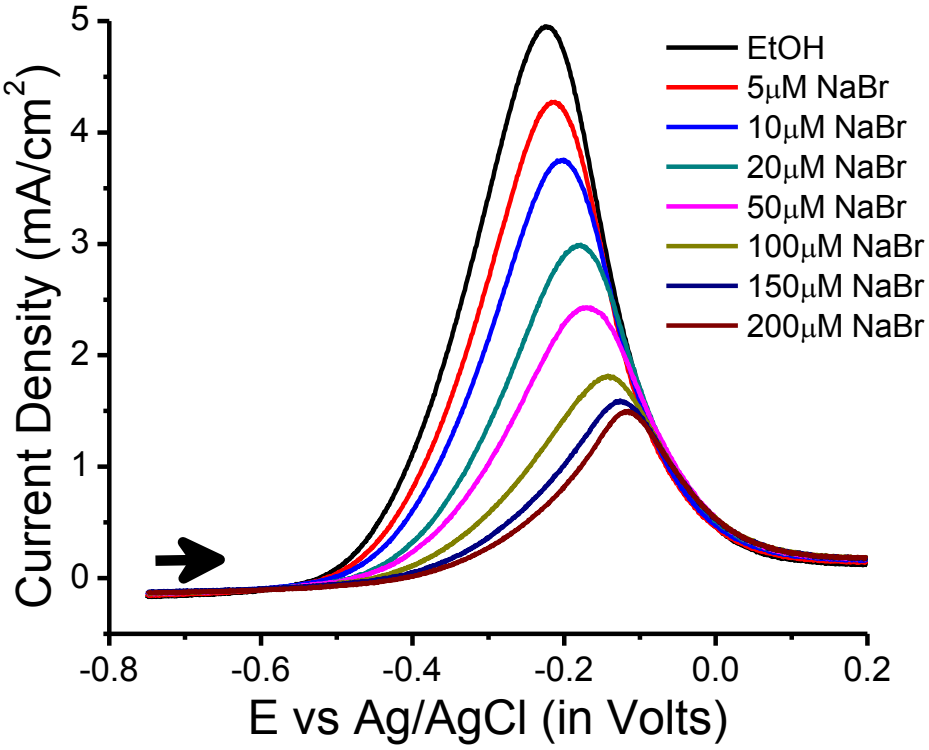

Figure 4.3. LSV Showing Influence of [Br^-] on Ethanol Oxidation on Palladium. Electrolyte: 1 M NaOH + 1 M EtOH. Scan Rate = 100 mV/s. Influence of [Br^-] was Studied by Stepwise Addition of Different Aliquots of 1 mM NaBr Stock Solution to the Electrolyte Solution to Produce the Final Concentrations Shown.

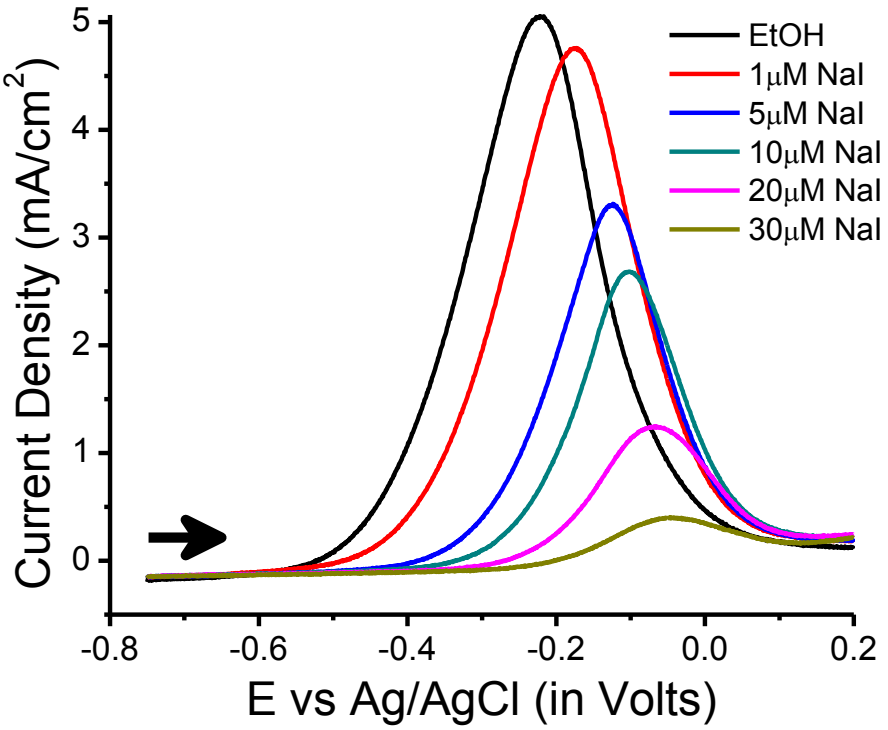

Figure 4.4. LSV Showing Influence of [I^-] on Ethanol Oxidation on Palladium. Electrolyte: 1 M NaOH + 1 M EtOH. Scan Rate = 100 mV/s. Influence of [I^-] was Studied by Stepwise Addition of Different Aliquots of 10 mM NaI Stock Solution to the Electrolyte Solution to Produce the Final Concentrations Shown.

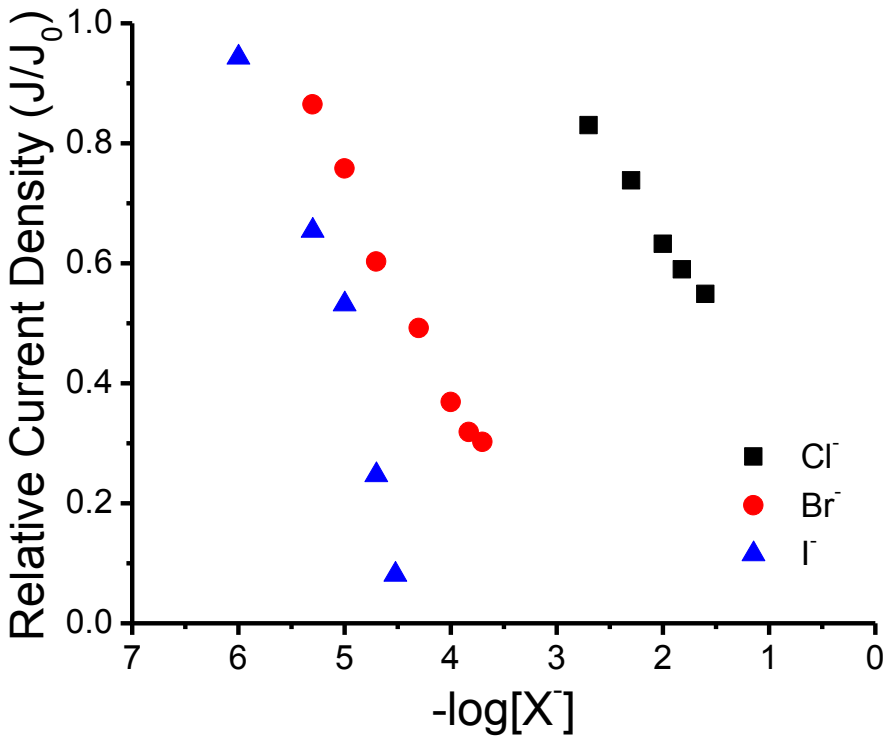

Figure 4.5. Plot of the Relative Decrease in Anodic Peak Current for Ethanol Oxidation versus Log[X^-] for Each of the Halides.

4.6. References:

[1] E. Antolini, E.R. Gonzalez, Alkaline direct alcohol fuel cells, J. Power Sources. 195 (2010) 3431–3450. doi:10.1016/j.jpowsour.2009.11.145.

[2] C. Lamy, A. Lima, V. LeRhun, F. Delime, C. Coutanceau, J.-M. Léger, Recent advances in the development of direct alcohol fuel cells (DAFC), J. Power Sources. 105 (2002) 283–296. doi:10.1016/S0378-7753(01)00954-5.

[3] D.M. Mackie, S. Liu, M. Benyamin, R. Ganguli, J.J. Sumner, Direct utilization of fermentation products in an alcohol fuel cell, J. Power Sources. 232 (2013) 34–41. doi:10.1016/j.jpowsour.2013.01.077.

[4] H. Tang, S. Wang, M. Pan, S.P. Jiang, Y. Ruan, Performance of direct methanol fuel cells prepared by hot-pressed MEA and catalyst-coated membrane (CCM), Electrochim. Acta. 52 (2007) 3714–3718. doi:10.1016/j.electacta.2006.10.053.

[5] M. Baldauf, W. Preidel, Status of the development of a direct methanol fuel cell, J. Power Sources. 84 (1999) 161–166. doi:10.1016/S0378-7753(99)00332-8.

[6] V.. Barragán, A. Heinzel, Estimation of the membrane methanol diffusion coefficient from open circuit voltage measurements in a direct methanol fuel cell, J. Power Sources. 104 (2002) 66–72. doi:10.1016/S0378-7753(01)00896-5.

[7] A.M. Zainoodin, S.K. Kamarudin, W.R.W. Daud, Electrode in direct methanol fuel cells, Int. J. Hydrogen Energy. 35 (2010) 4606–4621. doi:10.1016/j.ijhydene.2010.02.036.

[8] S. Song, W. Zhou, J. Tian, R. Cai, G. Sun, Q. Xin, *et al*., Ethanol crossover phenomena and its influence on the performance of DEFC, J. Power Sources. 145 (2005) 266–271. doi:10.1016/j.jpowsour.2004.12.065.

[9] T. Schaffer, V. Hacker, J.O. Besenhard, Innovative system designs for DMFC, J. Power Sources. 153 (2006) 217–227. doi:10.1016/j.jpowsour.2005.05.080.

[10] L. An, T.S. Zhao, R. Chen, Q.X. Wu, A novel direct ethanol fuel cell with high power density, J. Power Sources. 196 (2011) 6219–6222. doi:10.1016/j.jpowsour.2011.03.040.

[11] S. Sharma, B.G. Pollet, Support materials for PEMFC and DMFC electrocatalysts—A review, J. Power Sources. 208 (2012) 96–119. doi:10.1016/j.jpowsour.2012.02.011.

[12] S. Song, P. Tsiakaras, Recent progress in direct ethanol proton exchange membrane fuel cells (DE-PEMFCs), Appl. Catal. B Environ. 63 (2006) 187–193. doi:10.1016/j.apcatb.2005.09.018.

[13] E. Antolini, Catalysts for direct ethanol fuel cells, J. Power Sources. 170 (2007) 1–12. doi:10.1016/j.jpowsour.2007.04.009.

[14] S. Chen, M. Schell, Bistability and excitability in the electrochemical oxidation of ethanol, Electrochim. Acta. 44 (1999) 4773–4780. doi:10.1016/S0013-4686(99)00263-7.

[15] S. Chen, M. Schell, A comparison of multistability in the electrocatalyzed oxidations of methanol and ethanol in acid and alkaline solutions, J. Electroanal. Chem. 478 (1999) 108–117. doi:10.1016/S0022-0728(99)00421-0.

[16] C. Xu, P.K. Shen, X. Ji, R. Zeng, Y. Liu, Enhanced activity for ethanol electrooxidation on Pt–MgO/C catalysts, Electrochem. Commun. 7 (2005) 1305–1308. doi:10.1016/j.elecom.2005.09.015.

[17] Z.D. Wei, L.L. Li, Y.H. Luo, C. Yan, C.X. Sun, G.Z. Yin, *et al*., Electrooxidation of methanol on upd-Ru and upd-Sn modified Pt electrodes, J. Phys. Chem. B. 110 (2006) 26055–26061. doi:10.1021/jp0651891.

[18] J.S. Spendelow, G.Q. Lu, P.J.A. Kenis, A. Wieckowski, Electrooxidation of adsorbed CO on Pt(111) and Pt(111)/Ru in alkaline media and comparison with results from acidic media, J. Electroanal. Chem. 568 (2004) 215–224. doi:10.1016/j.jelechem.2004.01.018.

[19] S. Song, W. Zhou, Z. Liang, R. Cai, G. Sun, Q. Xin, *et al*., The effect of methanol and ethanol cross-over on the performance of PtRu/C-based anode DAFCs, Appl. Catal. B Environ. 55 (2005) 65–72. doi:10.1016/j.apcatb.2004.05.017.

[20] W.J. Zhou, S.Q. Song, W.Z. Li, Z.H. Zhou, G.Q. Sun, Q. Xin, *et al*., Direct ethanol fuel cells based on PtSn anodes: the effect of Sn content on the fuel cell performance, J. Power Sources. 140 (2005) 50–58. doi:10.1016/j.jpowsour.2004.08.003.

[21] C. Coutanceau, L. Demarconnay, C. Lamy, J.-M. Léger, Development of electrocatalysts for solid alkaline fuel cell (SAFC), J. Power Sources. 156 (2006) 14–19. doi:10.1016/j.jpowsour.2005.08.035.

[22] W. Xiao, D. Wang, X.W. Lou, Shape-Controlled Synthesis of MnO_2 Nanostructures with Enhanced Electrocatalytic Activity for Oxygen Reduction, J. Phys. Chem. C. 114 (2010) 1694–1700. doi:10.1021/jp909386d.

[23] F. Cheng, Y. Su, J. Liang, Z. Tao, J. Chen, MnO_2-based nanostructures as catalysts for electrochemical oxygen reduction in alkaline media, Chem. Mater. 22 (2010) 898–905. doi:10.1021/cm901698s.

[24] C. Shi, G.L. Zang, Z. Zhang, G.P. Sheng, Y.X. Huang, G.X. Zhao, *et al*., Synthesis of layered MnO_2 nanosheets for enhanced oxygen reduction reaction catalytic activity, Electrochim. Acta. 132 (2014) 239–243. doi:10.1016/j.electacta.2014.03.150.

[25] C. Wei, L. Yu, C. Cui, J. Lin, C. Wei, N. Mathews, *et al*., Ultrathin MnO_2 nanoflakes as efficient catalysts for oxygen reduction reaction., Chem. Commun. (Camb). 50 (2014) 7885–8. doi:10.1039/c4cc02781g.

[26] D.A.J. Rand, R. Woods, A study of the dissolution of platinum, palladium, rhodium and gold electrodes in 1 M sulphuric acid by cyclic voltammetry, J. Electroanal. Chem. Interfacial Electrochem. 35 (1972) 209–218. doi:10.1016/S0022-0728(72)80308-5.

[27] P.J. Kulesza, W. Lu, L.R. Faulkner, Cathodic fabrication of platinum microparticles via anodic dissolution of a platinum counter-electrode: Electrocatalytic probing and surface analysis of dispersed platinum, J. Electroanal. Chem. 336 (1992) 35–44. doi:10.1016/0022-0728(92)80260-B.

[28] M. Tian, B.E. Conway, Electrocatalysis in oscillatory kinetics of anodic oxidation of formic acid: At Pt; nanogravimetry and voltammetry studies on the role of reactive surface oxide, J. Electroanal. Chem. 616 (2008) 45–56. doi:10.1016/j.jelechem.2007.12.016.

[29] Y. Sugawara, A.P. Yadav, A. Nishikata, T. Tsuru, Dissolution and surface area loss of platinum nanoparticles under potential cycling, J. Electroanal. Chem. 662 (2011) 379–383. doi:10.1016/j.jelechem.2011.09.009.

[30] A. Kumar, D. A. Buttry, Size-dependent anodic dissolution of water-soluble palladium nanoparticles, J. Phys. Chem. C. 117 (2013) 26783–26789. doi:10.1021/jp408394h.

[31] S.A. Grigoriev, K.A. Dzhus, D.G. Bessarabov, P. Millet, Failure of PEM water electrolysis cells: Case study involving anode dissolution and membrane thinning, Int. J. Hydrogen Energy. 39 (2014) 20440–20446. doi:10.1016/j.ijhydene.2014.05.043.

[32] K.D. Snell, A.G. Keenan, Chloride inhibition of ethanol electrooxidation at a platinum electrode in aqueous acid solution, Electrochim. Acta. 26 (1981) 1339–1344. doi:10.1016/0013-4686(81)85119-5.

[33] J. Sobkowski, A. Wieckowski, The influence of halide ions on methanol adsorption and oxidation on a platinized electrode, J. Electroanal. Chem. Interfacial Electrochem. 41 (1973) 373–379. doi:10.1016/S0022-0728(73)80416-4.

[34] D.M. Novak, B.E. Conway, Competitive adsorption and state of charge of halide ions in monolayer oxide film growth processes at Pt anodes, J. Chem. Soc. Faraday Trans. 1. 77 (1981) 2341. doi:10.1039/f19817702341.

[35] M.W. Breiter, Voltammetric study of halide ion adsorption on platinum in perchloric acid solutions, Electrochim. Acta. 8 (1963) 925–935. doi:10.1016/0013-4686(62)87047-9.

[36] K. Sashikata, Y. Matsui, K. Itaya, M.P. Soriaga, Adsorbed-Iodine-Catalyzed Dissolution of Pd Single-Crystal Electrodes: Studies by Electrochemical Scanning Tunneling Microscopy, J. Phys. Chem. 100 (1996) 20027–20034. doi:10.1021/jp9620532.

[37] J.F. Rodriguez, T. Mebrahtu, M.P. Soriaga, The interaction of I_2(g), HI(g) and KI(aq) with Pd (111) electrode surfaces, J. Electroanal. Chem. Interfacial Electrochem. 264 (1989) 291–296. doi:10.1016/0022-0728(89)80164-0.

[38] J. Lipkowski, Z. Shi, A. Chen, B. Pettinger, C. Bilger, Ionic adsorption at the Au(111) electrode, Electrochim. Acta. 43 (1998) 2875–2888. doi:10.1016/S0013-4686(98)00028-0.

[39] Y.-G. Kim, J.H. Baricuatro, M.P. Soriaga, D. Wayne Suggs, Adsorbate-induced disorder-to-order surface reconstruction: iodine on Pd(111) revisited by EC-STM, J. Electroanal. Chem. 509 (2001) 170–174. doi:10.1016/S0022-0728(01)00514-9.

[40] J.A. Schimpf, J.B. Abreu, M.P. Soriaga, Electrochemical regeneration of clean and ordered Pd(100) surfaces by iodine adsorption-desorption: evidence from low-energy electron diffraction, J. Electroanal. Chem. 364 (1994) 247–249. doi:10.1016/0022-0728(93)02916-6.

[41] A. Kumar, D. A. Buttry, Size-Dependent Underpotential Deposition of Copper on Palladium Nanoparticles, J. Phys. Chem. C. (2015). doi:10.1021/acs.jpcc.5b03361.

[42] W. Niu, L. Zhang, G. Xu, Shape-controlled synthesis of single-crystalline palladium nanocrystals, ACS Nano. 4 (2010) 1987–1996. doi:10.1021/nn100093y.

[43] S.E. Lohse, N.D. Burrows, L. Scarabelli, L.M. Liz-Marzán, C.J. Murphy, Anisotropic noble metal nanocrystal growth: The role of halides, Chem. Mater. 26 (2014) 34–43. doi:10.1021/cm402384j.

[44] J. Zhang, C. Feng, Y. Deng, L. Liu, Y. Wu, B. Shen, *et al*., Shape-controlled synthesis of palladium single-crystalline nanoparticles: The effect of HCl oxidative etching and facet-dependent catalytic properties, Chem. Mater. 26 (2014) 1213–1218. doi:10.1021/cm403591g.

[45] R. Long, S. Zhou, B.J. Wiley, Y. Xiong, Oxidative etching for controlled synthesis of metal nanocrystals: atomic addition and subtraction., Chem. Soc. Rev. 43 (2014) 6288–310. doi:10.1039/c4cs00136b.

[46] Y. Xiong, H. Cai, B.J. Wiley, J. Wang, M.J. Kim, Y. Xia, Synthesis and mechanistic study of palladium nanobars and nanorods, J. Am. Chem. Soc. 129 (2007) 3665–3675. doi:10.1021/ja0688023.

[47] C.F. Zinola, a M.C. Luna, The Influence of Iodide Adsorption on Copper Underpotential Deposition on Polycrystalline Palladium Electrodes in Mildly Acidic Solutions, 397 (1999) 392–397. doi:10.1006/jcis.1998.5901.

[48] T.J. Schmidt, U.A. Paulus, H.A. Gasteiger, R.J. Behm, The oxygen reduction reaction on a Pt / carbon fuel cell catalyst in the presence of chloride anions, 508 (2001) 41–47.

[49] T.M. Arruda, B. Shyam, J.M. Ziegelbauer, S. Mukerjee, D.E. Ramaker, Investigation into the Competitive and Site-Specific Nature of Anion Adsorption on Pt Using In Situ X-ray Absorption Spectroscopy, (2008) 18087–18097.

[50] G. Denuault, C. Milhano, D. Pletcher, Mesoporous palladium-the surface electrochemistry of palladium in aqueous sodium hydroxide and the cathodic reduction of nitrite., Phys. Chem. Chem. Phys. 7 (2005) 3545–3551. doi:10.1039/b508835f.

[51] Z.X. Liang, T.S. Zhao, J.B. Xu, L.D. Zhu, Mechanism study of the ethanol oxidation reaction on palladium in alkaline media, Electrochim. Acta. 54 (2009) 2203–2208. doi:10.1016/j.electacta.2008.10.034.

[52] J. Liu, J. Ye, C. Xu, S.P. Jiang, Y. Tong, Kinetics of ethanol electrooxidation at Pd electrodeposited on Ti, Electrochem. Commun. 9 (2007) 2334–2339. doi:10.1016/j.elecom.2007.06.036.

[53] M. Grdeń, J. Kotowski, A. Czerwiński, The study of electrochemical palladium behavior using the quartz crystal microbalance, J. Solid State Electrochem. 4 (2000) 273–278. doi:10.1007/s100080050204.

[54] M.-C. Jeong, Voltammetric Studies on the Palladium Oxides in Alkaline Media, J. Electrochem. Soc. 140 (1993) 1986. doi:10.1149/1.2220750.

[55] S. Ghosh, H. Remita, P. Kar, S. Choudhury, S. Sardar, P. Beaunier, *et al*., Facile synthesis of Pd nanostructures in hexagonal mesophases as a promising electrocatalyst for ethanol oxidation, J. Mater. Chem. A. 3 (2015) 9517–9527. doi:10.1039/C5TA00923E.

[56] S. Sen Gupta, J. Datta, Electrode kinetics of ethanol oxidation on novel CuNi alloy supported catalysts synthesized from PTFE suspension, J. Power Sources. 145 (2005) 124–132. doi:10.1016/j.jpowsour.2005.01.066.

[57] M. Arenz, V. Stamenkovic, T.J. Schmidt, K. Wandelt, P.N. Ross, N.M. Markovic, The effect of specific chloride adsorption on the electrochemical behavior of ultrathin Pd films deposited on Pt(111) in acid solution, Surf. Sci. 523 (2003) 199–209. doi:10.1016/S0039-6028(02)02456-1.

APPENDIX A

COPYRIGHT PERMISSION

A. Copyright permission for figure 1.2.

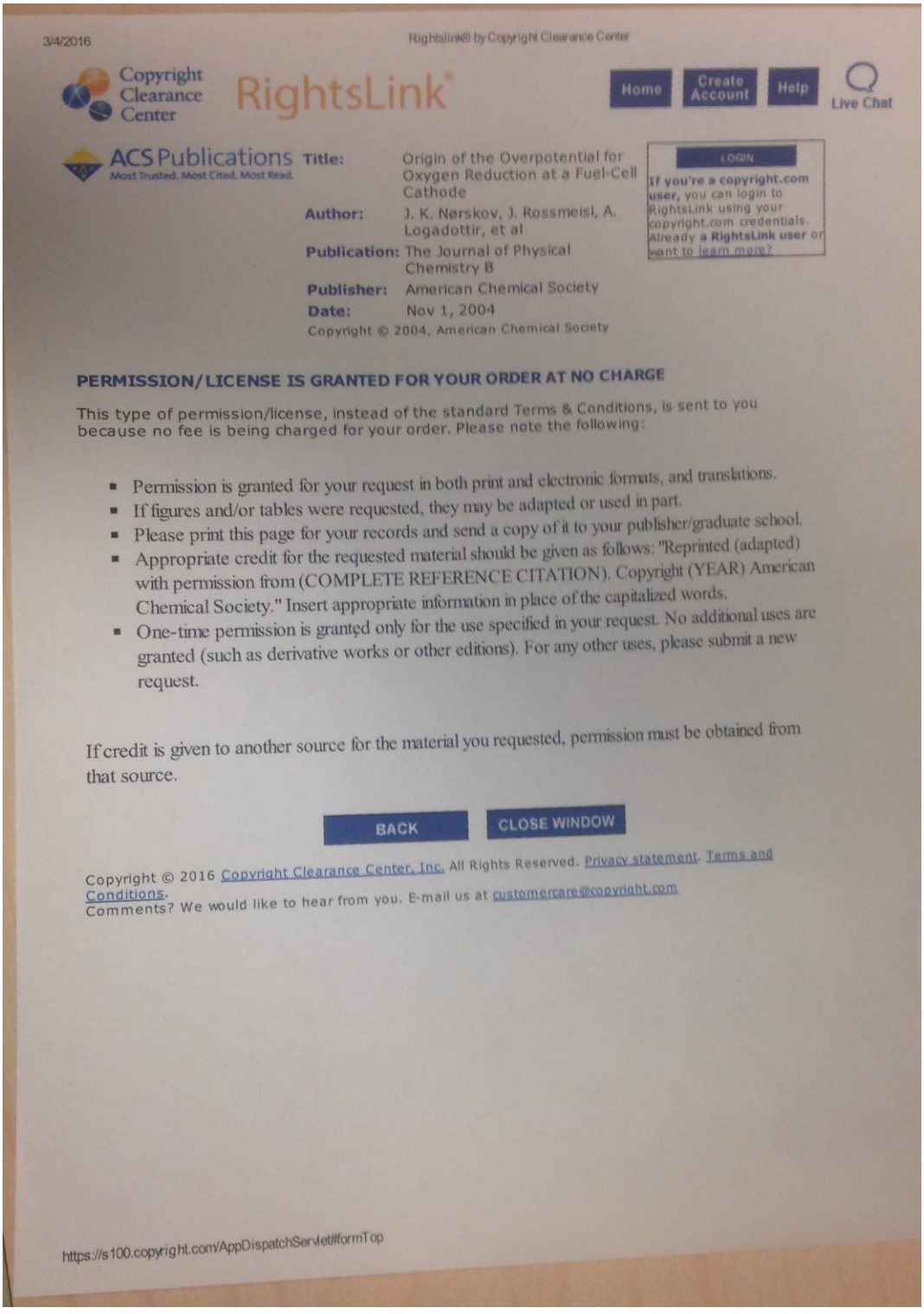

3/4/2016 Rightslink® by Copyright Clearance Center

Copyright Clearance Center RightsLink®

Home | Create Account | Help | Live Chat

ACS Publications
Most Trusted. Most Cited. Most Read.

Title: Origin of the Overpotential for Oxygen Reduction at a Fuel-Cell Cathode
Author: J. K. Nørskov, J. Rossmeisl, A. Logadottir, et al
Publication: The Journal of Physical Chemistry B
Publisher: American Chemical Society
Date: Nov 1, 2004
Copyright © 2004, American Chemical Society

LOGIN
If you're a copyright.com user, you can login to RightsLink using your copyright.com credentials. Already a RightsLink user or want to learn more?

PERMISSION/LICENSE IS GRANTED FOR YOUR ORDER AT NO CHARGE

This type of permission/license, instead of the standard Terms & Conditions, is sent to you because no fee is being charged for your order. Please note the following:

- Permission is granted for your request in both print and electronic formats, and translations.
- If figures and/or tables were requested, they may be adapted or used in part.
- Please print this page for your records and send a copy of it to your publisher/graduate school.
- Appropriate credit for the requested material should be given as follows: "Reprinted (adapted) with permission from (COMPLETE REFERENCE CITATION). Copyright (YEAR) American Chemical Society." Insert appropriate information in place of the capitalized words.
- One-time permission is granted only for the use specified in your request. No additional uses are granted (such as derivative works or other editions). For any other uses, please submit a new request.

If credit is given to another source for the material you requested, permission must be obtained from that source.

BACK CLOSE WINDOW

Copyright © 2016 Copyright Clearance Center, Inc. All Rights Reserved. Privacy statement. Terms and Conditions.
Comments? We would like to hear from you. E-mail us at customercare@copyright.com

https://s100.copyright.com/AppDispatchServlet#formTop

B. Copyright permission for figure 1.3.

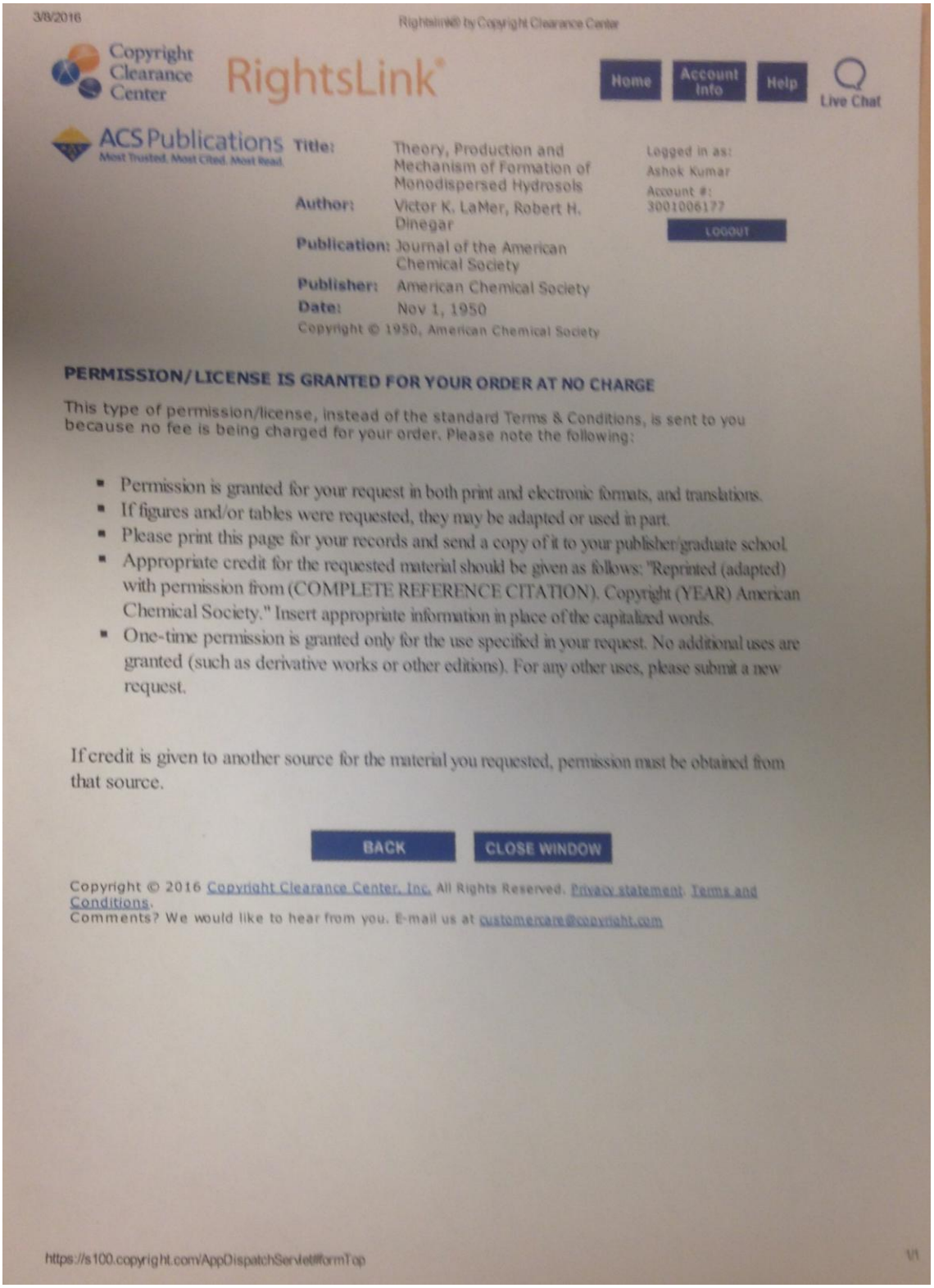

3/8/2016 RightsLink® by Copyright Clearance Center

Copyright Clearance Center RightsLink®

Home | Account Info | Help | Live Chat

ACS Publications Most Trusted. Most Cited. Most Read.

Title: Theory, Production and Mechanism of Formation of Monodispersed Hydrosols

Author: Victor K. LaMer, Robert H. Dinegar

Publication: Journal of the American Chemical Society

Publisher: American Chemical Society

Date: Nov 1, 1950

Copyright © 1950, American Chemical Society

Logged in as: Ashok Kumar
Account #: 3001006177
LOGOUT

PERMISSION/LICENSE IS GRANTED FOR YOUR ORDER AT NO CHARGE

This type of permission/license, instead of the standard Terms & Conditions, is sent to you because no fee is being charged for your order. Please note the following:

- Permission is granted for your request in both print and electronic formats, and translations.
- If figures and/or tables were requested, they may be adapted or used in part.
- Please print this page for your records and send a copy of it to your publisher/graduate school.
- Appropriate credit for the requested material should be given as follows: "Reprinted (adapted) with permission from (COMPLETE REFERENCE CITATION). Copyright (YEAR) American Chemical Society." Insert appropriate information in place of the capitalized words.
- One-time permission is granted only for the use specified in your request. No additional uses are granted (such as derivative works or other editions). For any other uses, please submit a new request.

If credit is given to another source for the material you requested, permission must be obtained from that source.

BACK | CLOSE WINDOW

Copyright © 2016 Copyright Clearance Center, Inc. All Rights Reserved. Privacy statement. Terms and Conditions.
Comments? We would like to hear from you. E-mail us at customercare@copyright.com

https://s100.copyright.com/AppDispatchServlet#formTop 1/1

C. Copyright permission for chapter 2.

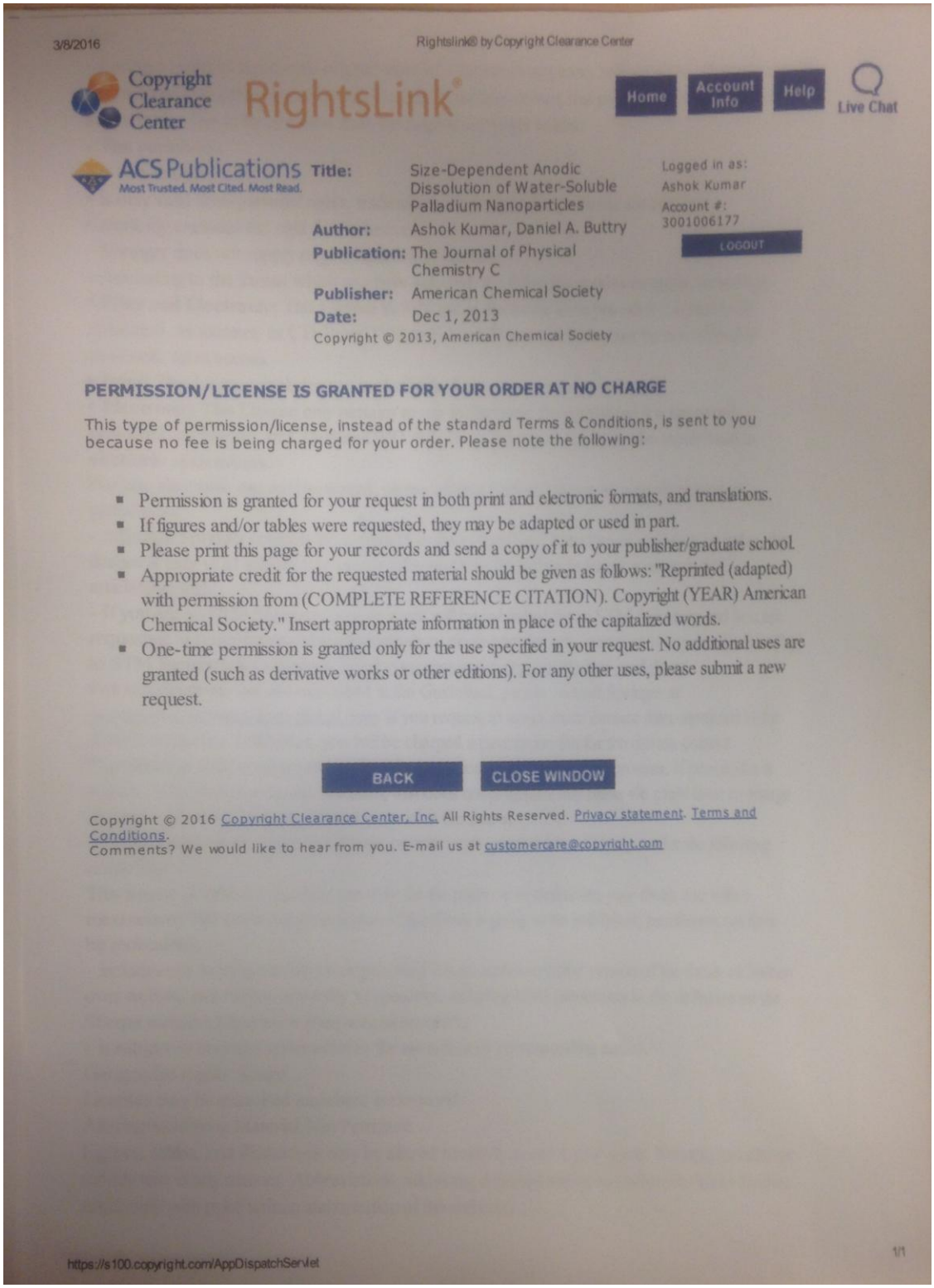

3/8/2016 Rightslink® by Copyright Clearance Center

Copyright Clearance Center RightsLink®

Home | Account Info | Help | Live Chat

ACS Publications Most Trusted. Most Cited. Most Read.

Title: Size-Dependent Anodic Dissolution of Water-Soluble Palladium Nanoparticles

Author: Ashok Kumar, Daniel A. Buttry

Publication: The Journal of Physical Chemistry C

Publisher: American Chemical Society

Date: Dec 1, 2013

Copyright © 2013, American Chemical Society

Logged in as: Ashok Kumar
Account #: 3001006177
LOGOUT

PERMISSION/LICENSE IS GRANTED FOR YOUR ORDER AT NO CHARGE

This type of permission/license, instead of the standard Terms & Conditions, is sent to you because no fee is being charged for your order. Please note the following:

- Permission is granted for your request in both print and electronic formats, and translations.
- If figures and/or tables were requested, they may be adapted or used in part.
- Please print this page for your records and send a copy of it to your publisher/graduate school.
- Appropriate credit for the requested material should be given as follows: "Reprinted (adapted) with permission from (COMPLETE REFERENCE CITATION). Copyright (YEAR) American Chemical Society." Insert appropriate information in place of the capitalized words.
- One-time permission is granted only for the use specified in your request. No additional uses are granted (such as derivative works or other editions). For any other uses, please submit a new request.

BACK CLOSE WINDOW

Copyright © 2016 Copyright Clearance Center, Inc. All Rights Reserved. Privacy statement. Terms and Conditions.
Comments? We would like to hear from you. E-mail us at customercare@copyright.com

https://s100.copyright.com/AppDispatchServlet 1/1

D. Copyright permission for chapter 3.

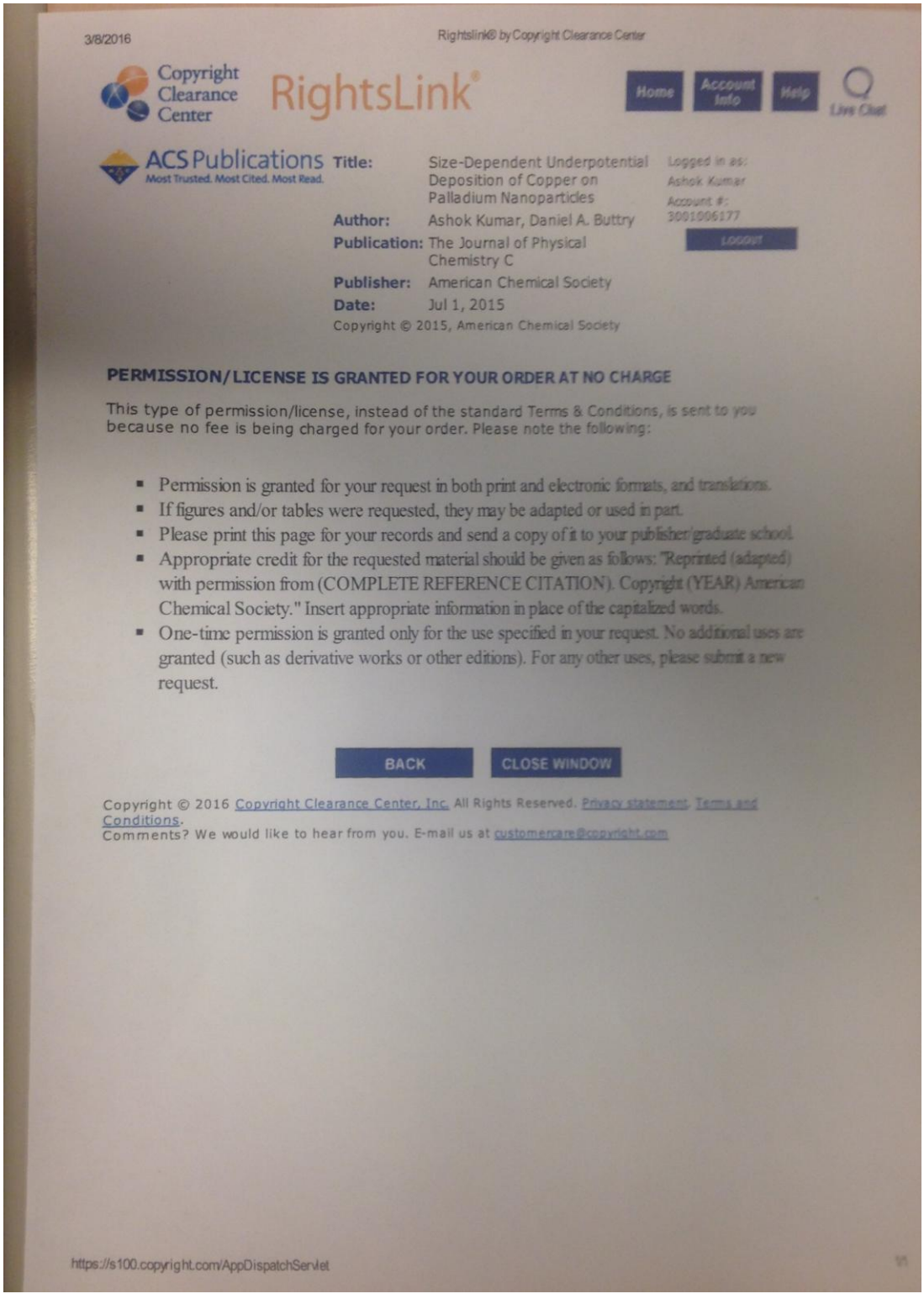

3/8/2016 Rightslink® by Copyright Clearance Center

Copyright Clearance Center RightsLink®

Home | Account Info | Help | Live Chat

ACS Publications Most Trusted. Most Cited. Most Read.

Title: Size-Dependent Underpotential Deposition of Copper on Palladium Nanoparticles

Author: Ashok Kumar, Daniel A. Buttry

Publication: The Journal of Physical Chemistry C

Publisher: American Chemical Society

Date: Jul 1, 2015

Copyright © 2015, American Chemical Society

Logged in as: Ashok Kumar
Account #: 3001006177
LOGOUT

PERMISSION/LICENSE IS GRANTED FOR YOUR ORDER AT NO CHARGE

This type of permission/license, instead of the standard Terms & Conditions, is sent to you because no fee is being charged for your order. Please note the following:

- Permission is granted for your request in both print and electronic formats, and translations.
- If figures and/or tables were requested, they may be adapted or used in part.
- Please print this page for your records and send a copy of it to your publisher/graduate school.
- Appropriate credit for the requested material should be given as follows: "Reprinted (adapted) with permission from (COMPLETE REFERENCE CITATION). Copyright (YEAR) American Chemical Society." Insert appropriate information in place of the capitalized words.
- One-time permission is granted only for the use specified in your request. No additional uses are granted (such as derivative works or other editions). For any other uses, please submit a new request.

BACK CLOSE WINDOW

Copyright © 2016 Copyright Clearance Center, Inc. All Rights Reserved. Privacy statement. Terms and Conditions.
Comments? We would like to hear from you. E-mail us at customercare@copyright.com

https://s100.copyright.com/AppDispatchServlet

E. Copyright permission for chapter 4.

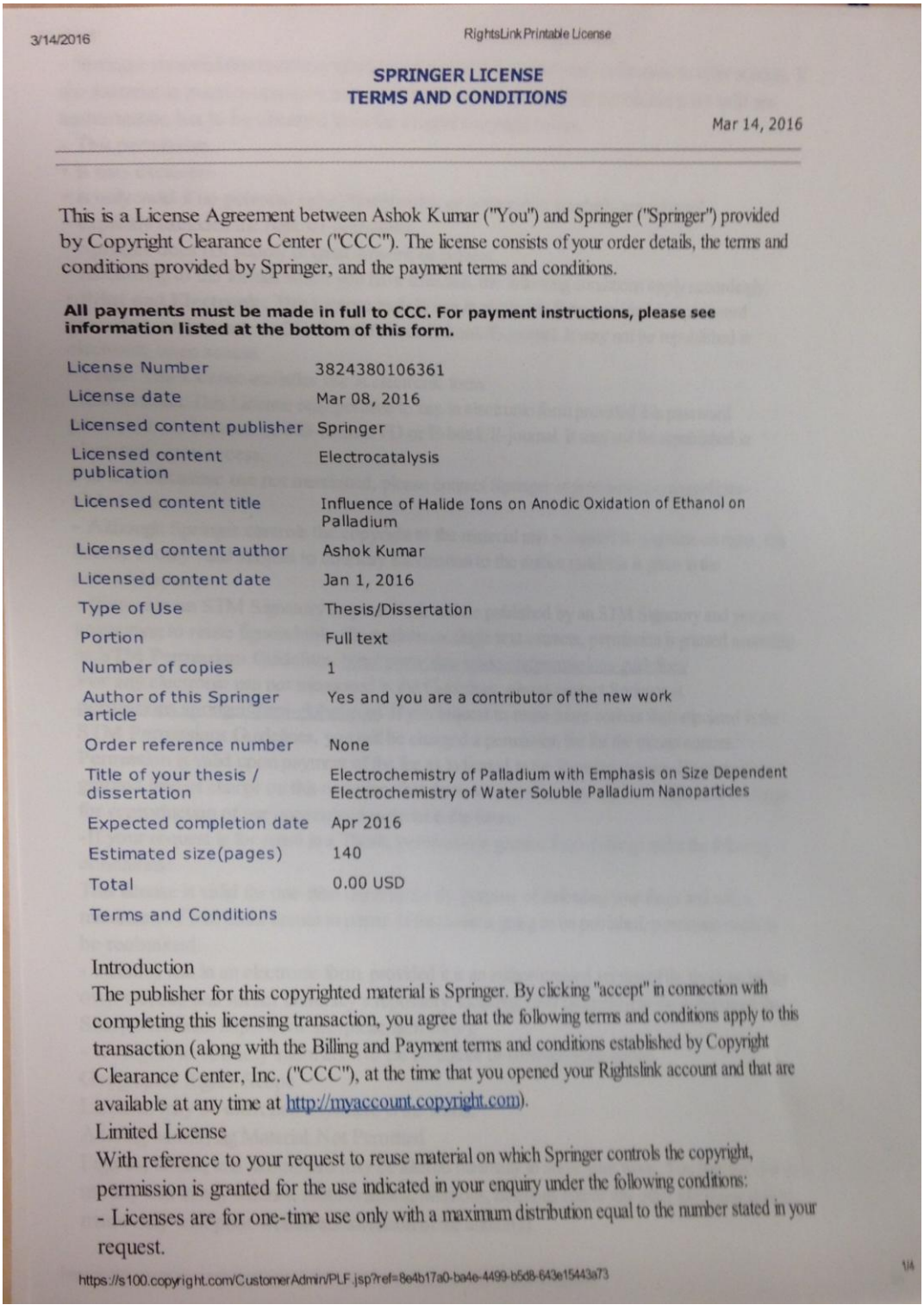

3/14/2016 RightsLink Printable License

SPRINGER LICENSE
TERMS AND CONDITIONS

Mar 14, 2016

This is a License Agreement between Ashok Kumar ("You") and Springer ("Springer") provided by Copyright Clearance Center ("CCC"). The license consists of your order details, the terms and conditions provided by Springer, and the payment terms and conditions.

All payments must be made in full to CCC. For payment instructions, please see information listed at the bottom of this form.

License Number	3824380106361
License date	Mar 08, 2016
Licensed content publisher	Springer
Licensed content publication	Electrocatalysis
Licensed content title	Influence of Halide Ions on Anodic Oxidation of Ethanol on Palladium
Licensed content author	Ashok Kumar
Licensed content date	Jan 1, 2016
Type of Use	Thesis/Dissertation
Portion	Full text
Number of copies	1
Author of this Springer article	Yes and you are a contributor of the new work
Order reference number	None
Title of your thesis / dissertation	Electrochemistry of Palladium with Emphasis on Size Dependent Electrochemistry of Water Soluble Palladium Nanoparticles
Expected completion date	Apr 2016
Estimated size(pages)	140
Total	0.00 USD
Terms and Conditions	

Introduction

The publisher for this copyrighted material is Springer. By clicking "accept" in connection with completing this licensing transaction, you agree that the following terms and conditions apply to this transaction (along with the Billing and Payment terms and conditions established by Copyright Clearance Center, Inc. ("CCC"), at the time that you opened your Rightslink account and that are available at any time at http://myaccount.copyright.com).

Limited License

With reference to your request to reuse material on which Springer controls the copyright, permission is granted for the use indicated in your enquiry under the following conditions:

- Licenses are for one-time use only with a maximum distribution equal to the number stated in your request.

https://s100.copyright.com/CustomerAdmin/PLF.jsp?ref=8e4b17a0-ba4e-4499-b5d8-643e15443a73 1/4